DEVELOPMENT OF A QUANTITATIVE MODEL OF STRESS IN A SEISMIC REGION AS A BASIS FOR EARTHQUAKE PREDICTION

Keiiti Aki
and
Keiichiro Ikeda

Department of Earth and Planetary Sciences
M.I.T.
Cambridge, Mass.

USGS CONTRACT NO. 14-08-0001-18205
Supported by the EARTHQUAKE HAZARDS REDUCTION PROGRAM

OPEN-FILE NO.81-269

Department of Earth and Planetary Sciences

M.I.T.

Cambridge, Mass.

Development of a Quantitative Model of Stress in a Seismic Region as a Basis for Earthquake Prediction

Technical Report - April 1979 - April 1980
Contract No. 14-08-0001-18205

Since this project has been renewed, and the details of progress have been reported in the renewal proposal, we shall summarize here only briefly what has been done in the past year.

Our goal in the project is to investigate earthquake precursors in relation to the stress in the earth. For this purpose, we determine incremental stress at depths from geodetic data obtained on the surface. We have completed the computer program for the geodetic data inversion and applied it to the data from the Palmdale area with some preliminary results.

The geodetic inverse problem is formulated in terms of known 3 component displacement and vanishing stress on the surface (Cauchy's boundary condition for an elliptic operator equation). Three dimensional finite element method provides a discretized operator. The input requires data both on vertical and horizontal displacements simultaneously. Such data are available for limited areas from geodimeter and leveling survey.

The inversion scheme is tested using artificial data generated by Mindlin's buried point source solution. The result was satisfactory for the 20-nodes isoparametric element scheme, which we are now using.

The scheme was applied to a small area near Palmdale, Calif. where 3 component data are available from geodimeter network and leveling survey from 1959 to 1976. The incremental stress obtained during the period of uplift (1959 to 1962) shows the dominance of horizontal tensional stress in the direction of N48°E with magnitude 2.1 bars at the depth of 3.75 km. During the period of downwarp, the maximum principal incremental stress become horizontal compression in the direction of N40°W with magnitude 2.2 bars at the depth of 3.75 km while minimum principal incremental stress was near vertical and tension. The compressional stress increases with depth to 4.2 bars at the depth of 6.5 km and 7.0 bars at the depth of 8.75 bars.

The sense and direction of incremental stress during the downwarp period are consistent with the fault plane solutions for earthquakes in the early period of swarm activities which coincides with the late period of downwarp. The magnitude of the incremental stress is compatible with the estimate from the observed geomagnetic change in the same period for the same area.

The above preliminary results were reported by the principal investigator at the Ewing Symposium on Earthquake Prediction held May 12-16, 1980, in which he proposed a probabilistic synthesis approach for uniting the results from laboratory, field and model studies on earthquake prediction. A new concept of "probability gain" was introduced for a given precursor, and its evaluation by various methods were discussed. The incremental stress to be determined by the current project may be used to estimate the probability gain. The probability gain can be translated into a quantitative measure of gradation of concern on earthquake occurrence useful for public offices concerned with earthquake hazard.

Reports

Ikeda, K. Three dimensional Geodetic Inversion Method for Stress Modelling in the Lithosphere, M.S. Thesis, M.I.T., January, 1980.

Aki, K. A probabilistic synthesis of precursory phenomena, presented at the Ewing Symposium on Earthquake Prediction, May 1980.

A PROBABILISTIC SYNTHESIS OF PRECURSORY PHENOMENA

Keiiti Aki

Department of Earth and Planetary Sciences

Massachusetts Institute of Technology

Abstract

The concept of probability gain associated with a precursor may be useful for unifying various areas of earthquake prediction research. Judging from the success of predicting the Haicheng earthquake of 1975, the probability gain at each stage of long-term, intermediate-term, short-term and imminent prediction in this case is estimated as a factor of about 30. For many independent precursors, the Baysian theorem shows that the total probability gain is approximately the product of individual gains.

The probability gain for an individual precursor may be calculated as its success rate divided by the precursor time (Utsu, 1979). The success rate can only be determined from the accumulation of experiences with actual earthquakes. The precursor time, on the other hand, may be studied experimentally and theoretically. A review of these studies leads to a suggestion that the loading rate may be faster for smaller earthquakes. The existence of so called "sensitive spots" where precursory strain, radon or other geochemical anomalies to show up even for distant earthquakes suggest that some sites may have stress amplification (concentration) effect which may also account for higher loading rate for a small earthquake.

The concept of fractals (a family of irregular or fragmented shapes) developed by Mandelbrot (1977) is applied to the fault plane to gain some insight into its geometry. If we use the idea of barrier model in which smaller earthquakes are generated by the segmentation of a large earthquake, the fractal dimension of the fault plane becomes equal to 3b/c where b is the b value of magnitude-frequency relation, and c is the log-moment vs magnitude slope ($c \tilde{-} 1.5$). For $1 < b < 1.5$, which is usually observed, the fractal dimension varies from 2 (filling up plane) to 3 (filling up volume). For $0.5 < b < 1.0$, which is sometimes observed for foreshocks, the model corresponds to fault lines trying to fill up a plane. The Goishi model of Otsuka (1972) and branching model of Vere-Jones (1976) have such geometry. Assuming that the total length of branches is proportional to earthquake energy, the b value for these models becomes 0.75, corresponding to the fractal dimension of 1.5.

The probability gain for the tectonic stress increase by $\Delta\sigma$ can be expressed as $\exp(\beta\Delta\sigma)$. The coefficient β has been obtained in laboratories and in field using various methods. The value of β varies wildly, but tends to show higher value when the stress is applied in a large scale. This may also be explained by a stress amplification due to the fractal nature of fault plane. Deterministic studies of inhomogeneities, irregularity and fragmentation of fault zone will be important for understanding precursor phenomena.

Introduction

The most impressive accomplishment in seismology during the last decade was the success of our Chinese colleagues in predicting several major earthquakes. Let us take the Haicheng earthquake of 1975 and consider the probability of its occurrence before the earthquake. When the warning of earthquake occurrence was issued and people were kept outdoors in cold winter temperatures, the hazard rate, that is, the probability of earthquake occurrence per unit time, must have been on the order of 1 per several hours. The area is normally aseismic and historic records indicate the hazard rate to be on the order of 1 per thousand years. In other words, the information gathered by Chinese colleagues was able to raise the probability by a factor of about 10^6. This remarkable accomplishment was made in four stages, namely, long-term, intermediate-term, short-term and imminent prediction. Figure 1 illustrates schematically how the unconditional hazard rate estimated from historic data was raised by each stage of prediction. Assuming an equal gain for all the stages, we find that each stage contributed to the probability gain of a factor of about 30. In order to achieve this amount of probability gain, many, many specialists and non-specialists were engaged in collecting information on various precursory phenomena. Some of the key precursors at each stage are indicated in Figure 1.

The purpose of the present paper is to unify various areas of earthquake prediction research by the concept of probability gain. The probability gain for a particular precursor may be studied empirically using past experiences with actual earthquakes. It may be studied in a laboratory

scale model under controlled conditions. More fundamentally, the probability gain may be determined by the increase of tectonic stress, which can be estimated from geodetic data. If these studies can develop a means to determine probability gain as a function of given precursors, the results can be translated into objective quantitative measure for the grade of concern about an earthquake occurrence, which will be helpful to the public offices in charge of public safety.

Let us start with a few definitions.

Definitions

First we specify the area in which an earthquake is predicted to occur. Then, we can define the average frequency of occurrence of earthquakes with a certain magnitude range in that area. For example, if the number N(M) of earthquakes with magnitude greater than M is recorded during the total time period T, the average rate of occurrence p_o per unit time is given by

$$p_o = \frac{N(M)}{T} \tag{1}$$

For a short time interval τ , then, the unconditional probability P(M) of occurrence of an earthquake with magnitude greater than M in that area is given by

$$P(M) = p_o\tau \tag{2}$$

We shall divide the time axis into consecutive segments with the constant interval τ as shown in Figure 2. The crosses indicate the occurrence

of an earthquake with magnitude greater than M. The interval τ is taken short enough so that each segment contains at most one earthquake. We shall write the total number of segments as

$$N_o = \frac{T}{\tau} \tag{3}$$

Let us now introduce precursors, and designate them as A, B, C, ... For example, A may be a swarm of small earthquakes which may be characterized by the duration, the maximum magnitude and the b value. B may be a ground upheaval characterized by the duration, extent and amount of uplift. C may be a Radon anomaly observed in the area characterized by the duration and amplitude. Suppose that, in the total period of observation, the precursor A showed up for time intervals shown in Figure 3.

Consider those segments during which the precursor A existed. Of those segments, let the number of segments containing an earthquake be n_A, and the number of segments containing no earthquake be $\tilde{n}_A$. Then, we can define the conditional probability $P(M|A)$ of occurrence of an earthquake within a time interval τ under the condition that the precursor A is existing as

$$P(M|A) = \frac{n_A}{n_A + \tilde{n}_A} \tag{4}$$

Since, for small τ , $P(M|A)$ is proportional to τ , we can write

$$P(M|A) = p_A \tau \tag{5}$$

P_A is the probability of an earthquake per unit time under the condition that the precursor A is existing.

We define similarly n_B, $\tilde{n}_B$ and p_B for the precursor B, and so on. Here, we simplified our problem by neglecting the details of each precursor phenomenon, which may be included by the explicit use of multiple parameters as done by Rhoades and Evison (1979).

Conditional Probability for Multiple Independent Precursors

Let us find the probability $P(M|A,B,C,...)$ of occurrence of an earthquake (with magnitude greater than M in a specified area) under the condition that n independent precursors A,B,C,... appeared simultaneously. According to the Bayes' theorem,

$$P(M|A,B,C) = \frac{P(A,B,C|M)\ P(M)}{P(A,B,C)}$$

$$= \frac{P(A,B,C|M)\ P(M)}{P(A,B,C|M)\ P(M) + P(A,B,C|\tilde{M})\ P(\tilde{M})} \qquad (6)$$

where $\tilde{M}$ means the non-occurrence of an earthquake.

Since we assume the statistical independence among the precursors,

$$P(A,B,C|M) = P(A|M)\ P(B|M)\ P(C|M) \qquad (7)$$

and

$$P(A,B,C|\tilde{M}) = P(A|\tilde{M})\ P(B|\tilde{M})\ P(C|\tilde{M}) \qquad (8)$$

On the other hand, from the definitions given in the preceding section,

$$P(A|M) = \frac{n_A}{N} \tag{9}$$

$$P(M) = \frac{N}{N_o} \tag{10}$$

$$P(A|\tilde{M}) = \frac{\tilde{n}_A}{N_o - N} \tag{11}$$

and

$$P(\tilde{M}) = \frac{N_o - N}{N_o} \tag{12}$$

Putting the equations (7) through (12) into (6), we obtain

$$P(M|A,B,C) = \frac{1}{1+\left(\frac{\tilde{n}_A}{n_A}\frac{\tilde{n}_B}{n_B}\frac{\tilde{n}_C}{n_C}\cdots\right)\left(\frac{N}{N_o - N}\right)^{n-1}} \tag{13}$$

Using equation (4), the above relation can be rewritten as

$$P(M|A,B,C) = \frac{1}{1 + \left(\frac{1}{P(M|A)}-1\right)\left(\frac{1}{P(M|B)}-1\right)\left(\frac{1}{P(M|C)}-1\right)\cdots \Big/ \left(\frac{1}{P(M)}-1\right)^{n-1}} \tag{14}$$

The above equation was obtained by Utsu (1979) without the use of the Bayes' theorem. For a small τ the above probability is proportional to τ . We can, then write

$$P(M|A,B,C) \tilde{-} p\tau,$$

where

$$p = p_o \cdot \frac{P_A}{P_o} \frac{P_B}{P_o} \frac{P_C}{P_o} \qquad (15)$$

The above extremely simple relation shows that, for multiple independent precursors, the conditional rate of earthquake occurrence can be obtained by multiplying the unconditional rate p_o by the ratios,

$$\frac{\text{conditional probability}}{\text{unconditional probability}}$$

for all the precursors. We shall call the above ratio as the probability gain of a precursor.

A quantitative measure of the grade of concern on an earthquake occurrence is illustrated in Figure 4, which shows the probability of occurrence per day of an earthquake with magnitude greater than a specified value. The unconditional probability is determined from the precursor data by equation (1). The precursors A, B, and C increase this probability approximately by a factor of $\frac{P_A}{P_o} \frac{P_B}{P_o} \frac{P_C}{P_o}$ as shown in equation (15). The example shown in Figure 4 corresponds to the earthquake with M > 6 1/2 in the Izu-Oshima area in Japan just before the earthquake of Jan. 14, 1978. Precursors A, B, and C are uplift (including gravity change), foreshocks, and Radon anomalies (including water-level change) respectively. The probability gain for each precursor was assigned by Utsu (1979) in a manner described later. The conditional probability for the three precursors almost reached the highest grade of concern VI. Although the evaluation of conditional probability was not made in real time, the Japan Meterological Agency nevertheless issued an earthquake information at 10h50m, on Jan. 14 stating

that there was a possiblity of occurrence of an earthquake causing a minor damage. An earthquake with M = 7 took place at 12h24m on the same day.

How to Assign the Probability Gain for a Particular Precursor

The evaluation of an earthquake prediction is very simple using the procedure described in the preceding section, if we know the probability gain p_A/p_o, p_B/p_o, ... for given precursors.

For the Izu-Oshima earthquake of 1978, Utsu (1979) estimated the probability gain in the following manner. The precursor A is the uplift in Izu Peninsula which was confirmed also by gravity change. The diameter of uplifted area is about 25 km, which may correspond to the source size of an earthquake with M = 6 1/2. According to a summary by Sato and Iuchi quoted in Utsu (1979), only 17% of anomalous uplifts were connected directly to earthquake occurrence. However, since the uplift in this case is so conspicuous, Utsu assigned the probability of 1/3 instead of 17%. He also assigned the life-time uplift (or precursor time) to be five years. This gives the conditional probability rate $p_A = \frac{1}{3x5x365}$ per day.

The precursor B is the earthquake swarm taking place in the area. According to statistics, one out of twenty swarms may be followed by a major earthquake. However, the Izu area is known for relatively frequent foreshocks. Utsu, thus, assigns the probability of 1/10 instead of 1/20 for the chance of a swarm to be followed by a major earthquake in this area. Utsu made a study of foreshocks for 26 major earthquakes, and found that the mainshock occurred with three days from the biggest foreshock for 19 cases out

of 26, and that the difference between the magnitude of main shock and that of the biggest foreshock was greater than 1.6 for 10 cases out of 26. Since the biggest foreshock in the present case was M 4.9, the difference between the magnitude of presumed main shock (M 6.5) and that of the biggest foreshock is 1.6. Thus, he assigned the conditional probability rate p_B to be $\frac{1}{10}\frac{19}{26}\frac{10}{26}\frac{1}{3} \simeq 10^{-2}$ per day.

Finally, the precursor C for the Izu-Oshima earthquake is the composite of Radon anomaly, anomalous water table change, and volumetric strain anomaly. He considers that these three precursors may be closely related, and treats them as one precursor. He just assigns the precursor time of 1 month, and the probability that the precursor is followed by a major earthquake to be 1/10. This gives $p_C = \frac{1}{300}$ per day,

With the above estimates of conditional probabilty rates p_A, p_B, p_C and the unconditional probability/p_o^{rate} based on the past seismicity in the area, he calculates the probability gains as shown in Figure 4. The precursor A (uplift) gives only the probability gain of about 2, while the precursors B (radon) and C (foreshock) gives the gain of about 100. The former, however, was important for assigning the magnitude of predicted earthquake. The main reason for the high gain of latter precursors is their short lifetime.

The probabilty gain is a function of magnitude of earthquake to be predicted. For a given earthquake swarm the probabilty that the swarm be accompanied by a major earthquake will decrease sharply with the magnitude of the latter. The longer lifetime of precursor for greater earthquakes as

proposed by various people also tend to diminish the probability gain for precursors of greater earthquakes.

On the other hand, a tremendous gain is possible, if a particular short-term precursor is expected with a high degree of certainty. For example, Sieh's (1978) suggestion that one out of several Parkfield earthquakes may become a foreshock of the next 1857 great Califoria earthquake will give a very high conditional probability rate, say, 10^{-1} per day. This means the probability gain of more than 10^{4}. With several additional precursors of moderate or small gains, it may be possible to issue a high-grade concern before the next 1857 earthquake.

Precursor Time for Various Models of Rock Failure

As described in the preceding section, Utsu (1979) estimates the probability gain for a given precursor to be equal its success rate divided by the precursor time. The success rate can only be determined from the accumulation of experiences with actual earthquakes. The precursor time, on the other hand, may be studied using rock samples in the laboratory under various conditions, or by analyzing models of rock failure theoretically. Here we shall make a review of proposed models with regard to the question "what determines the precursor time?".

Theoretical studies of the above problem were made by Rice (1979) and Rice and Rudnicki (1979) for a fluid-filled porous medium, and they concluded that not only the fault length of the impending earthquake but also the loading rate and the constitutive relation may play important parts. Their result showed that the precursor time is closer to proportional to L (fault

length) rather than to L^2 as suggested in various empirical formulas (Tsubokawa [1969], Scholtz, et al. [1973], Rikitake [1976]). Dieterich (1979) also suggests that the precursor time may be proportional to L on the basis of the precursory creep observed in his laboratory experiment and reproduced theoretically by a frictional model of slip-weakening instability. His precursor time is the travel time of precursory creep over the fault length, thus proportional to the latter.

Brady (1974) claims that the L^2 dependence of precursory time on fault length can be derived for a dry-dilatancy model without fluid diffusion. A close look at the derivation of his equation (19) reveals an unacceptable assumption made on the average strain $\bar{\varepsilon}$ within a volume element dV_{fr} due to closure of an average sized microcrack. The average strain can be written as

$$\bar{\varepsilon} = \frac{\int \varepsilon(\underset{\sim}{x}) dV}{dV_{fr}}$$

Since $\varepsilon(\underset{\sim}{x})$ is a decreasing function with distance from the microcrack, beyond a certain size of dV_{fr}, the numerator will reach a constant asymptotically. Since, by definition, dV_{fr} should be large enough to include many cracks, $\bar{\varepsilon}$ will be inversely proportional to dV_{fr} instead of a constant as assumed by Brady. If we correct for this, the precursor time becomes independent of L.

This conclusion is expected from a simple consideration that the successive stages of dilatancy model (Miachkin et al., 1975, Sobolev, et al., 1978) are primarily determined by the stress relative to the failure stress (independent of L), and the precursory time is mainly determined by the

loading rate. There is no obvious reason why the precursory time should depend on fault length, for a dry dilatancy model.

If the loading rate determines the precursor time, the empirical relation between precursor time and fault length means that the loading rate is higher for smaller earthquakes.

This magnitude dependence of loading rate is somewhat difficult to conceive for a homogenous continuum model of the earth and a common source model of stress for all earthquakes, that is, the plate motion.

One disturbing thing about the empirical relation between the precusor time and earthquake magnitude is the fact pointed out by Tsubokawa (1969) and Anderson and Whitcom (1975) that the slope of log precursor time vs. magnitude is identical to that of log recurrence time vs. magnitude. This means that the observed precursor time is roughly a fixed fraction of the recurrence time. Since no one tries to pick up a precursor for an earthquake before the time of occurrence of the preceding one, it may be suspected that those precursors may be just noises. On the other hand, these precursors may be real signals as demonstrated by the successful prediction of the Haicheng and other earthquakes.

If we accept the reality of precursors and the magnitude dependence of precursor time, we may have to accept also that the loading rate may be higher for smaller earthquakes.

A higher loading rate for a localized region relative to the surrounding is possible if the stress in the region is somehow amplified. Inhomogeneities such as joints and inclusions can cause such an amplification through stress concentration. The existence of so called "sensitive spots"

where precursory strain, radon or other geochemical anomalies tend to show up even for distant earthquakes, as well as the fact that even in the near-field of an earthquake, some precursory phenomena (such as the anomalous water table change) occur only at a small number of sites (wells) also suggest that some sites may be more sensitive because of the greater stress amplification.

Barrier Model and Fractal Dimensions of Fault Planes

The inhomogeneity of the fault zone, sometimes called "patches", "barriers" and "asperities", also introduce stress concentration. These inhomogeneities appear to exist in all scales. Microscopic pictures of the sections of rock sample after failure show that the zone of failure is not a continuous plane but fragmented. Similar fragmentation of fault has been observed at the site of rock burst in a deep mine (e.g., Spottiswoode and McGarr, 1975) and in the epicentral areas of major earthquakes (e.g., Tchalenko and Berberian, 1975). Das and Aki (1977) made a numerical experiment on rupture propagation over a fault plane with distributed barriers, and showed that some of the barriers may remain unbroken after the rupture propagation, offering a mechanism to account for fragmented fault.

The stress concentration around unbroken barriers may become the source of aftershocks (Otsuka, 1976). Aki (1978) summarized the relation between the barrier interval and the maximum slip obtained by various methods, and found that the barrier interval increases with the slip even for the same fault zone. This is consistent with the observed high Griffith fracture energy for greater earthquakes (Aki, 1979), because greater earthquakes break stronger fracture energy barriers with resultant longer barrier intervals.

Andrews (1978) pointed out, from a consideration of energetics, that the stationary occurrence of a large number of small earthquakes cannot be explained by the load of smoothly varying tectonic stress alone, but requires a generation of short wavelength self stress by a large earthquake, unless fault creep, varying in amplitude of all length scales prepares the fault for small earthquakes. The barrier model offers a physical mechanism for such a roughening of self stress in the fault zone after a major earthquake.

The above line of reasoning suggests a generic process of the whole ensemble of earthquakes, in which an earthquake prepares the stress field for the smaller earthquakes. This is similar to the phenomena of turbulence, in which a large eddy splits into smaller ones, generating a hierachy of eddies linked by a cascade.

The concept of "fractals" developed in a book by Mandelbrot (1977) may be useful for describing the geometry of the assemblage of fault planes. A fractal is a family of irregular or fragmented shapes. An example is the length of the coast of Britain, which increases indefinitely as the scales of map is made finer. Topologically, a coast is a line with dimension 1. To describe the departure of the coast line from a simple line with finite length, he introduces the fractal dimension. For example, the trace of Brownian moton of a particle has the fractal dimension of 2 because it fills up the plane, and the fractal dimension of west coast of Britain is determined to be about 1.25. One way to obtain the fractal dimension D is, given a segment, to find the number N of subsegments which has a linear dimension r times the segment. Then, D is given by $\log N/\log(1/r)$. For example, if a straight line is divided into N segments, $r = 1/N$ and therefore $D = 1$. If a square is divided into N squares, $r = 1/\sqrt{N}$ and therefore $D = 2$.

Assuming a process in which smaller earthquakes are generated by a large earthquake in the manner in which aftershocks are generated by the barrier model, we can interpret the magnitude-frequency relation and find the fractal dimension of fault plane (we allow an overlap of fault planes, in accordance with the barrier model). Let the number of earthquakes (in a given time-space range) with fault length greater than L be N(L). The slope of log N(L) against log L is 3b/c, where b is the slope of log frequency-magnitude relation and c is the slope of log moment-magnitude relation, and we assume that the seismic moment is proportional to L^3 (self-similarity). To be compatible with the process for generating segments, we shall restrict the possible fault length to be $L_n = r^n L_o$, where n is the integer.

From the n to (n + 1) step, the length is reduced by a factor r. In this process, the number of earthquakes is multipled by $(1/r)^{3b/c}$, because $\Delta L = (L_{n+1} - L_n)$ is proportional to L and $\Delta L \, dN/dL$ is proportional to $L^{3b/c}$ Thus, the fractal dimension of fault plane is D = 3b/c. We shall consider the usual case of c = 1.5 (Hanks and Kanarmori, 1979). Then, if b = 1, the fractal dimension of fault plane is 2, same as its topological dimension. If b = 1.5, on the other hand, the fractal dimension becomes 3, which corresponds to filling up volume with fault planes. In most cases, the observed b value falls between the above two extremes. The value slightly greater than 1 observed for the world, imply that the assemblage of fault planes, "the plate boundary" in the context of plate tectonics, is a little more than a plane.

For $0.5 < b < 1.0$, the fractal dimension becomes between 1 and 2. For them, one can no longer consider the fault as a plane, because the fractal dimension must be greater than the topological dimension. It is possible, however, to imagine fault lines trying to fill up a plane. As a matter of

fact, the goishi model of Otsuka (1972) (see also Saito et al., 1973 and Maruyama, 1978) and the branching model of Vere-Jones (1976) have such geometry. In fact, the corresponding log frequency-magnitude relation becomes linear (in the critical case) with the b value equal to 0.75, assuming that the total length of branches is proportional to earthquake energy. This suggests that the fractal dimension of the branching model is 1.5.

Otsuka'a model has been shown to be essentially the same as the model used in the study of percolation process. Otsuka proposed this model to describe the growth of an earthquake fault. His model is not based on the elasto-dynamics of rupture propagation along a fault plane, but is based on a probabilistic growth of a tree-like shape. Seismological observations clearly show that an earthquake involves a propagation of rupture with the speed comparable to elastic wave velocities and is not a percolation process. On the other hand, his model may be useful for studying the stage of preparation of a large earthquake. The barrier model used for generating a hierachy of earthquakes is adequate for aftershocks and probably for the normal earthquake, but not for foreshocks which will precede a larger earthquake. If there is a basic generic difference between foreshocks and normal earthquakes, there remains a hope to discriminate them. Smaller b values observed for some foreshocks than for aftershocks certainly agree with the idea that the percolation model applies to the former and the barrier model to the latter. Needless to say, the precursor time will be longer for larger earthquakes if the percolation model is applicable to the preparation stage. The cross section of branches at the earth's surface will be points, and may be very difficult to be detected without numerous observations. This may explain the reason for the Chinese successful predictions.

Probability Gain by an Increase in Tectonic Stress

So far, we have mainly considered the geometry of the assemblage of fault planes, somewhat phenomenologically without paying much attention to the detailed state of stress and dynamic process going on over the fault plane. More explicit discussions of these subjects have been given by Hanks (1979) and Andrews (1980). Here we shall stay out of the stress distribution in the fault zone and consider only its response to applied external stress, namely, the problem of estimating the probability gain of an earthquake occurrence by an increase in tectonic stress.

How the probability of earthquake occurrence depends on the tectonic stress is an extremely complex problem. According to Mogi (1962), the probability of occurence of fracture in a rock sample increases exponentially with the applied stress. When a constant stress σ is applied at $t = o$, he found that the probability of occurrence of fracture between t and $t + dt$ is independent of t and given by

$$\mu(t)dt = \mu_o \exp(\beta\sigma) \tag{16}$$

where $\mu(t)$ is what we called "hazard rate" earlier, and β is determined as $0.37\ \text{bar}^{-1}$ for the tensile fracture of granite samples in the atmosphere. The experiment by Scholtz (1972) on static fatigue of quartz under uniaxial compression shows the same functional dependence on stress, but with β about one hundred times smaller than Mogi's value. The probability gain due to stress increase by $\Delta\sigma$ is simply $\exp(\beta\Delta\sigma)$, which will be wildly different whether we use Mogi's value or Scholtz's value for β .

The coefficient β can be estimated from the recurrence time of major earthquakes in a fault zone and the associated stress drop. For the Hokkaido-Kuril region, Utsu (1972) constructed a statistical model based on equation (16) and determined the model parameter by fitting the data on recurrence time. Combining Utsu's result with the average stress accumulation rate (0.3 bar per year) inferred from the stress drops in major earthquakes in this zone (Fukao and Furumoto, 1979), we find that β is 1.1 bar^{-1}. Earlier, Hagiwara (1974) obtained β of about 0.3 bar^{-1} by applying equation (16) to the statistical distribution of ultimate strain obtained by geodetic measurements.

From time to time, we find reports on an apparent sensitivity of earthquake occurrence to small stress changes such as due to earth tide and atmospheric pressure. For example, Conrad (1932) showed an impressive evidence for the increase of local earthquake frequency by 30% due to the atmospheric pressure gradient across the Alps by 5^{mm} Hg (6.7×10^{-3} bars) or greater. This gives β to be about 40 bar^{-1}.

In this conference, Barry Raleigh reported about the increase of seismicity in southern California by a factor of 2 which was associated with a strain change of 10^{-6}. This corresponds to the value of β about 2 bar^{-1}, which is much greater than laboratory values but comparable to the Hokkaido-Kuril result.

The value of β estimated by various methods, thus, ranges from 0.004 to 40 bar^{-1} over 4 decades. There is some suggestion of increasing β with increasing scale length. In other words, the probability of earthquake occurrence is more sensitive to stress change, when stress is applied in a larger scale.

Earlier, we have discussed about the scale dependence of loading rate, and suggested that stress concentration or amplification may be occurring in a cascade from a larger scale to successively smaller scales. The scale dependence of β may also be attributed to such stress amplification.

Discussion

I feel that fractal models of fault planes would be useful for understanding the precursory phenomena, especially with regard to their sensitivity to tectonic stress. The currently most reliable data for estimating tectonic stress are geodetic data supplied from levelling and geodimeter survey. One promising approach toward understanding precursory phenomena is to determine the stress change at depth from geodetic data, and then correlate the estimated stress change with the stress-sensitive phenomena such as changes in seismicity and magnetic field. A preliminary result from the Palmdale area obtained by Ikeda (1980) is encouraging. He inverted the geodetic data into 3-D stress distribution and found that the state of incremental stress during the downwarp period was in agreement with the fault plane solutions for the swarm of earthquakes during the same period given by McNally et al. (1978). From the magnitude of incremental stress (estimated at about 10 bars) and increase in the frequency of small earthquakes, the β-value was estimated to be about 0.3 bar . This magnitude of stress increase was consistent with that estimated by Johnston et al. (1979) from the observed magnetic anomaly.

In the present paper, we discussed the fractal aspect of fault planes only from the statistical point. For the purpose of earthquake prediction, however, it may be necessary to study them deterministically. For example, we need to know where the sensitive spots are in order to observe precursors. Recent work by Bakun et al. (1980) on the relation between detailed seismicity and geometry of fault fragmentation along a part of the the San Andreas fault demonstrated that such a deterministric approach may be feasible and promising.

Acknowledgement

I thank Joe Andrews for directing me to the most interesting book by Mandelbrot. This work was supported by the U.S. Geological Survey under contract 14-08-0001-19150.

Reference

Aki, K., A quantitative model of stress in a seismic region as a basis for earthquake prediction Proc. Conf. III, Fault Mechanics and its relation to earthquake prediction, U.S. Geological Survey Open-file Report 78-380, 7-30, 1978.

Aki, K., Characterization of Barriers on an Earthquake Fault, J. Geophys. Res., 84, 6140-6148, 1979.

Anderson, D. L. and J. H. Whitcom, Time-dependent seismology, J. Geophys. Res., 80, 718-732, 1975.

Andrews, D. J., Coupling of energy between tectonic processes and earthquakes, J. Geophys. Res., 83, 2259-2264, 1978.

Andrews, D. J., Stochastic Fault model - I Static Case, J. Geophys. Res., in press, 1980.

Bakun. W. H., R. M. Stewart, C. G. Bufe, and S. M. Marks, Implication of seismicity for failure of a section of the San Andreas fault, Bull. Seis. Soc. Am., 70, 185-201, 1;980.

Brady, B. T., Theory of earthquakes, I. A scale independent theory of rock failure, Pageoph 112, 701-725, 1974.

Conrad, V., Die Zietlich Folge der Erdbeben und Bebenaulosande Ursachem, Handbuch der Geophysik, Bd. IV, 1997-1185, 1932.

Das, S. and K. Aki, Fault plane with barriers: A versatile earthquake model, J. Geophys. Res., 82, 5658-5670, 1977.

Dieterich, J. H., Modeling of Rock Friction. 1. Experimental results and constitutive equations. 2. Simulation of preseismic slip, J. Geophys. Res., 84, 2161-2175.

Fukao, Y., and M. Furumoto, Stress drop, wave spectrum and recurrence interval of great earthquakes - implication from the Etorofu earthquake of Nov. 6, 1958, Geophys. J. Roy. Astr. Soc., 57 23-40, 1979.

Hagiwara, Y., Probability of earthquake occurrence estimated from results of rock fracture experiments, Tectonophysics, 23, 99-103, 1974.

Hanks, T. C., b-values and $\omega^{-\gamma}$ seismic source models: Implications for tectonic stress variations along active crustal fault zones and the estimation of high-frequency strong ground motion, J. Geophys. Res., 84 2235-2242, 1979.

Hanks, T. C. and H. Kanamori, A moment magnitude scale, J. Geophys. Res., 84, 2348-2350, 1979.

Ikeda, K., 3-dimensional geodetic inversion method for stress modelling in the lithosphere, MS thesis, M.I.T., Jan. 1980.

Johnston, M. J. S., F. J. Williams, J. McWhister and B. E. Williams, Tectonomagnetic anomaly during the southern California downwarp, J. Geophys. Reviews, 84, 6026-6030, 1979.

Mandelbrot, B. B., Fractals, W. H. Freeman and Co., San Francisco, pp. 365, 1977.

Maruyama, T., Frequency distribution of the sizes of fractures generated in the Branching Process -- Elementary Analysis, Bull. Earth. Res. Inst. 53, 407-421, 1978.

Miachkin, V. I., W. F. Brace, G. A. Sobolev, J. H. Dieterich, Two models for earthquake forerunners, Pure Appl., Geophys. 113.

McNally, K. C., H. Kanamori, J., Pechmann and G. Enis, Seismicity increase along the San Andreas fault, southern California, Science, 201, 814, 1978,

Mogi, K., Study of elastic shocks caused by the fracture of heterogeneous material and its relation to earthquake phenomena, Bull. Earth. Res. Inst., Univ. Tokyo, 40, 125-173, 1962.

Otsuka, M. A simulation of earthquake occurrence, 5, an interpretation of aftershock phenomena, Zisin, Ser. II, 29, 137-146, 1976.

Otsuka, M., A chain-reaction type source model as a tool to interpret the magnitude-frequency relation of earthquakes, J. Phys. Earth., 20, 35-45, 1972.

Rhoades, D. A., and F. F. Evison, Long-range earthquake forecasting based on a single predictor, Geoph, J. R., Astro. Soc. 59, 43-56, 1979

Rice, J.R., and J. W. Rudnicki, Earthquake precursor effects due to pore fluid stabilization of weakening fault, J. Geophhys. Res., 84, 2177-2194, 1979,

Rice, J. R., Theory of precursory processes in the inception of earthquake rupture, Gerl. Beitr. Geoph. Leipzig 88, 91-127, 1979.

Rikitake, T., Earthquake prediction. Elsevier, Amsterdam, 1976

Saito, M., M. Kikuchi and K. Kudo, An analytic solution for Otsuka's goishi model, Zisin, II, 26, 19-25, 1973.

Scholtz, C. H., L. R. Sykes and Y. P. Aggarwal, Earthquake predicton: A physical basis, Science, 181, 803-810, 1973.

Scholtz, C. H., Static fatigue of quartz, J. Geophys. Res., 77, 2104-2114, 1972.

Sieh, K. E., 1978, Central California foreshocks of the great 1857 earthquakes, Bull. Seis. Soc. Am., 68, 1731-1750, 1978.

Sobolvev, G., H. Spetzler and B. Salov, Precursors to failure in rocks while underoing anelastic deformations, J. Geophys. Res., 83, 1775.

Spottiswoode, S. M. and A. McGarr, Source parameters of tremors in a deep-level gold mine, Bull Seis. Soc. Am., 65, 93-112, 1975.

Tchalenko, J. S. and M. Berberian, Dasht-e Bayas Fault, Iran: Earthquake and earlier related structures in bedrock, Geol. Soc. Am. Bull., 86, 703-709, 1975.

Tsubokawa, I., 1969, On relation between duration of crustal movement and magnitude of earthquake expected, J. Geod. Soc. Japan, 15, 75-88, 1969.

Utsu, T., Large earthquakes near Hokkaido and the expectancy of the occurrence of a large earthquake off Nemuro, Rep. Coord. Comm. for Earthq. Prediction, Geographic Survey Inst. Ministry of Construction, Japan, 7, 7-13, 1972.

Utsu, T., Calculation of the probability of success of an earthquake prediction (in the case of Izu-Oshima-Kinkai earthquake of 1978), Rep. Coord. Comm. for Earthquake Prediction, 164-166, 1979.

Vere-Jones, D., A branching model for crack propagation, Pageoph, 114, 711-725, 1976.

Figure Captions

Fig. 1. The successful prediction of the Haicheng earthquake implies that the hazard rate (probability of occurrence of earthquake per unit time) had been increased from about 1 per 1000 years to 1 per several hours through acquisition of precursory information. The probability gain at each of four stages of prediction is about a factor of 30.

Fig. 2. The cross indicates an earthquake. The time interval τ is taken short enough so that each interval contains, at most, one earthquake.

Fig. 3. The precursor A occurs in time intervals marked A.

Fig. 4. The probability gains calculated by Utsu (1979) for precursors A (uplift), B (foreshock) and C (radon and water table) for the Izu-Oshima earthquake of 1978.

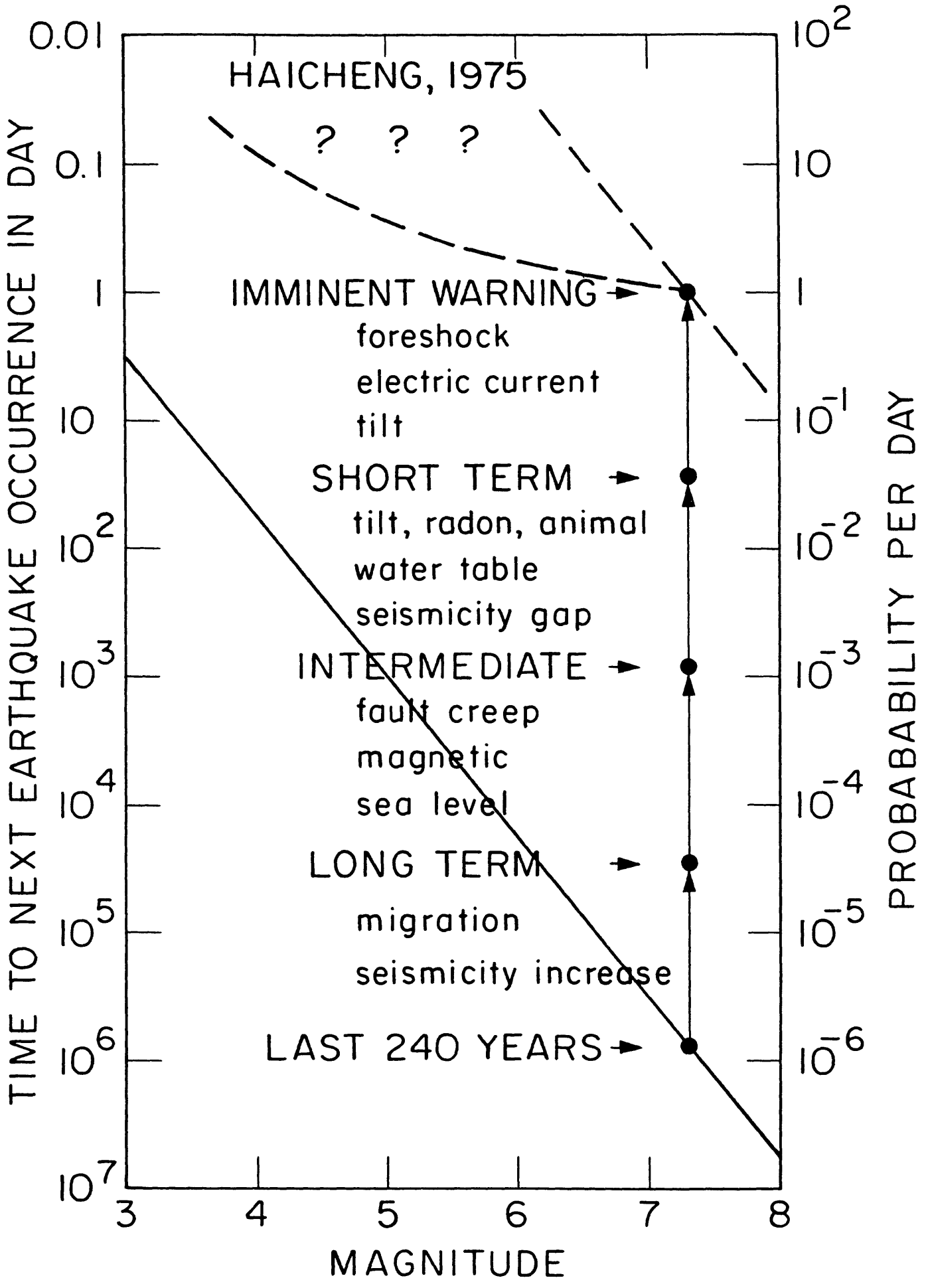
HAICHENG, 1975
? ? ?
IMMINENT WARNING
foreshock
electric current
tilt
SHORT TERM
tilt, radon, animal
water table
seismicity gap
INTERMEDIATE
fault creep
magnetic
sea level
LONG TERM
migration
seismicity increase
LAST 240 YEARS
TIME TO NEXT EARTHQUAKE OCCURRENCE IN DAY
PROBABABILITY PER DAY
MAGNITUDE
0.01
0.1
1
10
10^2
10^3
10^4
10^5
10^6
10^7
10^2
10
1
10^-1
10^-2
10^-3
10^-4
10^-5
10^-6
3
4
5
6
7
8

F 1

FIG 2

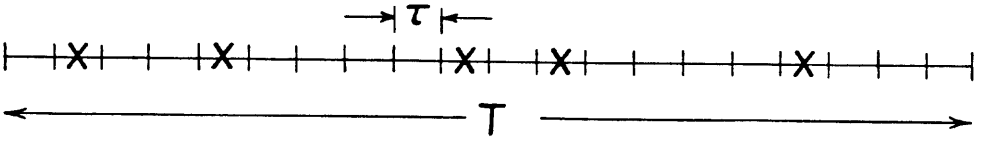

FIG 3

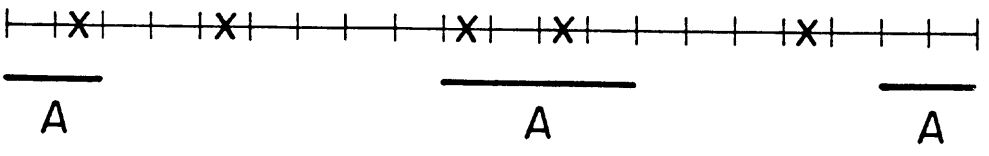

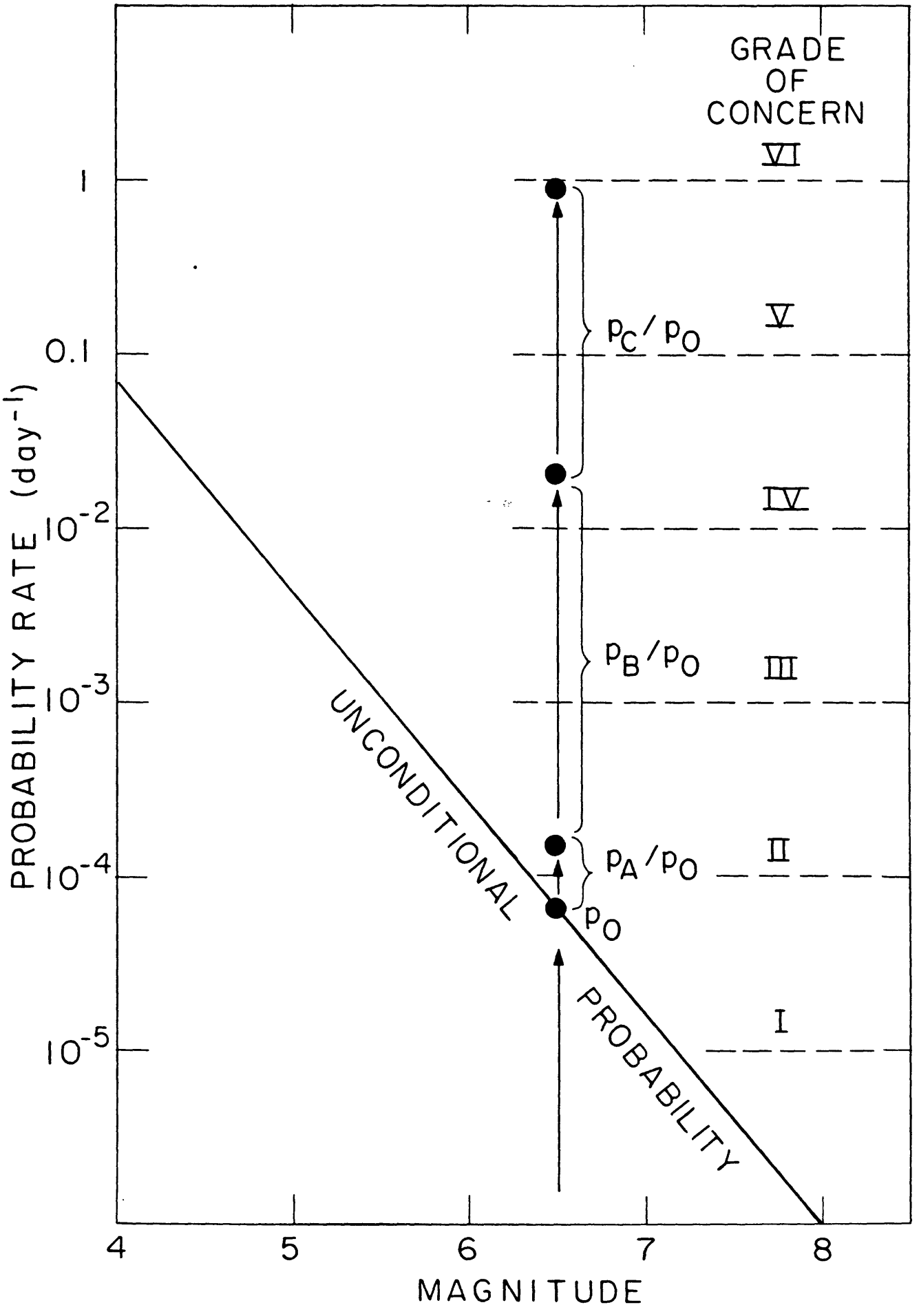
GRADE OF CONCERN
VI
V
IV
III
II
I
1
0.1
10^{-2}
10^{-3}
10^{-4}
10^{-5}
PROBABILITY RATE (day^{-1})
p_C / p_O
p_B / p_O
p_A / p_O
p_O
UNCONDITIONAL PROBABILITY
4
5
6
7
8
MAGNITUDE

IG 4

THREE DIMENSIONAL GEODETIC INVERSION METHOD FOR STRESS MODELLING IN THE LITHOSPHERE

BY

KEIICHIRO IKEDA

B.S. University of Tokyo (1974)
M. Eng. University of Tokyo (1976)

SUBMITTED IN PARTIAL FULFILLMENT OF THE REQUIREMENT OF
THE DEGREE OF
MASTER OF SCIENCE

AT THE

MASSACHUSETTS INSTITUTE OF TECHNOLOGY

January 1980

Signature of Author: _____
Department of Earth and Planetary Sciences
January 18, 1980

Certified by: _____
Keiiti Aki
Thesis Supervisor

Accepted by: _____
Theodore R. Madden
Chairman, Departmental Graduate Committee

THREE DIMENSIONAL GEODETIC INVERSION METHOD FOR STRESS MODELLING IN THE LITHOSPHERE

by

KEIICHIRO IKEDA

Submitted to the Department of Earth and Planetary Sciences on January 18, 1980 in partial fulfillment of the requirement for the Degree of Master of Science in Earth and Planetary Sciences.

ABSTRACT

The goal of the present project is to determine the distribution of incremental stress inside the earth under a seismic region as a basis for quantitative studies of stress-induced earthquake precursors. We formulated an inverse problem for incremental stress in the earth to be determined from three-component displacements observed on the free surface. A body was cut out of the earth under the surface at which displacements are known from geodetic measurements.

A special finite-element method is designed to give a unique determination of stress in the interior of the volume from known surface displacements and the free surface condition. The scheme was successfully tested using artificial data for a point source buried in a homogeneous half-space. We are currently applying it to the actual data from southern California geodimeter network and levelling data during the Palmdale uplift episode. A preliminary result indicates that the state of stress at the depth of a few km can be considerably different from the horizontal stress measured on the surface. The estimated incremental stress shows an encouraging agreement with observations on geomagnetic field and earthquake swarm activities.

Thesis Supervisor: Dr. Keiiti Aki
Title: Professor of Earth and Planetary Sciences

Acknowledgements

I would like to express my sincere gratitude to Professor Keiiti Aki for his guidance and advice throughout the course of this research. I also wish to thank Judy Roos and Dorothy Frank for their assistance in the editing and the typing of the manuscript.

This research was supported by U.S. Geological Survey under contract number 14-08-0001-18205.

List of Contents

List of Figures and Tables

Chapter 1. INTRODUCTION

A precise knowledge of the state of stress in the lithosphere in a seismically active region is desirable since the stress is believed to be the cause of an earthquake.

Many studies have been done to infer the state of stress in the lithosphere. Laboratory studies suggest high shear stress up to 2 kb along the San Andreas fault (Stesky and Brace, 1973, Stesky, 1975), while heat flow studies give low upper limit around 250 bar for possible shear stress there (Brune et al., 1969, Lachenbruch and Sass, 1973). This low shear stress is consistent with the value suggested from the studies of driving force for plate tectonics (Forsyth and Uyeda, 1975, Richardson and Solomon, 1977, Richardson, 1978), and seismic studies on stress drop (Aki, 1966, Wyss, 1970, Wyss and Molnar, 1972), although recent discussion on plate tectonics and earthquake stress-drop (Hanks, 1977) suggest high shear stress of the order of a kilobar.

The lack of agreements among these studies show a fundamental difficulty to know the state of stress in the lithosphere precisely. On the other hand the stress increment in the lithosphere may be easier to estimate than absolute stress since repeated geodetic measurements can give the incremental displacements at the surface.

The incremental stress may be related to earthquake precursors in many ways. Sassa and Nishimura (1956) reported rapid tilt changes in which so-called S-shaped changes in

the tilt-vector diagram were observed to occur a few hours prior to the Nanki earthquake of 1950. The magnitude of tilt was of the order of 0.1" at a distance of 100 km from the epicenter. They observed similar tilt changes prior to some other earthquakes. There have been many precursory anomalous changes in land level such as reported for the Niigata earthquake of 1964 (Danbara, 1973). Castle et al. (1974) studied levelling data near San Fernando and found that anomalous level changes with maximum value of 200 mm had taken place in a few years preceding the San Fernando earthquake of 1971. An aseismic creep along the fault at depth or a dilatancy are considered as causing these land deformations prior to earthquakes though exact mechanism is not known (Wyss, 1977; Thatcher, 1976). These land deformations are believed to be one of the most promising precursors for earthquakes because they have been frequently observed prior to many shallow earthquakes (Rikitake, 1975, 1976).

On the other hand, other precursors such as changes in V_p/V_s, resistivity, geomagnetic field are still under debate although they are also quite promising precursors, especially in view of the dilatancy-diffusion hypothesis (Nur, 1969). After Semenov (1969) observed that the ratios of travel times of S and P waves significantly varied prior to earthquakes in Russia, this has been followed by both verifications and contradictions. For example Whitcomb

et al. (1973) reported 10% change in V_p/V_s over the three years prior to the San Fernando earthquake of 1971 and Stewart (1973) showed a V_p decrease by 20% prior to the Pt. Mugu earthquake of 1973 while no change in V_p/V_s was observed in the Bear Valley earthquake of 1972 (Bakun et al., 1973). Bakun et al. attributed their negative results to the stress level at shallow depths which might be too low for dilatancy to take place. The laboratory experiments showed that volumetric strain necessary to explain the observed large V_p/V_s change was much greater than the stress level expected in the Bear Valley (Hadley, 1975).

Electrical resistivity change up to 24% was observed two months before the Bear Valley earthquake of 1972 by Mazzella and Morrison (1974). Laboratory experiments showed dramatic changes in the electrical properties of rock prior to failure (Brace and Orange, 1978a) in agreement with some field observations. On the other hand, a theoretical study of resistivity change based on a model of strike slip fault showed that the observed resistivity changes were several orders of magnitude larger than predicted for the expected stress change.

The geomagnetic change due to the piezomagnetic effect of rock under incremental stress is known to be very effective as a procursor as well as an indirect way to estimate the incremental stress at depth. Theoretical

study shows, assuming optimum material constants such as high magnetization and high stress sensitivity, the stress change caused by slip on a fault at shallow depth is sufficient to produce the geomagnetic field change observed on the surface (Johnston, 1978, Johnston et al., 1979).

The discrepancy between the theory on the stress-induced precursory phenomena based on laboratory data and precursory phenomena observed in the field may be attributed to the scale effect of specimen as well as the state of incremental stress at depth. The purpose of this thesis work is to develop an inversion method based on the finite element method using geodetic data on three-component displacement obtained at the earth's surface for finding the distribution of incremental stress at depths in a seismically active region. Such a distribution of incremental stress in the lithosphere will be useful together with laboratory observation on rock properties (Brace and Orange, 1968a, 1968b, Nur, 1969, Brace, 1972, Hadley, 1975, Stesky, 1975, Johnston, 1978) to find the cause of precursory phenomena. We applied the inversion method to the Palmdale uplift, southern California and obtained some preliminary encouraging results.

Chapter 2. FINITE ELEMENT METHOD

1. General Formulation

In order to develop a finite element scheme for elasticity problems, we have to decide the type of generalized coordinate and the order of interpolation function as well as the shape of an element. If we use nodal displacements as a generalized coordinate, we have so-called finite element displacement method based on minimum potential energy principle. If we choose stress as a generalized coordinate, we have so-called conjugate finite element method based on minimum complementary energy principle. If we use displacements together with stress as a generalized coordinate, we have so-called hybrid finite element method. The last one seems most adequate for applying to our inversion, but the theory as well as numerical technique of this method is still not well established, and therefore we need further study for applying it to our inverse problem (Tong and Rosett, 1978, Oden and Reddy, 1976). Since fairly well established theory and numerical technique exist for the displacement finite element method, we shall formulate our finite element scheme and inversion scheme according to this method.

We shall define displacements within an element in a matrix form as

$$[U] = \begin{bmatrix} u \\ v \\ w \end{bmatrix} \tag{1}$$

where u,v,w are displacements in x,y,z direction. This displacement vector is presented in terms of interpolation functions and the generalized coordinate, i.e., nodal displacements in the displacement based finite element method. In matrix, they are:

$$[U] = [D(x,y,z)]\ [U^n] \tag{2}$$

where [U] is displacement vector, defined before, D(x,y,z) is interpolation matrix which gives [U] at an arbitrary point from the nodal displacement matrix $[U^n]$. $[U^n]$ can be written explicitly as

$$[U^n]^T = [u_1 v_1 w_1\ u_2 v_2 w_2 \ldots u_k v_k w_k] \tag{3}$$

where u_i, v_i, w_i are x,y,z components of displacement vector at ith node. The value of k depends on the degree of interpolation function and shape of an element, and k=20 if parabolic interpolation is used in a hexahedral element. T denotes transpose of a matrix.

We shall define strain tensor [e], traction vector [T], force vector [F], and elasticity matrix [C]. They are:

$$[e]^T = [\varepsilon_{xx}\ \varepsilon_{yy}\ \varepsilon_{zz}\ \gamma_{xy}\ \gamma_{xz}\ \gamma_{yz}] \tag{4}$$

$$[T]^T = [T_x\ T_y\ T_z] \tag{5}$$

$$[F]^T = [F_x\ F_y\ F_z] \tag{6}$$

where ε_{ij}, γ_{ij} are six components of a strain tensor in which we use engineering shear strain. T_i or F_i (i = x,y,z) are the x,y,z components of surface traction vector and force vector. The elasticity matrix is in case of isotropic material,

$$[C] = \begin{bmatrix} \lambda+2\mu & \lambda & \lambda & o & o & o \\ \lambda & \lambda+2\mu & \lambda & o & o & o \\ \lambda & \lambda & \lambda+2\mu & o & o & o \\ o & o & o & \mu & o & o \\ o & o & o & o & \mu & o \\ o & o & o & o & o & \mu \end{bmatrix} \tag{7}$$

where λ, μ are Lame's constants.

We can define strain matrix [e] in terms of strain-transformation matrix [E] and nodal displacement matrix. This is:

$$[e] = [E]\ [U^n] \tag{8}$$

$$[E] = \begin{bmatrix} \frac{\partial}{\partial x}[D] & o & o \\ o & \frac{\partial}{\partial y}[D] & o \\ o & o & \frac{\partial}{\partial z}[D] \\ \frac{\partial}{\partial y}[D] & \frac{\partial}{\partial x}[D] & o \\ \frac{\partial}{\partial z}[D] & o & \frac{\partial}{\partial x}[D] \\ o & \frac{\partial}{\partial z}[D] & \frac{\partial}{\partial y}[D] \end{bmatrix} \tag{9}$$

where [D] was defined in [2]. The total potential energy of an elastic body can be presented as (Tong and Rosett, 1978)

$$\pi = \int_v \frac{1}{2}[e]^T[C][e]dv - \int_v [U]^T[F]dv - \int_v [U]^T[T]ds \qquad (10)$$

where π is total potential energy, s is boundary surface and integration covers whole volume of a body. This is the quantity to be minimized.

The above potential energy can be expressed as a sum of energy for each element, i.e.,

$$\pi = \sum_{n=1}^{m} \pi_n \qquad (11)$$

where m is the total number of elements. Substitution of eq. (8) into eq. (10) yields

$$\pi_n = \frac{1}{2}[U^n]_n^T[K]_n[U^n]_n - [U^n]_n^T[R]_n \qquad (12)$$

where $[\ ]_n$ represents nth element, and $[K]_n$ and $[R]_n$ are element stiffness matrix and element load matrix. Explicitly they are

$$[K]_n = \int_v [E]_n^T[C][E]_n dv \qquad (13)$$

and

$$[R]_n = \int_v [D]^T[F]dv + \int_s [D]^T[T]ds\,. \qquad (14)$$

Making the potential energy in each element, presented by eq. (12) stationary with respect to generalized coordinate, i.e., nodal displacement, we have a linear equation for each element as:

$$[K]_n[U^n]_n = [R]_n . \qquad (15)$$

2. Isoparametric element

The choice of an interpolation function is an important part of the finite element method and depends on the type of element to be used and on desired accuracy. The concept of isoparametric element developed by Zienkiewicz, and his associate [Zienkiewicz,1972] is one of the most versatile interpolations because of its flexibility.

The basic concept in the isoparametric element formulation is to express the element coordinates and its displacements by the same interpolation function using the natural coordinate system of the element. The coordinate interpolations in a three-dimensional element are as:

$$x = \sum_{i=1}^{\ell} h_i x_i$$

$$y = \sum_{i=1}^{\ell} h_i y_i \qquad (16)$$

$$z = \sum_{i=1}^{\ell} h_i z_i$$

where x,y,z are the coordinates at any point of the element and x_i, y_i, z_i $(i = 1,\ell)$ are the coordinates of the ith node in the element, and ℓ denotes the total number of nodes in the element.

The unknown quantities in eq. (16) i.e. the interpolation function h_i, have the fundamental property that its value in the natural coordinate system is unity at the ith node and is zero at all other nodes. Using this condition the interpolation function h_i corresponding to a specific nodal point configuration can be derived. In the case of our three-dimensional 20 nodes parabolic interpolation in hexahedral element, these interpolation functions are given by the following equations.

$$h_1 = \frac{1}{8}(1+r)(1+s)(1+t)(r+s+t-z)$$

$$h_2 = \frac{1}{8}(1-r)(1+s)(1+t)(-r+s+t-z)$$

$$h_3 = \frac{1}{8}(1-r)(1-s)(1+t)(-r-s+t+z)$$

$$h_4 = \frac{1}{8}(1+r)(1-s)(1+t)(r-s+t-z)$$

$$h_5 = \frac{1}{8}(1+r)(1+s)(1-t)(r+s-t-z)$$

$$h_6 = \frac{1}{8}(1-r)(1+s)(1-t)(-r+s-t-z)$$

$$h_7 = \frac{1}{8}(1-r)(1-s)(1-t)(-r-s-t-z) \qquad (17)$$

$$h_8 = \frac{1}{8}(1+r)(1-s)(1-t)(r-s-t-z)$$

$$h_9 = \frac{1}{4}(1-r^2)(1+s)(1+t)$$

$$h_{10} = \frac{1}{4}(1-r)(1-s^2)(1+t)$$

$$h_{11} = \frac{1}{4}(1-r^2)(1-s)(1+t)$$

$$h_{12} = \frac{1}{4}(1+r)(1-s^2)(1+t)$$

$$h_{13} = \frac{1}{4}(1-r^2)(1+s)(1-t)$$

$$h_{14} = \frac{1}{4}(1-r)(1-s^2)(1-t)$$

$$h_{15} = \frac{1}{4}(1-r^2)(1-s)(1-t)$$

$$h_{16} = \frac{1}{4}(1+r)(1-s^2)(1-t)$$

$$h_{17} = \frac{1}{4}(1+r)(1+s)(1-t^2)$$

$$h_{18} = \frac{1}{4}(1-r)(1+s)(1-t^2)$$

$$h_{19} = \frac{1}{4}(1-r)(1-s)(1-t^2)$$

$$h_{20} = \frac{1}{4}(1+r)(1-s)(1-t^2) \qquad (17) \text{ (cont'd)}$$

where r,s,t are natural coordinate whose values range from -1 to 1 as shown in Fig. 1.

The displacements in an element are interpolated by the same relation as the coordinates in the isoparametric interpolation, i.e., for displacement at any point of the element, we have:

$$u = \sum_{i=1}^{\ell} h_i u_i$$

$$v = \sum_{i=1}^{\ell} h_i v_i \qquad (18)$$

$$w_i = \sum_{i=1}^{\ell} h_i w_i$$

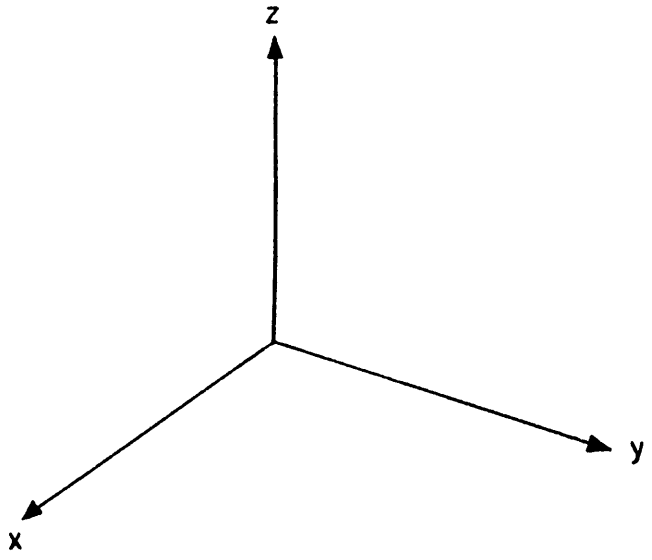

LOCAL COORDINATE SYSTEM

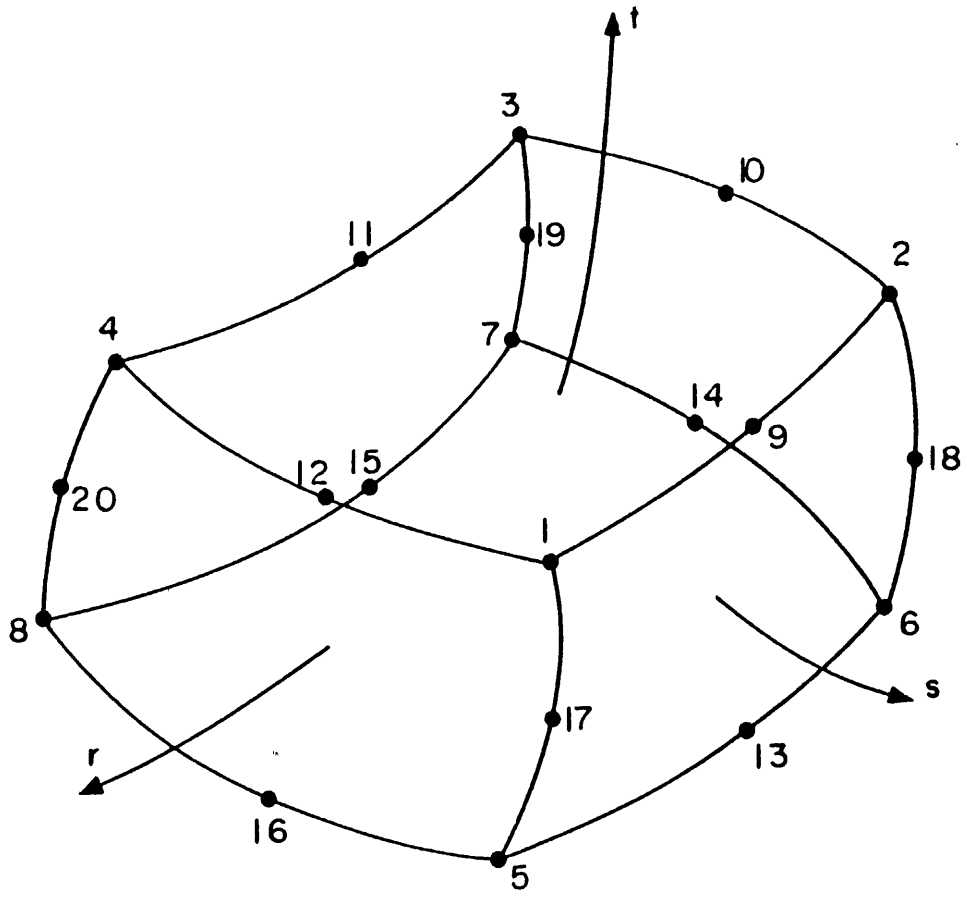

NATURAL COORDINATE SYSTEM

Fig. 1 Isoparametric 20 nodes element

where u,v,w are displacement component at any point in the element and u_i, v_i, w_i $(i = 1, \ell)$ are these components of nodal displacements of the element.

In order to evaluate the stiffness matrix [K] of an element, we need to calculate the strain-transformation matrix [E]. Since the element displacements are presented in the natural coordinate system as shown in eq. (17) we must relate the derivatives in the local x,y,z coordinates to the derivatives in the r,s,t natural coordinates. Using a chain rule for partial derivatives, the relations are:

$$\frac{\partial}{\partial x} = \frac{\partial}{\partial r}\frac{\partial r}{\partial x} + \frac{\partial}{\partial s}\frac{\partial s}{\partial x} + \frac{\partial}{\partial t}\frac{\partial t}{\partial x}$$

$$\frac{\partial}{\partial y} = \frac{\partial}{\partial r}\frac{\partial r}{\partial y} + \frac{\partial}{\partial s}\frac{\partial s}{\partial y} + \frac{\partial}{\partial t}\frac{\partial t}{\partial y} \qquad (19)$$

$$\frac{\partial}{\partial z} = \frac{\partial}{\partial r}\frac{\partial r}{\partial x} + \frac{\partial}{\partial s}\frac{\partial s}{\partial z} + \frac{\partial}{\partial t}\frac{\partial t}{\partial z} .$$

These equations show that we need the explicit inverse relationship between x,y,z and s,r,t, i.e. we need to know the functions

$$r = f_1(x,y,z)$$

$$s = f_2(x,y,z) \tag{20}$$

$$t = f_3(x,y,z)$$

which are generally difficult to obtain explicitly and it is natural recourse to use a numerical procedure.

The relation between the derivatives in the r,s,t coordinate system and derivatives in the x,y,z coordinates system can also be written using the chain rule:

$$\frac{\partial}{\partial r} = \frac{\partial}{\partial x}\frac{\partial x}{\partial r} + \frac{\partial}{\partial y}\frac{\partial y}{\partial r} + \frac{\partial}{\partial z}\frac{\partial z}{\partial r}$$

$$\frac{\partial}{\partial s} = \frac{\partial}{\partial x}\frac{\partial x}{\partial s} + \frac{\partial}{\partial y}\frac{\partial y}{\partial s} + \frac{\partial}{\partial z}\frac{\partial z}{\partial s} \tag{21}$$

$$\frac{\partial}{\partial t} = \frac{\partial}{\partial x}\frac{\partial x}{\partial t} + \frac{\partial}{\partial y}\frac{\partial y}{\partial t} + \frac{\partial}{\partial z}\frac{\partial z}{\partial t}$$

in matrix form we have

$$\frac{\partial}{\partial [r]} = [J] \frac{\partial}{\partial [x]} \tag{22}$$

where [J] is the Jacobian operator matrix i.e.

$$[J] = \begin{bmatrix} \frac{\partial x}{\partial r} & \frac{\partial y}{\partial r} & \frac{\partial z}{\partial r} \\ \frac{\partial x}{\partial s} & \frac{\partial y}{\partial s} & \frac{\partial z}{\partial s} \\ \frac{\partial x}{\partial t} & \frac{\partial y}{\partial t} & \frac{\partial z}{\partial t} \end{bmatrix} \tag{23}$$

Since we can evaluate Jacobian operator matrix [J] explicitly using eq. (17), we can get the inverse relationship between derivatives in two coordinate systems as

$$\frac{\partial}{\partial [x]} = [J]^{-1} \frac{\partial}{\partial [r]} \tag{24}$$

provided that matrix [J] is non-singular. This condition is satisfied if the mapping between these two coordinate systems, i.e. eq. (20) is one to one.

Using eq. (18) and eq. (24) we evaluate derivatives needed to construct the strain transformation matrix [E].

The element stiffness matrix corresponding to the local degree of freedom is derived as

$$[K] = \int_v [E]^T [C] [E] dv \tag{25}$$

where [C] is elasticity matrix defined before.

Since strain-transformation matrix [E] is a function of the natural coordinate r,s,t, the volume integral dv should be written in terms of this coordinate system. That is:

$$dv = \det [J] \, drdsdt \tag{26}$$

where det denotes determinant of Jacobian operator matrix. Since explicit solution for $[J]^{-1}$ seldom exists, we must use numerical integration to evaluate the volume integral in eq. (25). We have

$$[K] = \sum_{i=1}^{m} \sum_{j=1}^{m} \sum_{k=1}^{m} \alpha_i \alpha_j \alpha_k \, [E]^T_{ijk} [C] [E]_{ijk} \det[J]_{ijk} \tag{27}$$

where $[\ ]_{ijk}$ represents a quantity evaluated at a point r_i, s_j, t_k, m is the total number of sampling points for numerical integration, and α_i, α_j, α_k are weight at these points. The sampling points and weighting factors depend on the integration scheme to be used. We used Gauss-Legendre quadrature method, for which the sampling points and weights are shown in Fig. 2 and Table 1.

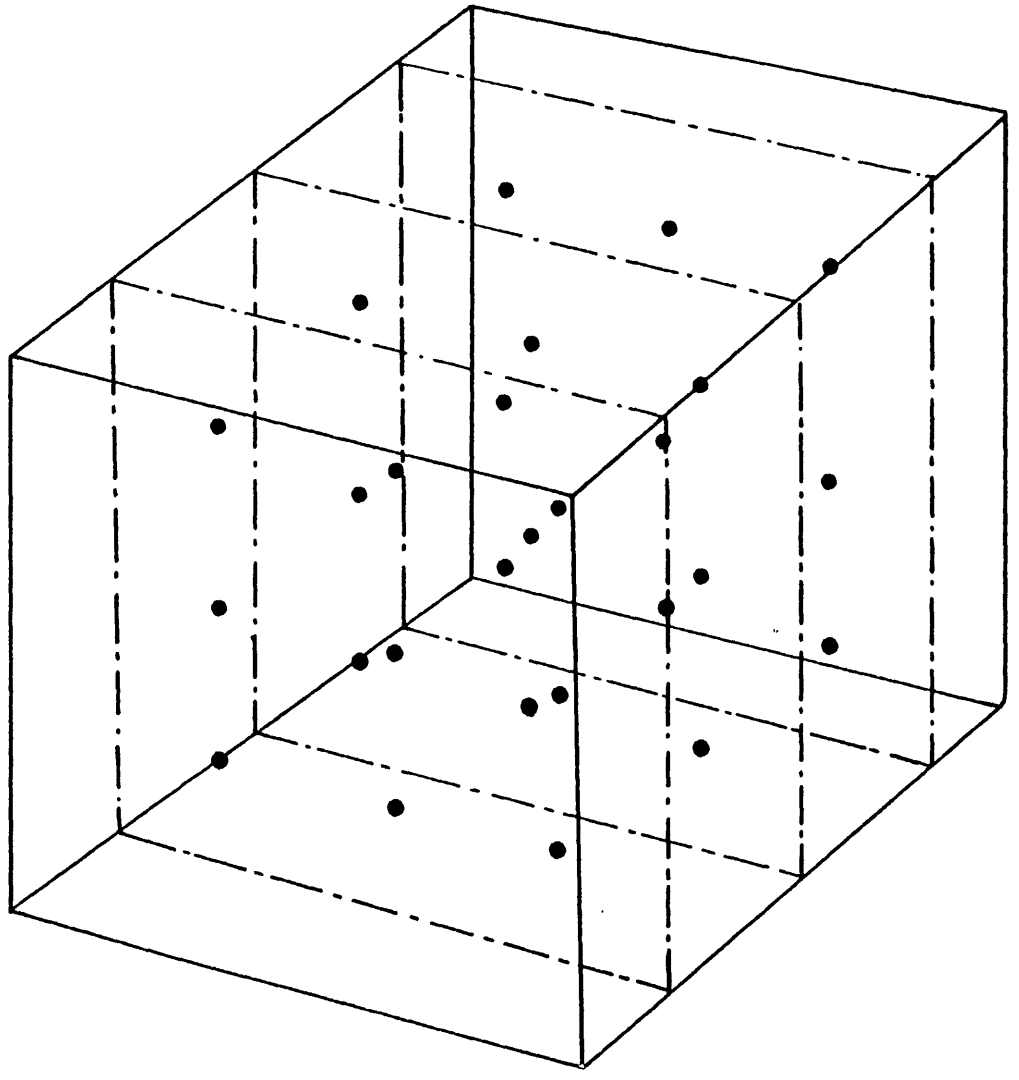

Fig. 2 Sampling points for numerical integration

3. Assembling Matrix for the Whole Body

The final stage of finite element method is to assemble $[K]_n$ matrix and $[R]_n$ matrix in each element to global matrix [K] and [R] to attain the equilibrium condition of the whole body. Since matrix [K] is a transfer matrix which represents contributions of each component of nodal displacement matrix $[U_n]$ to components of the load matrix [R], this is nothing but a summation and re-numbering of matrix for each element.

For example, if we re-number the ith node of the ℓth element as the mth node of the global system, and the jth node of ℓth element as the nth node of the global system, we have

$$[K_{mn}]_g = \sum_{\ell'} [K_{ij}]_{\ell'},$$

$$[R_m]_g = \sum_{\ell'} [R_i]_{\ell'}, \tag{28}$$

$$[R_n]_g = \sum_{\ell'} [R_j]_{\ell'},$$

where $[K_{ij}]$ is ij-component of stiffness matrix [K] and subscript g represents global matrix and the summation is taken over elements ℓ' sharing the particular node. After assembling whole element matrix using eq. (28) we have linear equations to be solved, i.e. we have

$$[K]\ [U] = [R]. \tag{29}$$

Chapter 3. GEODETIC INVERSION SCHEME

1. General Theory

The use of the finite element method in inverse problem, especially in parameter estimation problem, has been studied in many fields in science and engineering during the last decade. In geophysics some inversions based on the finite element method were studied. Most of them used the observed surface displacements associated with an earthquake to estimate fault parameters such as slip vector (Jangle and Frazar, 1973), visco-elastic constant of surrounding material (Smith, 1973), and stress drop (McCowan et al., 1977) with specified boundary conditions.

In our geodetic inverse problem, we want to calculate the stress and displacements inside the earth's crust without specifying anything on the internal boundary inside the earth. The only boundary conditions available to us are displacements and free surface condition on the surface boundary. Mathematically this is known as a Cauchy boundary condition for an elliptic equation and in general results in unstable solutions for the entire region (Morse and Feshbach, 1953).

Suppose that the problem is reduced to a linear operator equation $Lx = y$, where x is the desired solution. When this problem is ill-posed, there are basically two methods for remedy (Lunz, 1979). One is known as the regularization

method in which we use a priori choice of the space of the permitted solution to avoid instability by modifying the functional to be minimized. For example, we minimize

$$J(x) = ||Lx - y|| + \alpha\psi(x) \tag{30}$$

instead of solving the equation $Lx = y$ directly where $||\ ||$ denotes an appropriate norm, $\alpha > 0$ and Ψ is a functional defined on a solution space. This method is equivalent to the damped least squares (Levenbergs, 1944), the stochastic inverse (Franklin, 1970) and the generalized inverse (Wiggins, 1972) depending on the property of ψ and the norm used.

Another way to solve this ill-posed operator equation is the so-called expansion method. In this method we choose finite dimensional space X_n and look for a solution in this space. If $[\psi_{in}]$ denotes a basis for X_n, we look for a solution of the form

$$x_n = \sum_{i=1}^{h} \alpha_i \psi_{in} \tag{31}$$

such that

$$Lx_n \simeq y. \tag{32}$$

The latter method seems more convenient than the former if we use the finite element method to discretize the operator L, because of a large amount of computation for calculating the norm. On the other hand, in the expansion method we can choose any solution space so that accuracy and economic factor can be satisfied at the same time. This can be attained by appropriate choice of expansion by eq. (31) with specific mesh configurations which assure the same number of knowns and unknowns.

2. Inversion Scheme

Using the finite element method derived in a previous chapter, we can have discretized form of the operator equation Lx = y. Written explicitly, this equation is in a partitioned form,

$$\begin{array}{c} \\ k \\ \ell \\ m \\ n \end{array} \begin{array}{c} \begin{array}{cccc} k & \ell & m & n \end{array} \\ \begin{bmatrix} K_{11} & K_{12} & K_{13} & K_{14} \\ K_{21} & K_{22} & K_{23} & K_{24} \\ K_{31} & K_{32} & K_{33} & K_{34} \\ K_{41} & K_{42} & K_{43} & K_{44} \end{bmatrix} \end{array} \begin{bmatrix} U_1^* \\ U_2^* \\ U_3 \\ U_4 \end{bmatrix} = \begin{bmatrix} R_1^* \\ R_2 \\ R_3^* \\ R_4 \end{bmatrix} \qquad (33)$$

where K_{11} is a (k x k) matrix. K_{12} is a (k x ℓ) matrix, K_{13} is a k x m matrix, K_{14} is a (k x n) matrix, K_{22} is a (ℓ x ℓ) matrix, K_{23} is a (ℓ x m) matrix, K_{24} is a (ℓ x n) matrix, K_{33} is a (m x m) matrix, K_{34} is a (m x n) matrix, K_{44} is a (n x n) matrix, and K_{21}, K_{31}, K_{32}, K_{41}, K_{42}, K_{43} are transpose of K_{12}, K_{13}, K_{23}, K_{14}, K_{24}, K_{34}, respectively. U_1^* is a (k x 1) matrix, U_2^* is a (ℓ x 1) matrix, U_3 is a (m x 1) matrix. U_4 is a (n x 1) matrix, R_1^* is a (k x 1) matrix, R_2 is a (ℓ x 1) matrix, R_3^* is a (m x 1) matrix, and R_4 is a (n x 1) matrix, and a star represents that elements of that matrix are known quantities. These known quantities are observed three components on the surface, stress free condition on the surface and the force balance condition inside the boundaries. The latter two conditions give zero values to the load matrix [R].

The above matrix equation can be modified to give a more convenient form to analyze, that is:

$$\begin{bmatrix} K_{13} & K_{14} & 0 & 0 \\ K_{23} & K_{24} & -I & 0 \\ K_{33} & K_{34} & 0 & 0 \\ K_{43} & K_{44} & 0 & -I \end{bmatrix} \begin{bmatrix} U_3 \\ U_4 \\ R_2 \\ R_4 \end{bmatrix} = \begin{bmatrix} -K_{11} & -K_{12} & I & 0 \\ -K_{21} & -K_{22} & 0 & 0 \\ -K_{31} & -K_{32} & 0 & I \\ -K_{41} & -K_{42} & 0 & 0 \end{bmatrix} \begin{bmatrix} U_1^* \\ U_2^* \\ R_1^* \\ R_3^* \end{bmatrix} \qquad (34)$$

where [I] denotes a unit matrix of appropriate order. As can be seen from the above equation, our problem is overdetermined if $\ell + m + 2n <$ rank of $L_n = k + \ell + m + n$ underdetermined if $k + \ell + m + n <$ rank of $L_n = \ell + m + 2n$, and ill-posed if rank of $L_n < k + \ell + m + n$ and rank of $L_n < \ell + m + 2n$, and well-posed if rank of $L_n = k + \ell + m + n = \ell + m + 2n$, where L_n represents the matrix on L.H.S. of eq. (34).

We need, therefore, to have rank of $L_n = k + \ell + m + n = \ell + m + 2n$ or $k = n$. This last condition shows that the number of surface nodes where we have both stress free condition and displacements observation (this excludes the boundary nodes on the surface) need to be the same as the number of boundary nodes inside the earth where we know neither tractions nor displacements. To attain this condition, we need to choose a special family of the finite element mesh configuration. This is mathematically equivalent to specify the base of solution space in expansion method as was shown in eq. (31).

The simplest mesh configuration which satisfies the condition is shown in Fig. 3. This mesh configuration has a certain advantage that it allows us to increase the order of interpolation function without changing the whole configuration. This is shown in Fig. 4. The values of k, ℓ, m, n in cases of 8 nodes of interpolation and 20-nodes interpolation are presented in Table 2.

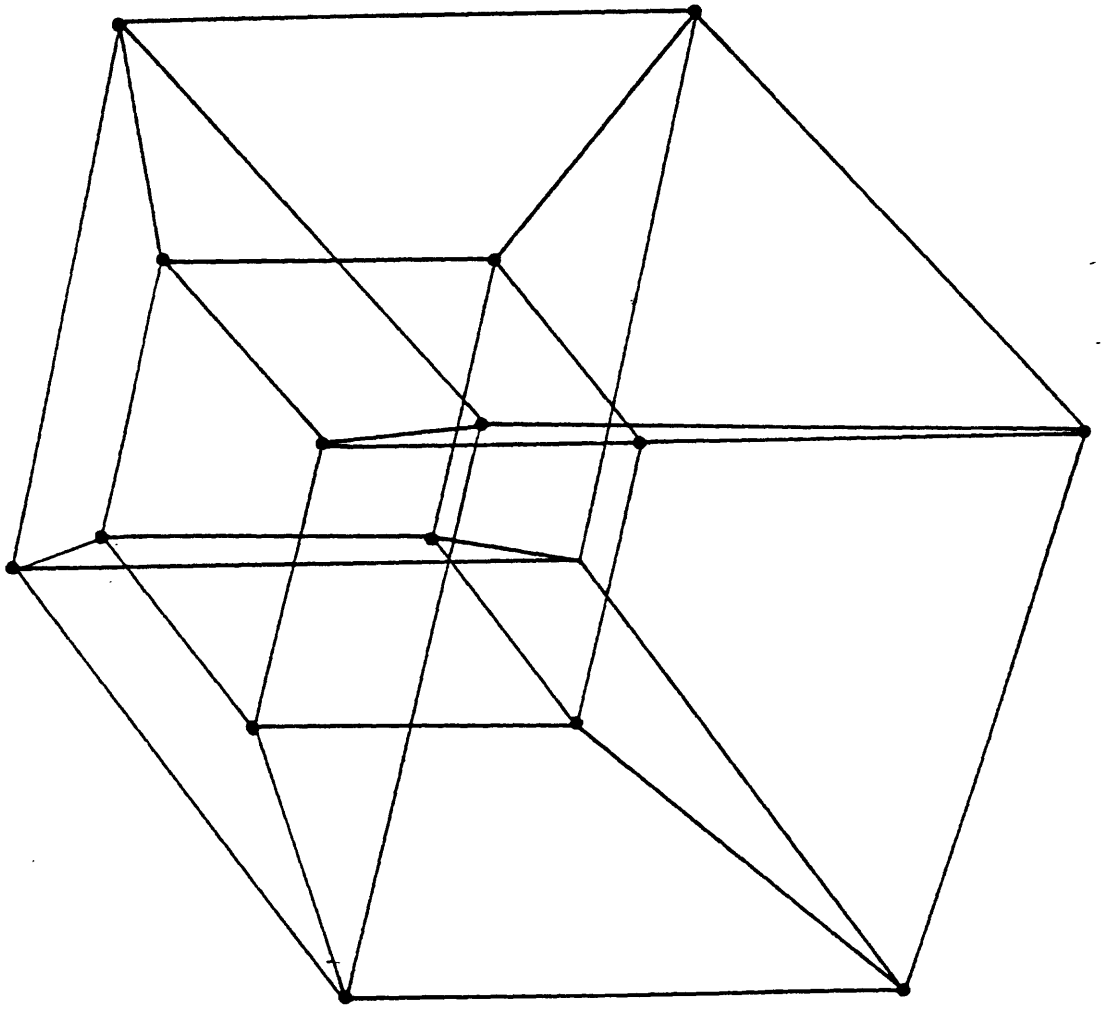

Fig. 3 Mesh configuration by 8 nodes element

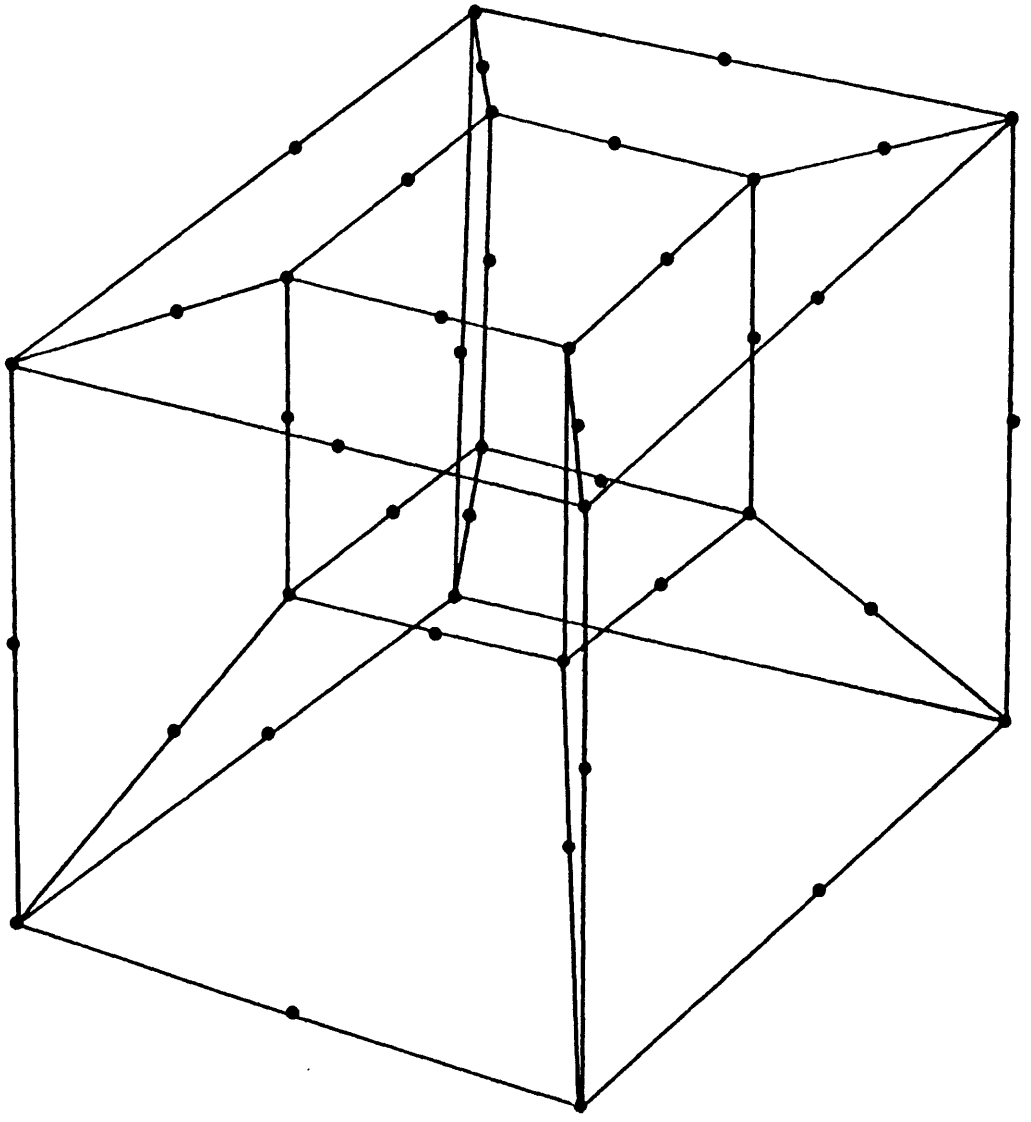

Fig. 4 Mesh configuration by 20 nodes element - I

Since in the parabolic interpolation using 20 nodes in an element, the highest term is square, we expect that a strain change in the element is at most linear. Thus if we have to approximate a rapidly changing stress field inside a block, the block must be further subdivided. We can improve the accuracy of solution by subdividing the inner block in Fig. 4 into 7 small blocks as shown in Fig. 5. The values of k, ℓ, m, n are also shown in Table 2. It is clear that the condition k = n still holds after this subdivision.

3. Error Analysis

There are two sources of error in this finite element inversion scheme. The first one is inherent to the property of matrix L_n in eq. (34). As shown earlier, for the problem to be well-posed it is necessary to have rank of $L_n = k + \ell + m + n$ in addition to the condition k = n. This condition is satisfied, in principle, by the family of mesh configuration as shown previously, but numerically the system can be near rank-deficient.

To measure the well-posedness of the problem, it is convenient to use a condition number K defined as

$$K = \frac{\max \; || \; \lambda \; ||}{\min \; || \; \lambda \; ||} \tag{35}$$

where λ is an eigenvalue of matrix L_n.

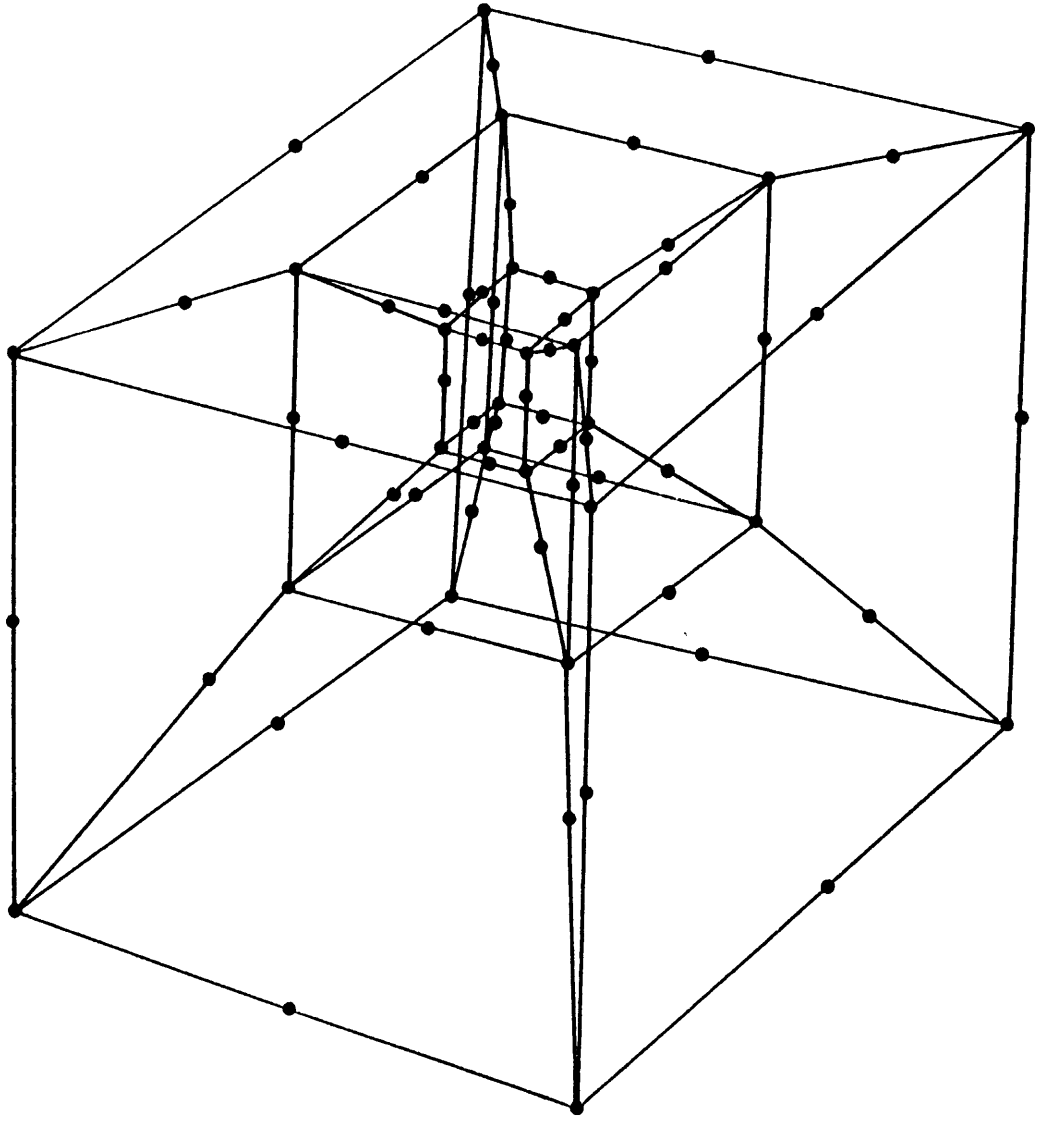

Fig. 5 Mesh configuration by 20 nodes element – II

For the block whose dimension is 10 x 10 x 10 km, condition number around 10^5 to 10^6 depending on the configuration of inner nodes is obtained by calculating the eigenvalue of matrix L_n. Using formula on the relation between the accuracy of fixed point arithmetic and condition number K, (Wilkinson, 1969) i.e.,

$$s \geq t - \log_{10} K \tag{36}$$

where s is the number of digits of precision in the solution and t is the number of digits of arithmetic used in the computer, we can have rough estimate on the truncation error involved in this finite element inversion. Eq. 36 shows that we have 1 digit to 0 digit of accuracies if we use 6-digit arithmetic in the computer. Therefore the use of double precision arithmetic is necessary.

The other source of error in our finite element inversion scheme is the error due to the use of specific mesh configuration with high order interpolation. Since the transformations of local coordinates x,y,z to natural coordinates r,s,t may be non-linear if the element is deformed from a rectangular as in Fig. 4, the error associated with the interpolation function may change considerably.

This situation becomes clear if we choose two-dimensional 8-nodes element as an example. (This element corresponds to a 20-nodes element in three-dimensions). This element is shown in Fig. 6. The transformation between (x,y) and (r,s)

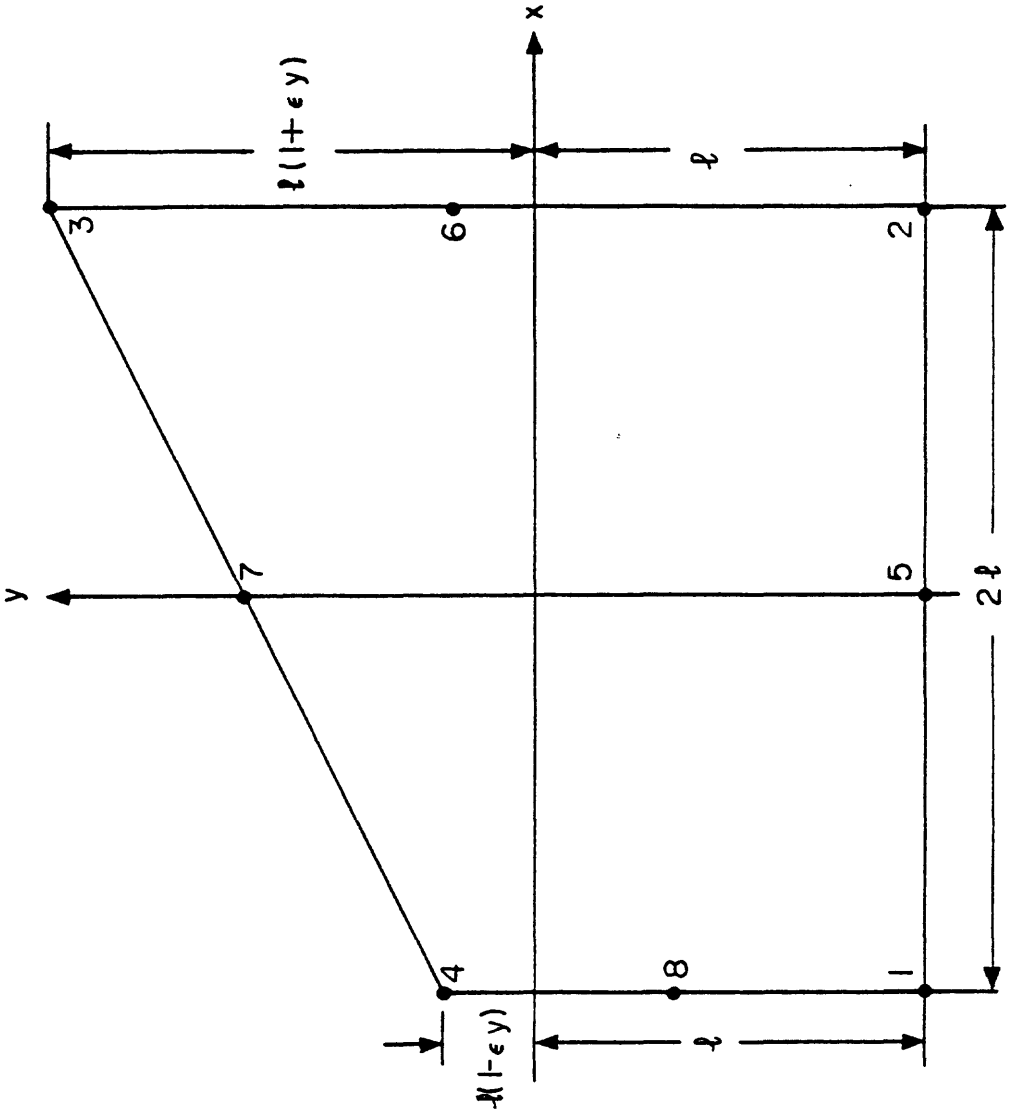

Fig. 6 Two-dimensional 8 nodes element

coordinates are simply,

$$x = \ell r$$

$$y = \ell\{s + \frac{\varepsilon_y}{2} r\ (1 + s)\} \tag{37}$$

where ε_y is the slope of upper edge shown in Fig. 6. For example, consider function $\tilde{u} = y^2$, which have nodal values $\tilde{u}_i = y_i{}^2$. The interpolation formula gives

$$\tilde{u} = \sum_{i=1}^{8} h_i(r,s) y_i^2 \tag{38}$$

where $h_i(r,s)$ is the interpolation function similar to eq. (19) to eq. (38).

Inserting eq. (11) into eq. (12), we obtain

$$\tilde{u} = \sum_{i=1}^{8} h_i(r,s)\,\ell^2[(s_i + \frac{\varepsilon_y}{2} r_i(1 + s_i)]^2$$

$$= \sum_{i=1}^{8} h_i(r,s)\,\ell^2(r_i + \frac{\varepsilon_y}{2} s_i)^2 + \sum_{i=1}^{8} 2h_i(r,s)\,\ell^2(s_i + \frac{\varepsilon_y}{2} r_i)$$

$$r_i s_i \frac{\varepsilon_y}{\ell^2} + \sum_{i=1}^{8} h_i(r,s) + \frac{\ell^2 \varepsilon_y{}^2}{4} r_i^2 s_i^2 \tag{39}$$

Since the order of interpolation function $h_i(r,s)$ is at most cubic in r and s, it is impossible to describe a function which contains a fourth power term in r and s exactly. Since the first two terms on RHS of equation (39) are parabolic and can be completely described, we have

$$u = \ell^2(s + \frac{\varepsilon_y}{2}r)^2 + \varepsilon_y^2(s + \frac{\varepsilon_y}{2}r)rs + \sum_{i=1}^{8} h_i(r,s)\frac{\ell^2}{4}\varepsilon_y^2 r_i^2 s_i^2$$

$$= y^2 + \frac{\ell^2}{4}\varepsilon_y^2 \left(\sum_{i=1}^{8} h_i(r,s) r_i^2 s_i^2 - r^2 s^2\right) \qquad (40)$$

This equation shows that the error depends on ℓ and ε_y and may be very sensitive to the mesh configuration.

The above error analysis gives us only a rough idea of the error involved. An optimum mesh configuration must be found by trial and error, since the complete error analysis for an optimization is too complicated. The mesh configuration shown in Fig. 7 appears to be near optimum for the case of a buried point force model used in our test.

4. Testing With Artificial Data

In order to find the optimal mesh configuration, we used artificial data generated by a buried point force in a homogeneous half-space. Displacements at the free surface, known as Mindlin's solution (Mindlin, 1936), are used as an input to our inverse scheme. The calculated stress and displacements at depths by our inverse scheme are then compared with the true stress and displacement generated by the point force.

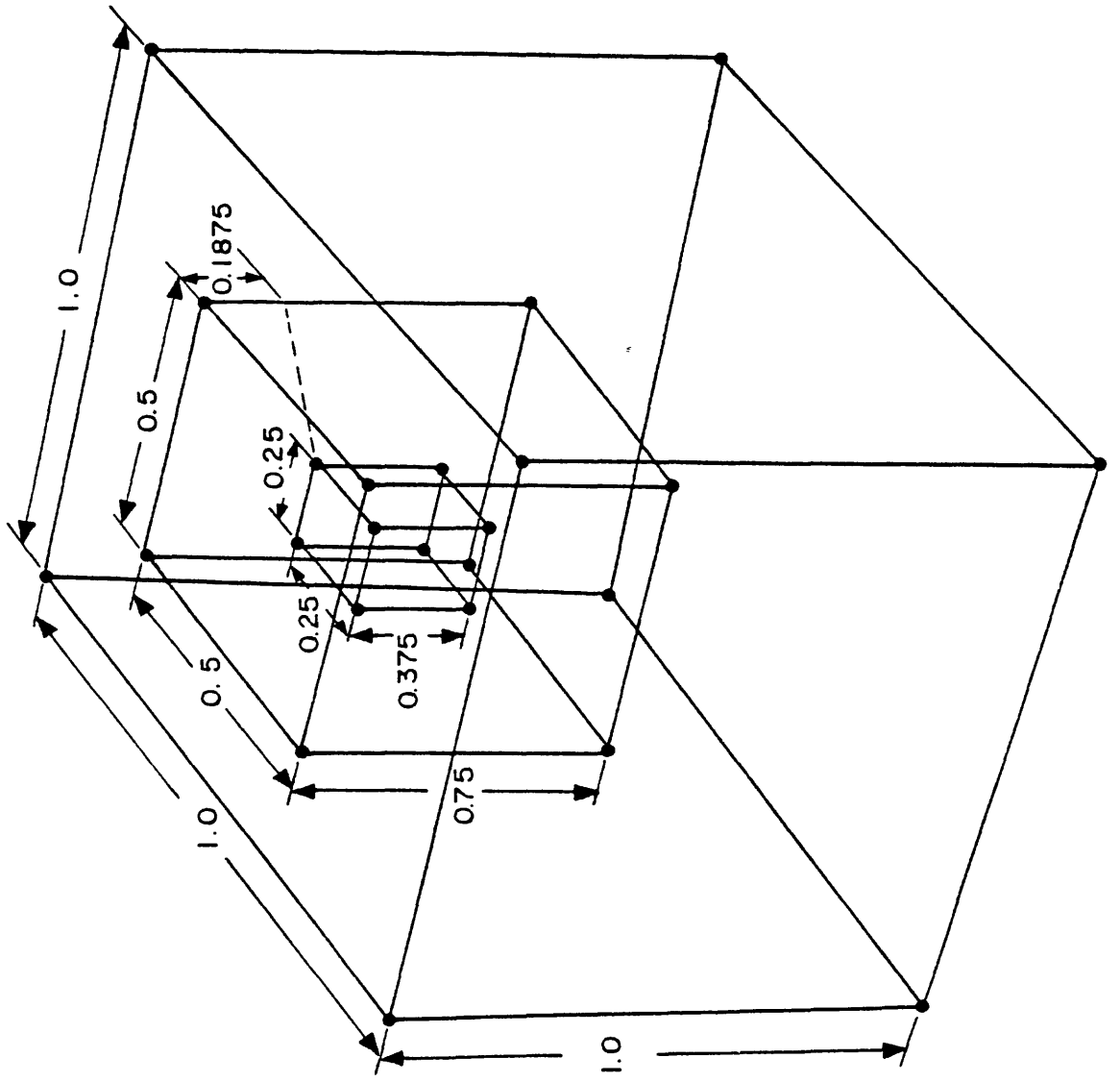

Fig. 7 Optimum mesh configuration

We used the configuration shown in Fig. 5, and the block size (outer boundary) was chosen to be 10 x 10 x 10 km or 20 x 20 x 20 km. The whole block was cut out of the half-space which contains a point force directed upward at depths 15 to 100 km. The horizontal location of block is also varied relative to the point force. An example of block location is depicted in Fig. 8. Figs. 9 and 10 represent the absolute error between the true displacement and stress in the center of each element and those obtained by our inversion scheme. Figs. 11 and 12 show the relative error between the true value and inverted one. These values are shown for various depths of the point source and a fixed horizontal distance (14 km). It is shown that for the point force at the depth of 25 km to 35 km, the accuracy of our inversion scheme is within 5% for displacement and within 30% for stress components. Compared with the sensitivity of error to the change of the depth of point source, the sensitivity to the horizontal distance is small.

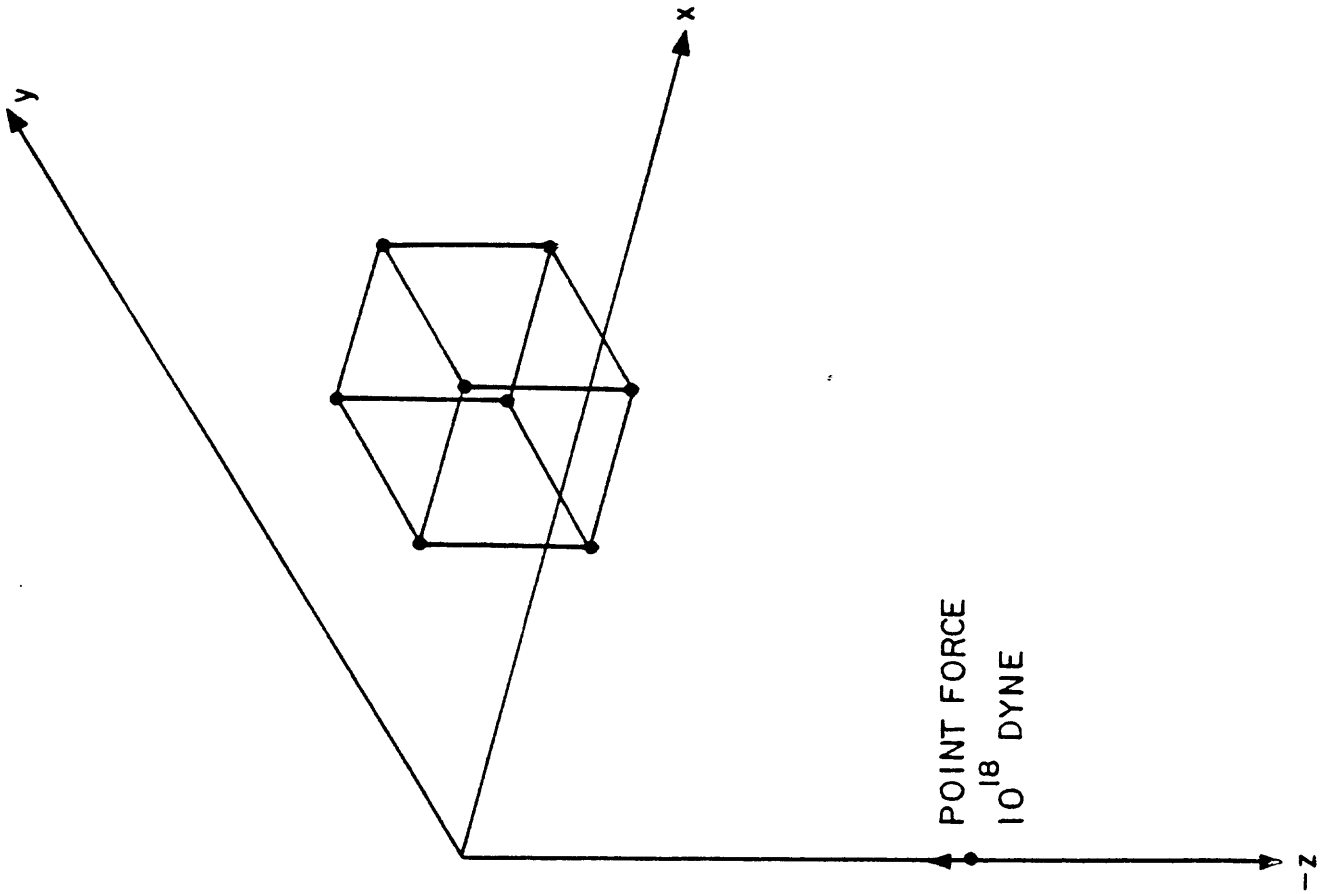

Fig. 8 Model for artificial data

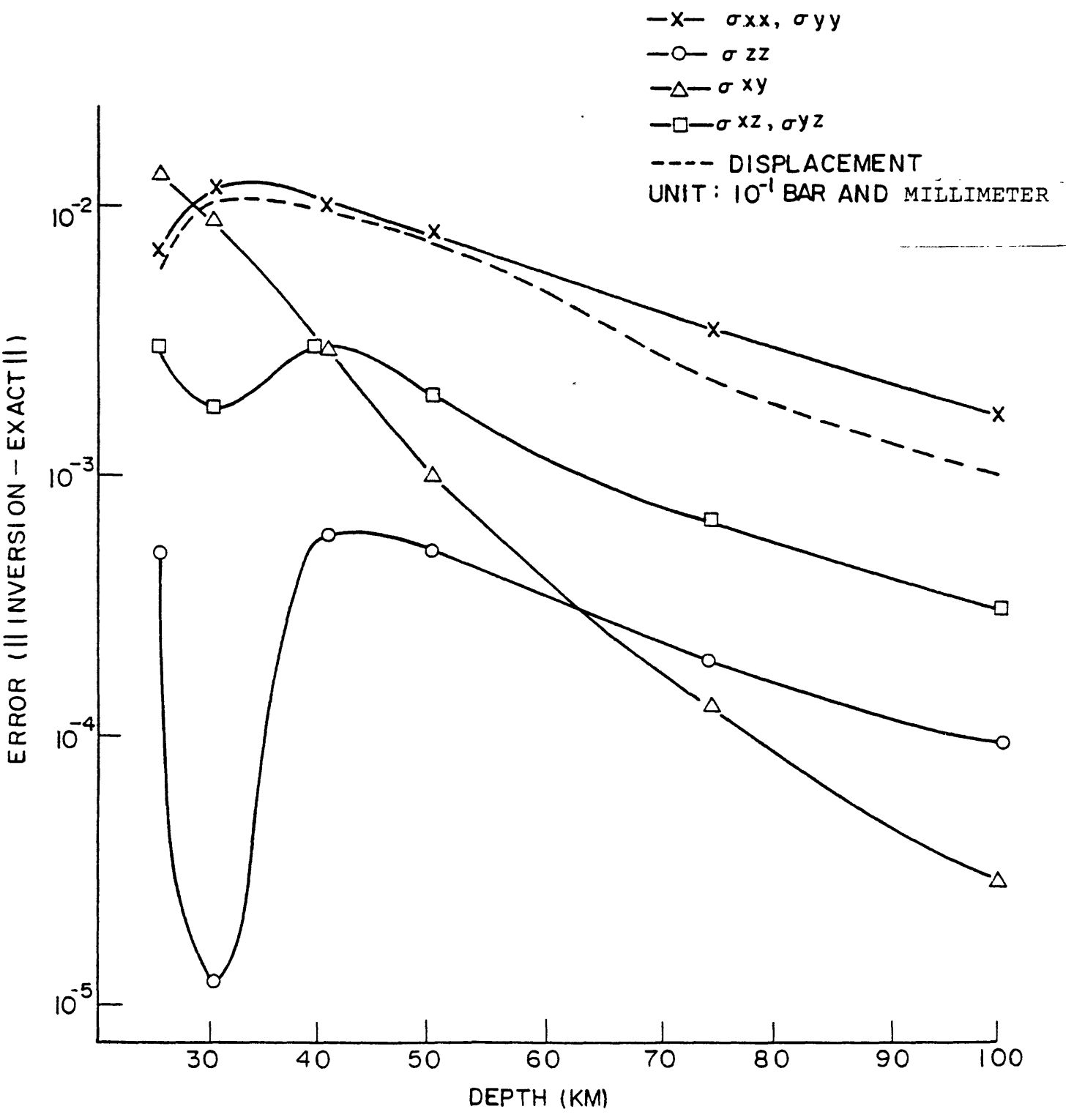

Fig. 9 Error in inversion — 10 x 10 x 10 km block

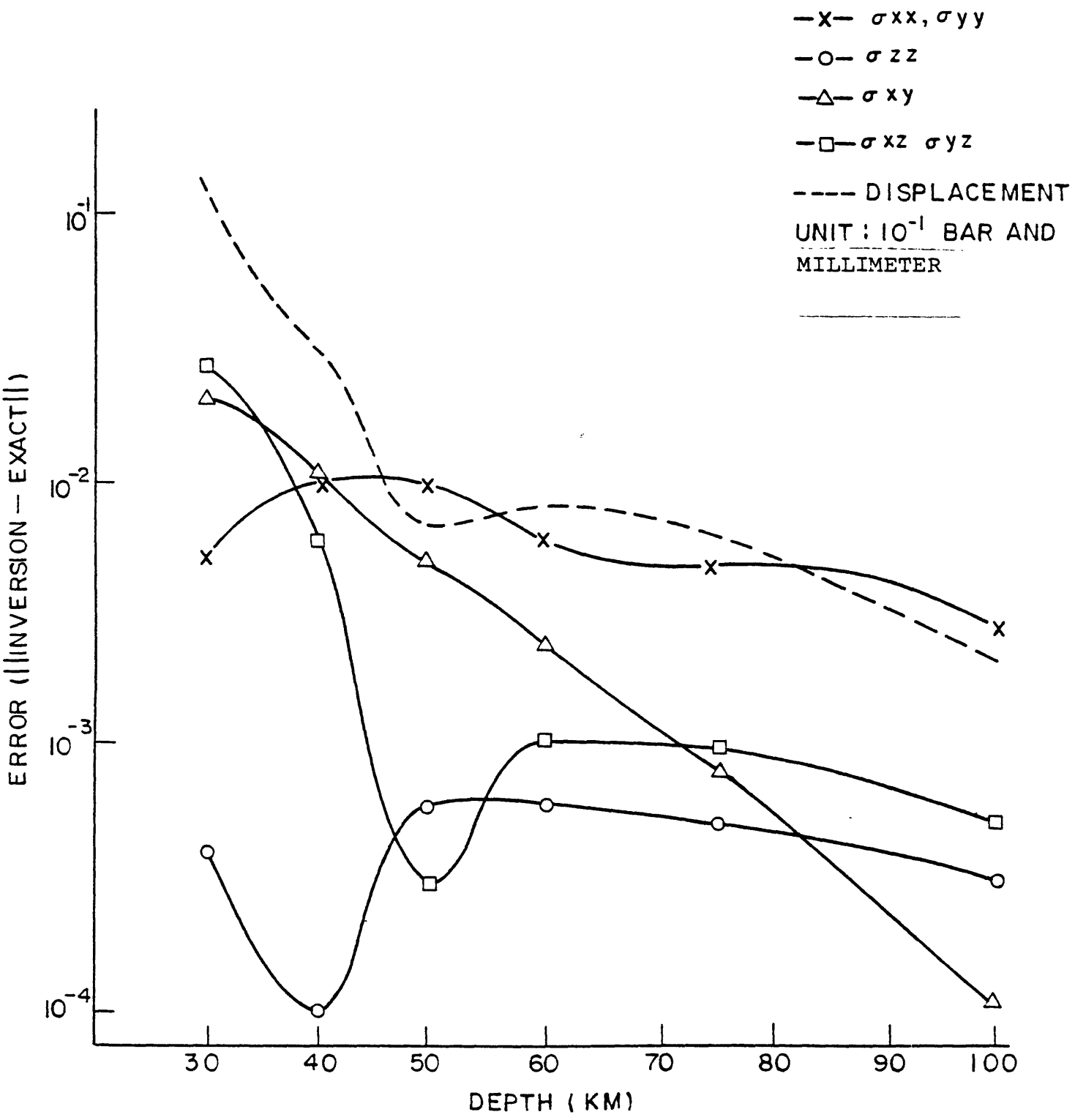

Fig. 10 Error in inversion— 20 x 20 x 20 KM block

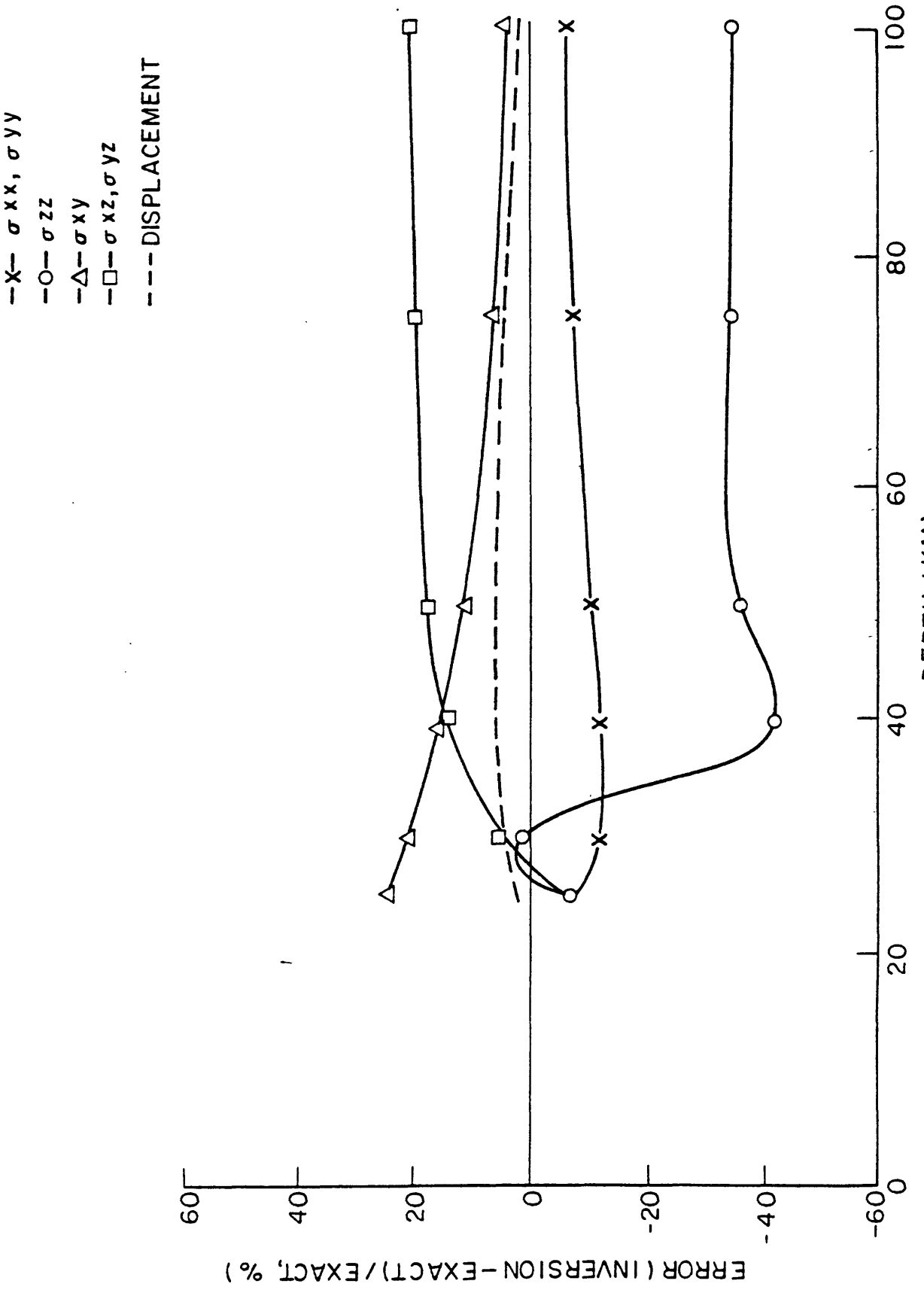

Fig. 11 Error in the inversion - 10 x 10 x 10 km block

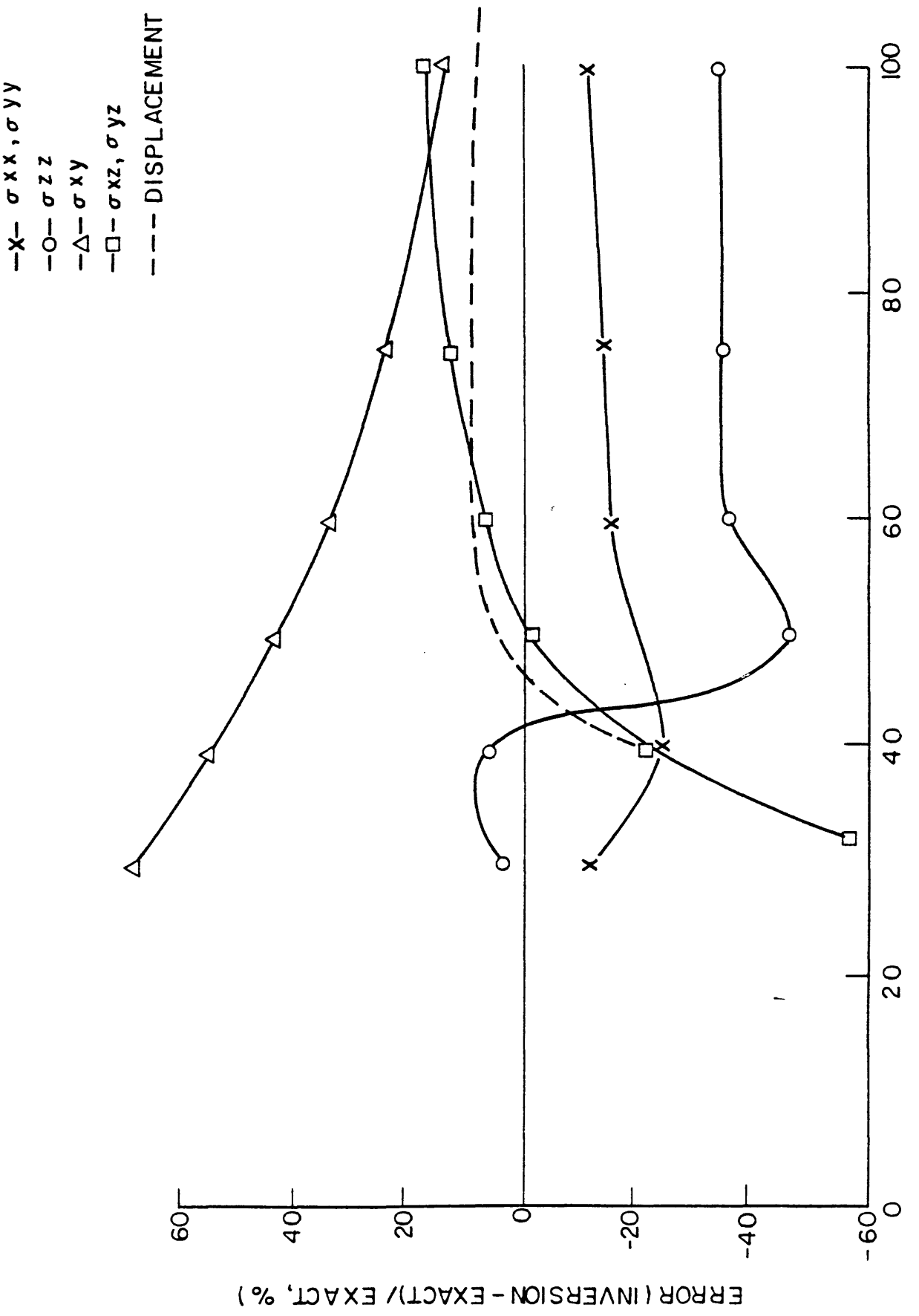

Fig. 12 Error in the inversion – 20 x 20 x 20 KM block

Chapter 4. PALMDALE UPLIFT

1. Levelling Data

The anomalous uplift in Southern California, so-called Palmdale bulge was first discovered in 1975 and reported by Castle et al., in 1976 (Castle et al., 1976). The pattern of uplift is shown in Fig. 13. This first survey was mainly based on the levelling data obtained between 1959 and 1968, and large scale high precision levelling survey was conducted since then. The result of these continued surveys revealed that the bulge was wider than estimated at first and also greater in displacement (Castle, 1978). These surveys also revealed that part of initial uplift subsided since 1974 although the space-time history of this subsidence or "downwarp" is quite uncertain. These results are shown in Fig. 14.

According to Castle (Castle, 1978), the whole episode of uplift occurred as follows:

(1) The uplift began near the intersection of Garlock fault and San Andreas fault in late 1959 and spread eastward which is confirmed by the continuous levelling near Palmdale showing that this area uplifted 20 cm during 1959-1962 period. This is shown in Fig. 15. The uplift gradually increased by another 15 cm in the next 10 years.

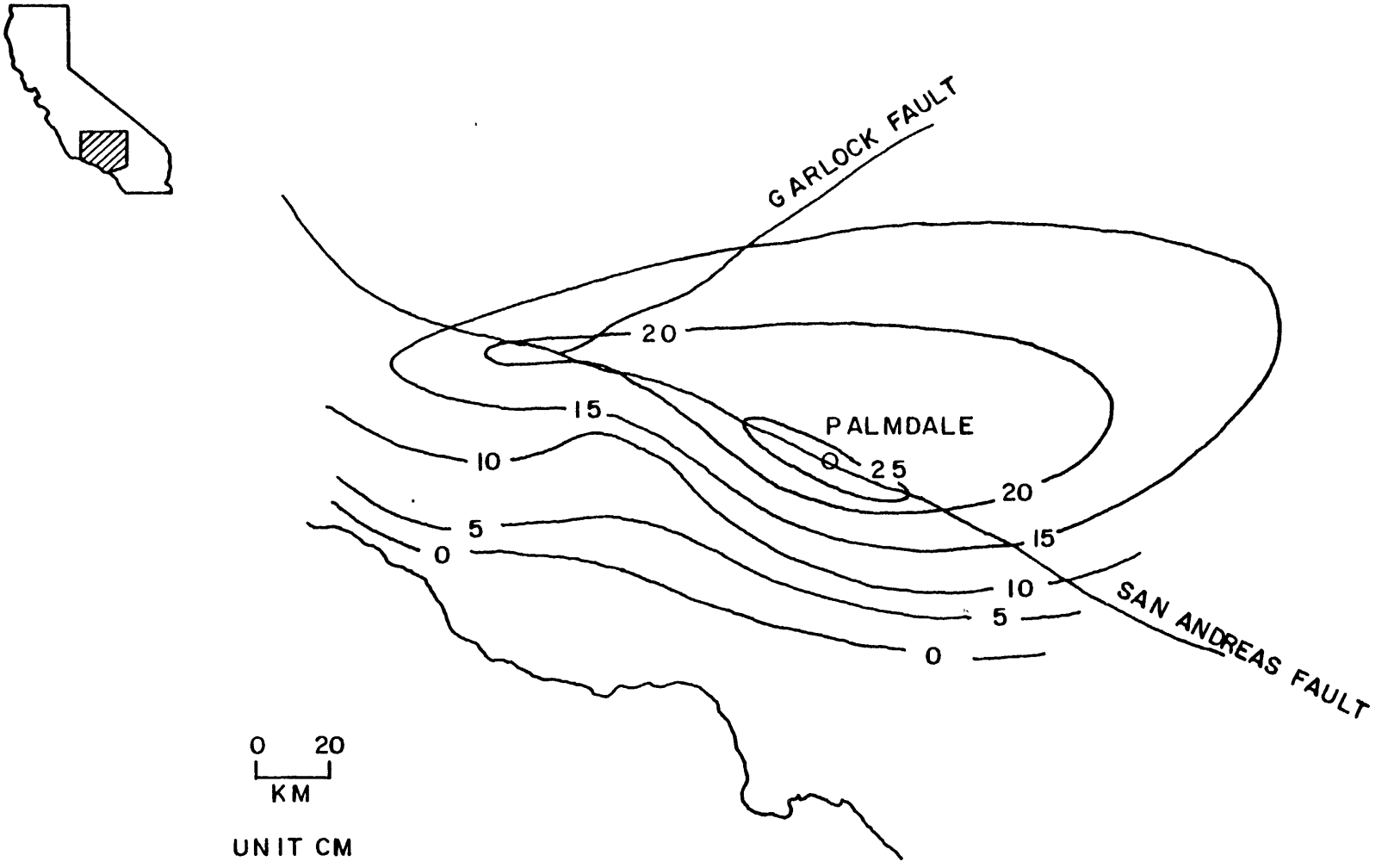

Fig. 13 Palmdale Uplift 1959-1974 (From Castle et al., 1976)

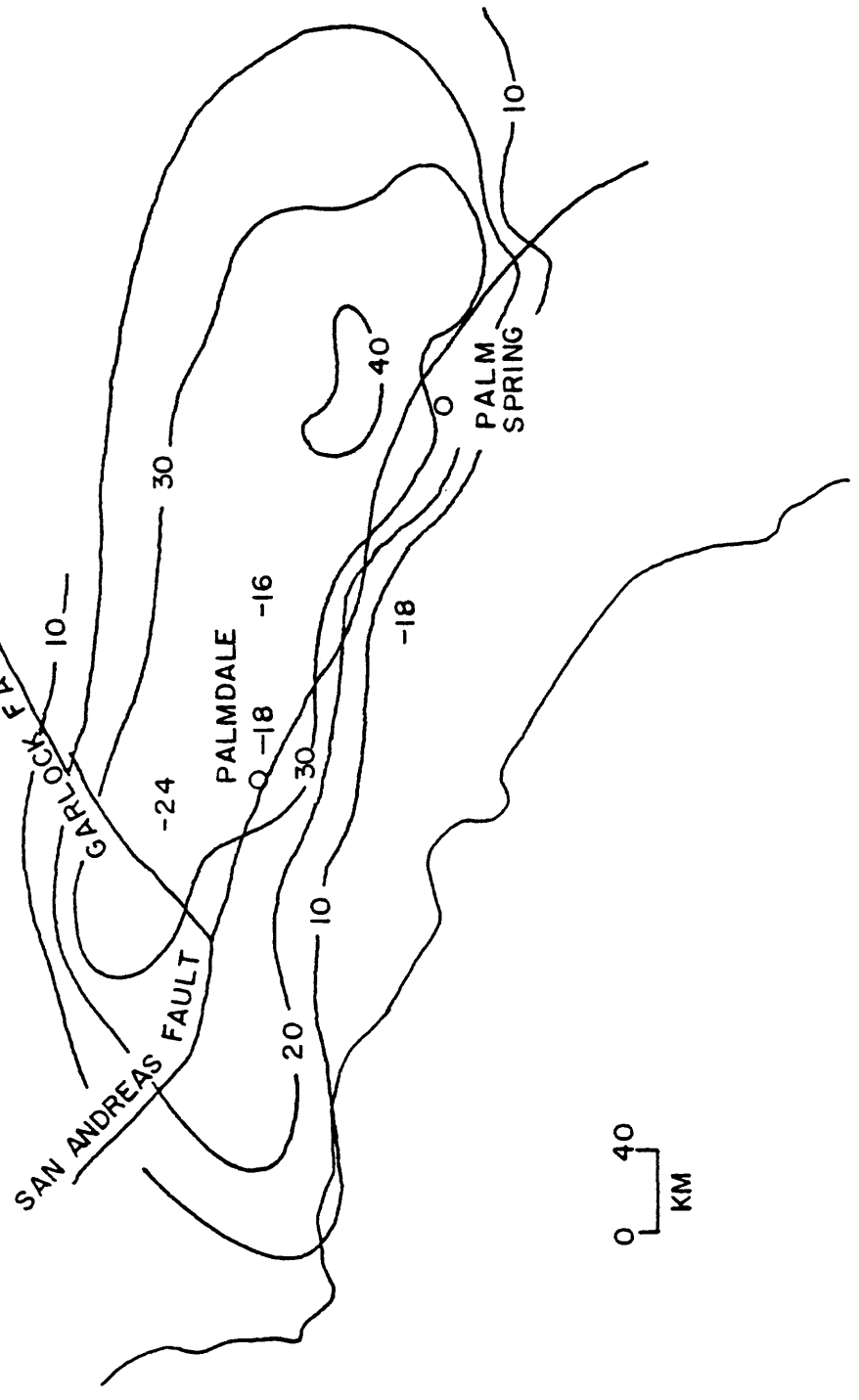

Fig. 14 Palmdale uplift and downwarp 1959-1978 (From Castle, 1978)

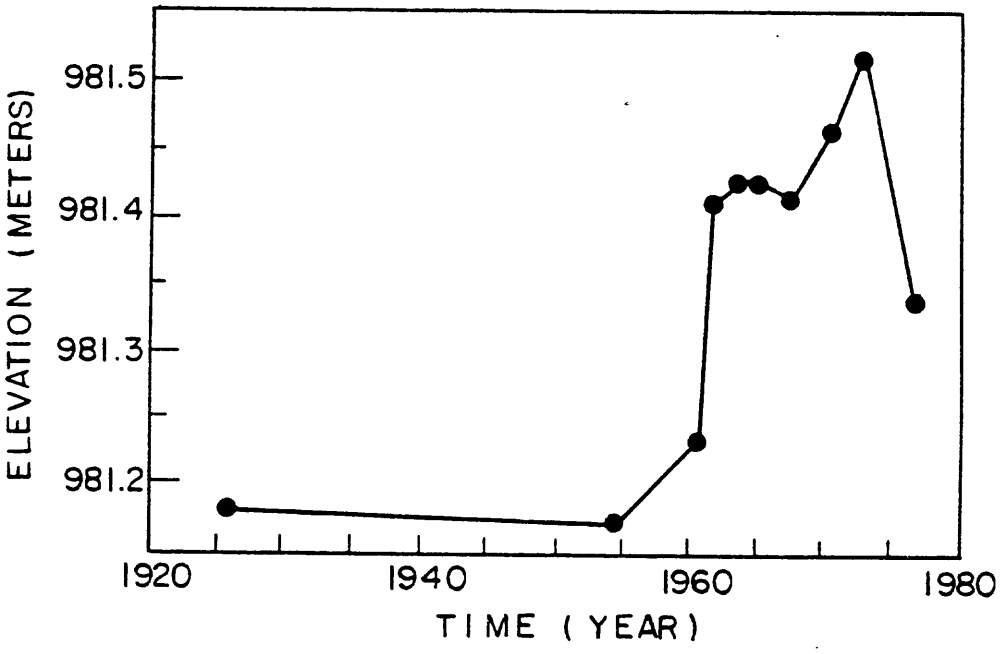

Fig. 15 Levelling data near Palmdale (From Savage and Prescott, 1979)

(2) Between late 1972 and early 1974, the area of uplift expanded to the southeast, where a maximum uplift of 45 cm occurred near Yucca Valley.

(3) Between late 1974 and late 1976, much of the uplift subsided. This downwarp reached 18 cm near Palmdale, 16 cm near Cajon, and 24 cm in Mojave.

2. Triangulation Data

Since Reid's suggestion on monitoring a strain accumulation as an earthquake precursor (Reid, 1910), extensive triangulation survey has been conducted in California by many organizations (Savage et al., 1973, Thatcher, 1976). These data show that the general trend of horizontal strain accumulation near Big Bend is 0.3 ∿ 0.4 microstrain per year of contraction in NS direction and 0.0 ∿ 0.1 microstrain per year of extension in EW direction. This pattern of strain accumulation is consistent with the regional stress expected here from plate tectonics (Atwater and Molnar, 1973).

After the discovery of Palmdale Bulge, interest in the relationship between horizontal strain accumulation and uplift during the uplift period is increased and many data were re-analyzed.

Using triangulation network near Big Bend (Fig. 16), Thatcher discussed that the direction of strain axises were significantly different from the long term regional trend during the uplift period 1959-1963. He also suggested that the compressional axes are perpendicular to the contour

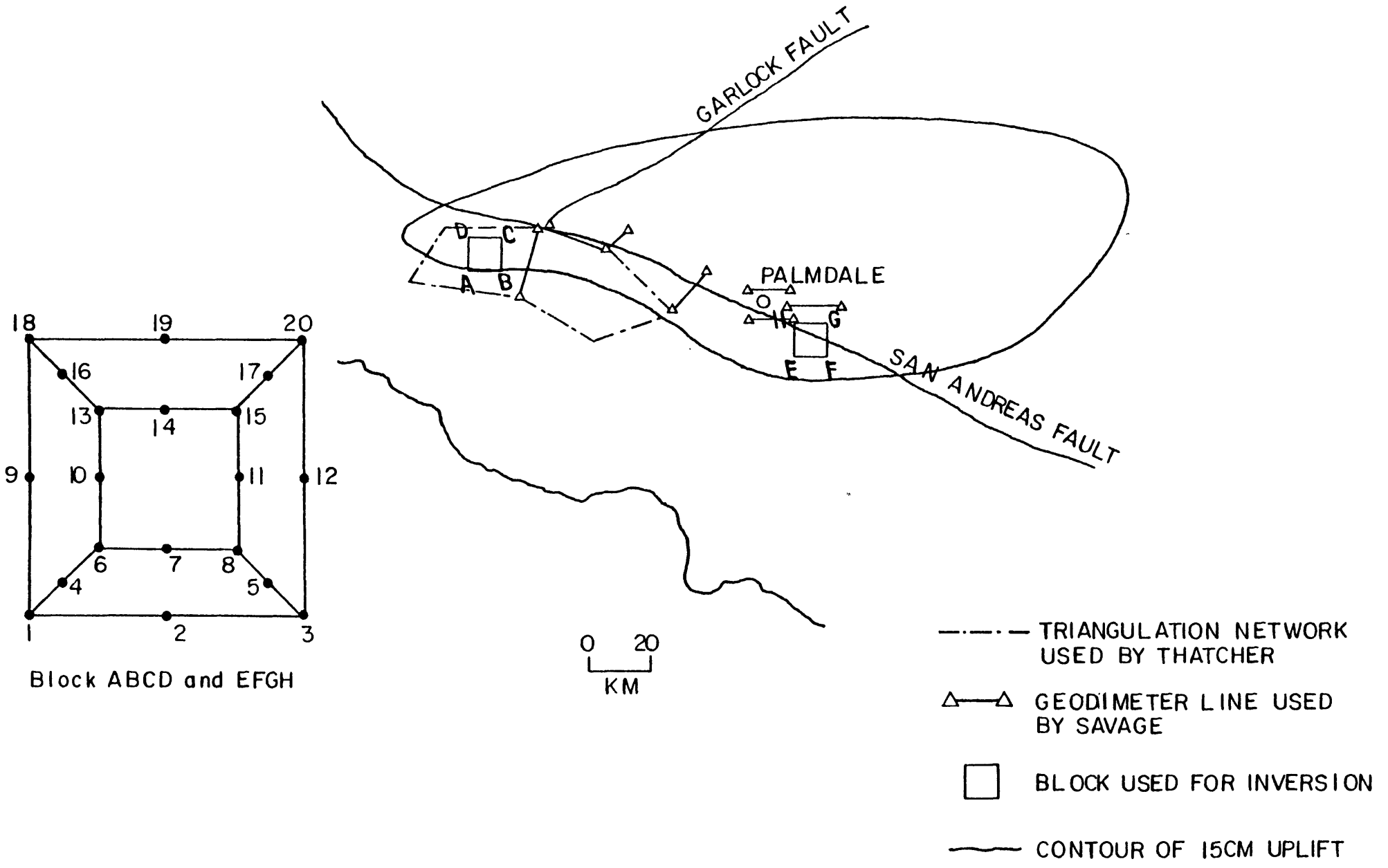

Block ABCD and EFGH

Fig. 16 Geodimeter network and block used for inversion

of uplift almost everywhere (Thatcher, 1976). But his data were based on Frank's method that uses only the change of angle in a triangulation network and therefore we can include any amount of dilatation on his data. As Savage and Prescott stated, this fact makes his result quite model dependent (Savage and Prescott, 1979).

Savage et al. analyzed geodometer data along the San Andreas fault (Fig. 16) and revealed no special change during the period 1950-1972 (Savage et al., 1973). The obtained data shows 0.4 microstrain per year of contraction in N13°E direction and 0.13 microstrain per year of extension in the direction of N77°W near the intersection of Garlock fault and San Andreas fault. Near Palmdale, they observed 0.35 microstrain per year of contraction in the direction of N7°E and 0.07 microstrain per year of extension in the direction of N83°W. These results are based on the change of the length of lines and are therefore not model dependent. Savage et al. also analyzed the strain rate near Palmdale in the period of 1972 to 1978 and revealed that the strain accumulations are 0.3 microstrain per year in NS direction and no strain accumulation in EW direction (Savage et al., 1978).

3. Geomagnetic Anomaly

Geomagnetic survey using high precision proton magnetometer were conducted along the 30 km segment of San Andreas fault between Palmdale and San Bernardino in the period 1973-1978 (Johnston et al., 1979). The location

is shown in Fig. 17. The observed anomalous changes were maximum of 10 gamma near Cajon and 5 gamma near Palmdale. These changes are shown in Fig. 17. The increase of magnetic field occurred between the period 1974-1976, which corresponds to the period of partial downwarp of Palmdale bulge. The peak of change was reached in May 1976.

Johnston et al., (1979) discussed that this anomalous change of geomagnetic field can be attributed to the local stress change at the depth less than 10 km. According to his discussion, 5 bar of stress change is sufficient to cause 5 gamma change on the surface if magnetization is 10^{-2} e.m.u. and 50 bar is needed for 5 gamma change if magnetization is 10^{-3} e.m.u. 10^{-2} e.m.u. of magnetization is probably the upper bound in this region (Johnston, 1978).

4. Seismological Data

There is a quite extensive catalog of earthquakes in this region during the period 1931 to 1972 (Heilman et al., 1973) and during the period 1972 to 1974 (Friedman et al., 1976) that show the relative quietness in this region during the period of uplift 1959-1974.

McNally et al. (1978) presented data on an earthquake swarm occurred between late 1976 and late 1977. According to them, in November 1976 an increase in the number of small earthquakes with local magnietuce (M_L) 2.0 to 3.0 began in Palmdale area, near Juniper Hills to the southeast and Lake Hughes to the northwest. In the year that followed, 1 November 1976 to 1 November 1977, the

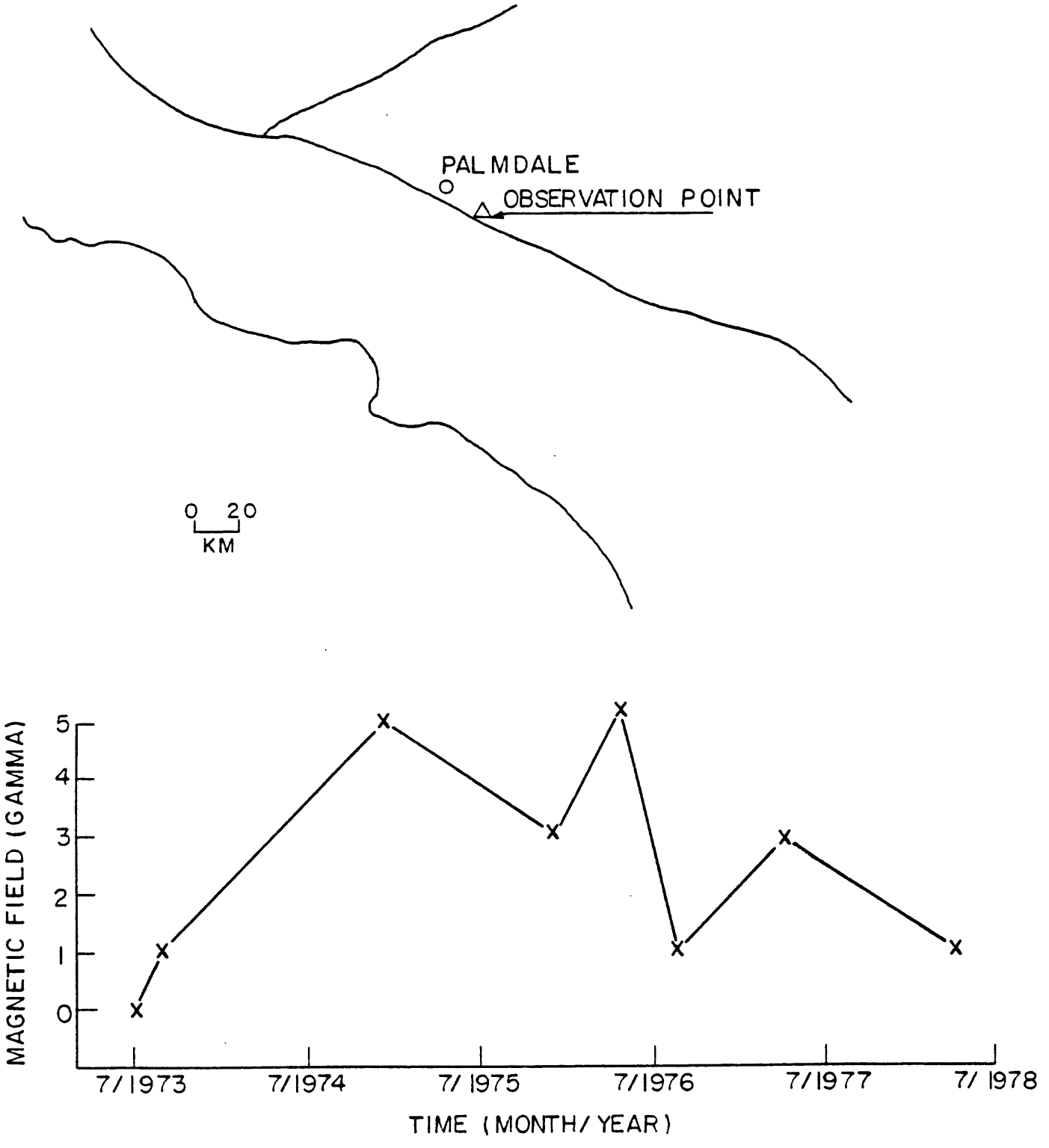

Fig. 17 Geomagnetic data near Palmdale (From Johnston et al. 1979)

number of earthquakes with $M_L \simeq 2.0$ was more than an order of magnitude greater than the long term average for these two areas.

Most earthquakes in the 1976-1977 period are clustered in a small volume with linear dimensions of 3 km (maximum at the depth of 8 km. The fault plane solutions for the largest four earthquakes occurred in the Juniper Hills region in 1976-1977 are shown in Fig. 18, together with the epicenters of these events.

These figures of fault plane solutions show that the axis of maximum compression rotates with time in the clockwise direction from a horizontal northwest-southeast orientation to a horizontal north-south orientation which is more consistent with the regional stress field.

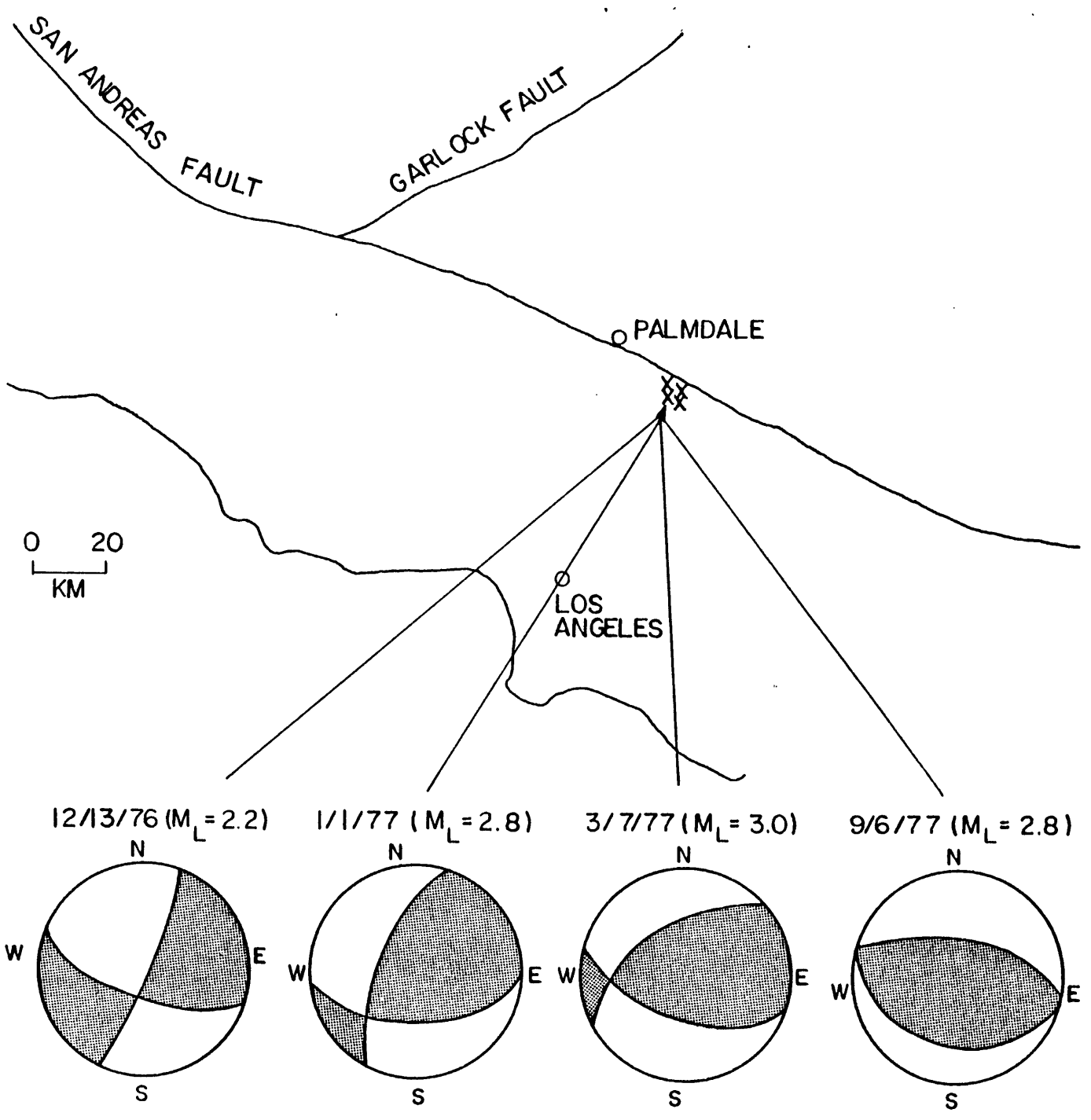

Fig. 18 Earthquake Swarm near Palmdale (From McNally et al. 1978)

Chapter 5. INVERSION OF PALMDALE DATA

1. Data Input

In order to apply our inversion scheme to Palmdale Bulge, the displacement at nodes on the surface are calculated using Savage's data for Block ABCD and Block EFGH shown in Fig. 16. Horizontal displacements are calculated assuming a constant strain rate uniform within each block. One nodal point on the surface was arbitrarily fixed. Vertical displacements are read from a contour map given by Castle et al., (Castle et al., 1976). Rigidity 3×10^{11} dyne/cm^2 and Poisson ratio 0.25 are assumed. It is assumed that through the period of whole episode of uplift and downwarp, the shape of contour does not change, i.e. the distribution of contour line at 1974 (Fig. 13), is preserved. Data used for inversion for the uplift 1959-1962, downwarp 1974-1977 for Block ABCD and Block EFGH are shown in Table 3. Since the temporal distribution of downwarp is not clear, the whole downwarp is assumed to have taken place in one year.

2. Result of Inversion

With these three-component displacements data as input to our inversion scheme, we obtained the stress inside the block. The result is shown for the center of each block at depths 3.75 km, 6.5 km and 8.75 km in Fig. 19 through 21, where the principal axes are shown using the Schmidt net (lower hemisphere).

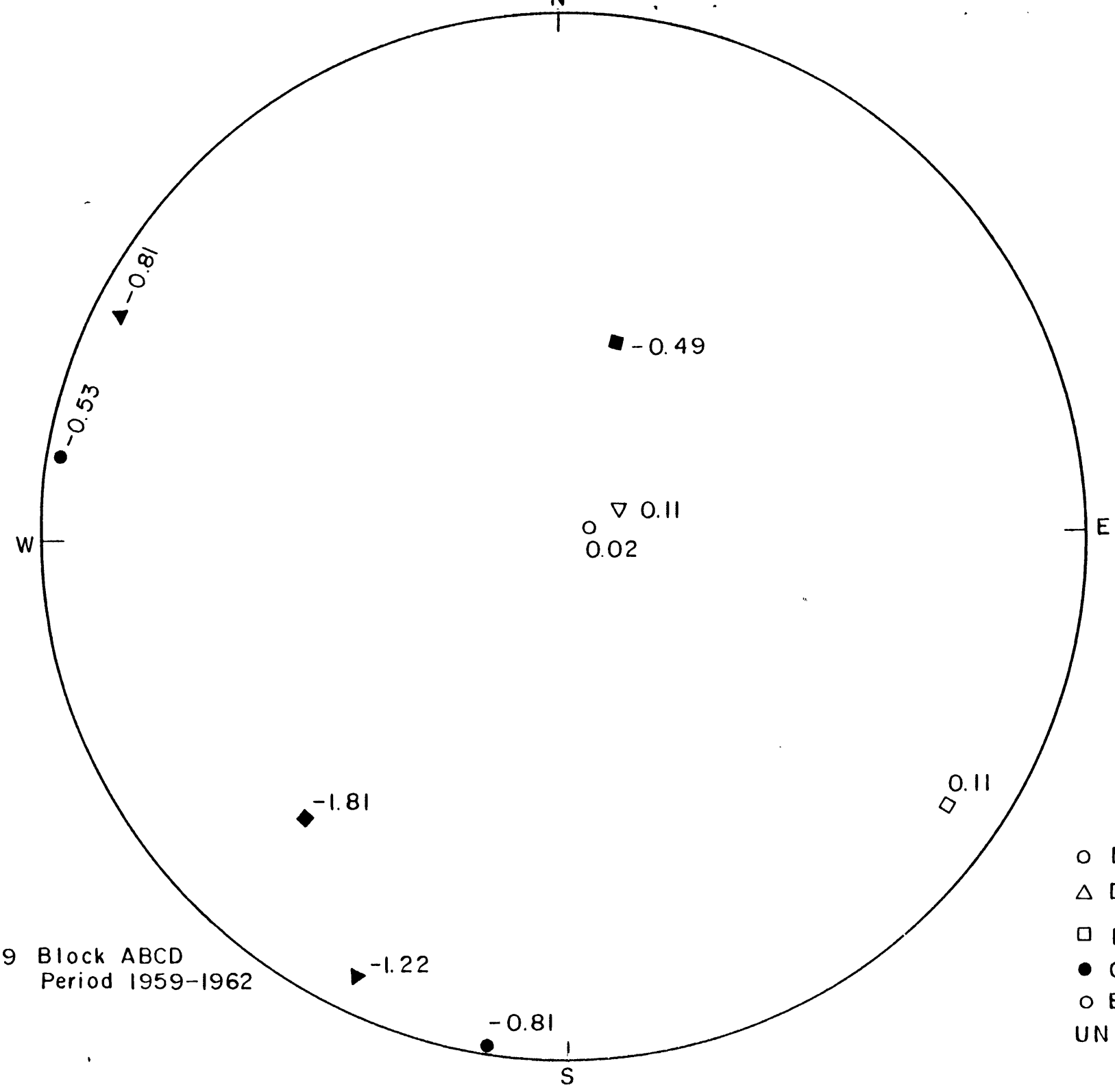

Fig. 19 Block ABCD
Period 1959-1962

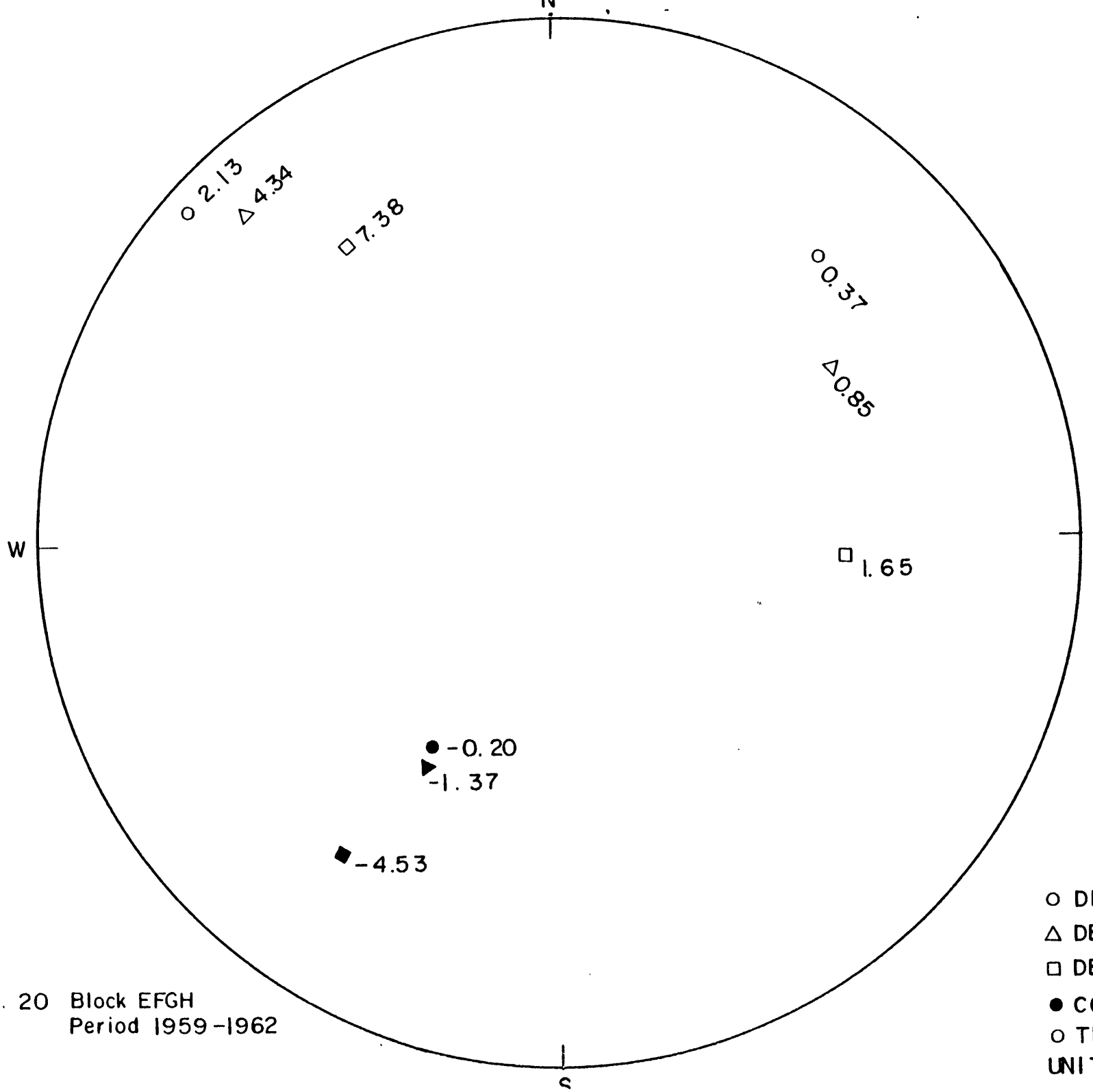

Fig. 20 Block EFGH
Period 1959-1962

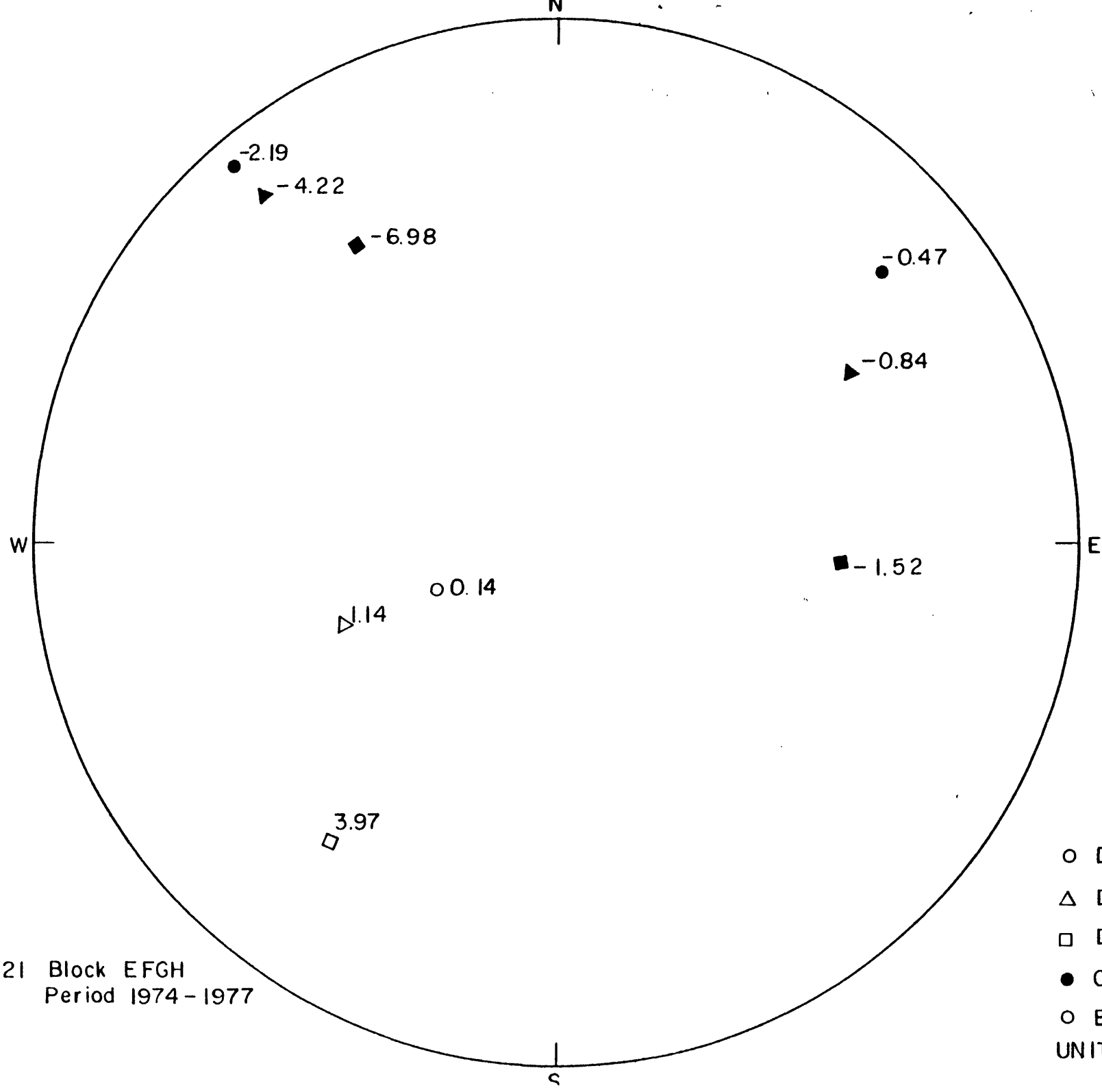

Fig. 21 Block EFGH
Period 1974 - 1977

The magnitude of principal stress is indicated by numeral in bar in these figures.

Since there is no direct evidence for downwarp in block ABCD, inversion was applied only to the uplift stage for this block. The result from Block ABCD shows that during the period of the uplift at a depth of 3.75 Km, the maximum compressional axis is oriented in the direction of N9°E with magnitude 0.8 bar.

The results from Block EFGH during the period 1959-1962, i.e., the period of uplift is quite interesting because they are showing dominance of tensional stress in that region during uplift. The direction of maximum tension is almost horizontal in the direction of N48°W with the magnitude 2.1 bar at a depth of 3.75 Km. Inversion for the same block during the period 1974-1977, i.e. the period of downwarp gives the horizontal compression axis in the direction of N40°W with magnitude 2.2 bar at a depth of 3.75 Km. This compressional stress increases with depth to 4.2 bar at 6.5 Km and 7.0 bar at 8.75 Km depth without changing directions so much.

Although we don't know exact spatio-temporal distributions of downwarp and we had to make assumptions about the distribution of displacements, the obtained state of stress at depth seems quite compatible with the data obtained by seismological and geomagnetic observations mentioned earlier.

The direction and sense of principle axis during the downwarp period are consistent with the fault plane solutions obtained for earthquakes in the early period of the swarm before the clockwise rotation of axis started.

The magnitude of stress obtained for Block EFGH during the downwarp by this inversion ranges from 2.1 bar at 3.75 Km depth to 7.0 bar at 8.75 Km depth. This result is again compatible with the estimate of Johnston (Johnston 1977, Johnston et al., 1979) for a stress change to account for the observed geomagnetic change of 5 gamma during the period 1974-1978. If the magnetization is 10^{-2} e.m.u., a stress change of 5 bars will produce the observed change in magnetic field.

The state of incremental stress at depth was horizontal tension during the uplift period 1969-1974 and horizontal compression during the downwarp period 1974-1976. The incremental stress before the uplift period was probably horizontal compression but with the rate an order of magnitude smaller than that during the downwarp period. The sudden increase of seismicity during the downwarp period may be due to accelerated horizontal compression.

3. Discussion

Mogi (1962) made laboratory fracture experiments on numerous rock-specimen for the purpose of determining the probability $\lambda(t)$ of fracture occurrence per unit time at time t measured after the application of a constant stress. He obtained the following formula for $\lambda(t)$ in the case of granite specimen under bending,

$$\lambda(t) = Ae^{BS} \tag{41}$$

where $\lambda(t)$ is called "hazard rate" and S denotes stress. The two constants A, B for the bending experiments of granite-specimen were determined as $A = 2.0 \times 10^{-12}$/year and $B = 0.37$ cm^2/Kg (Mogi, 1962).

Hagiwara (1974) modified the above equation to give the hazard rate in terms of ultimate strain which is determined for actual earthquakes statistically using the data on land deformations associated with them (Rikitake, 1974). The equation is

$$\lambda(\varepsilon) = \frac{A}{\dot{\varepsilon}} e^{BE\varepsilon} \tag{42}$$

where $\lambda(\varepsilon)\Delta\varepsilon$ is the conditional probability of fracture occurrence in a strain interval ε and $\varepsilon + \Delta\varepsilon$, $\dot{\varepsilon}$ is strain rate, and E is Young's modula. The associated reliability function, or the probability with which the ultimate strain exceed ε, can be written as

$$R(\varepsilon) = \exp\left\{ - \frac{A}{BE\dot{\varepsilon}} \exp(BE\varepsilon - 1)\right\}. \qquad (43)$$

This equation was used to derive the two constants A, B from the statistical distribution of actual ultimate strain assuming Gaussian distribution for the ultimate strain. Using the mean value of ultimate strain as 5.3×10^{-5} with the standard deviation of 3.3×10^{-5} as shown by Rikitake (1974), Young's modulus as 2.0×10^{11} dyne/cm^2 and constant strain rate as 5.0×10^{-7}/year, the values $A = 0.99 \times 10^{-3}$/year and $B = 0.3$ cm^2/Kg were obtained. It is noticed that if the ultimate strain obtained from the San Francisco earthquake in 1906 is also used in the above calculation, we obtain the values $A = 1.4 \times 10^{-3}$/year and $B = 0.19$ cm^2/Kg. These variations of constants A, B indicate, together with Scholtz's fracture experiments under the compression test of quartz specimen (Scholtz, 1972) which gave smaller values for B in two orders of magnitude, that these constants may vary significantly for different rocks, different stress conditions and different tectonic history of seismic regions.

Denoting two consecutive periods during stress build-up in an area as period I and period II, we have from eq. (41)

$$\lambda_I = Ae^{B(\sigma_o+\sigma_I)}$$

$$\lambda_{II} = Ae^{B(\sigma_o+\sigma_I+\sigma_{II})} \qquad (43)$$

where λ_I, λ_{II} are the probability of fracture occurrences per unit time at the ends of period I and II respectively, σ_I and σ_{II} are incremental stress during the period I and II respectively, and σ_o is the initial stress at the beginning of period I. The value of B can be determined if we know λ_I and λ_{II}, i.e. we have

$$B = \frac{1}{\sigma_{II}} \ln(\frac{\lambda_{II}}{\lambda_I}). \qquad (44)$$

We can estimate the value of A if we know the initial stress σ_o, or alternatively, we can estimate the stress σ_o if the value of A is determined statistically from past data. The equation to be used is

$$\sigma_o = \frac{1}{B} \ln(\frac{\lambda_I}{A}) - \sigma_I. \qquad (45)$$

According to McNally et al. (1978), the average number of earthquake per year at Juniper Hills before 1953 is 0.6 for events larger than $M_L \tilde{-} 2.0$ and is 15.0 in the period of November 1976 to November 1977. The incremental stress at the focal region is 0.12 bar per year before 1953 and about 7.0 bar in the 1976 to 1977 period as estimated by our inversion. Putting these numbers into eq. (44), the value of B is estimated as $B \sim 0.47$ cm^2/Kg. This is

quite comparable to the values obtained by Mogi (1962) and Hagiwara (1974) though it is much larger than the value obtained by Scholtz (1972). This large value of B may be due to the special condition of the particular section of the San Andreas fault.

Though there are observations which indicate a wide variability of the value B (Aki, 1978), the two values obtained from geodetic data, i.e. Hagiwara's statistical data on ultimate strain and our inversion of geodetic data combined with seismic data, and the value obtained from Mogi's experiments are quite comparable and suggests that B may be independent of the scale effect to a certain extent. It may also be possible to extrapolate the value of A obtained from laboratory experiments to the value for actual earthquakes in a large region to estimate the absolute value of probability of the earthquake occurrence. This is a fundamentally important problem for earthquake prediction and will be the subject of our future research.

Chapter 6. CONCLUSION

Our inversion scheme for determining incremental stress was successfully tested using artificial data generated by a buried point source in a homogeneous half-space.

The scheme was applied to the geodetic data from the Palmdale Bulge, including trilateration, triangulation and levelling data. Most significant conclusion is that the horizontal stress at depth as shallow as a few km can be significantly different from the horizontal stress measured on the surface from trilateration and triangulation alone.

We obtained an encouraging agreement between our estimate of incremental stress and data from geomagnetic and seismic observations for the period of downwarp. During this period, we estimated about 4.2 bars incremental horizontal compression at a depth of 6.5 km. This is compatible with the change of magnetic field by 5 gamma observed by Johnston et al. (Johnston et al., 1979) and increase of seismicity by an order of magnitude observed by McNally et al. (McNally et al., 1978).

These results show that our inversion scheme may be useful for studying various stress-induced earthquake precursor phenomena as a basis for earthquake prediction.

BIBLIOGRAPHY

Aki, K., Generation and propagation of G waves from Niigata earthquake of Jan. 16, 1964. Part 2. Estimation of earthquake moment, released energy, and stress-strain drop from the G wave spectrum, Bull. Earthq. Res. Inst., 44, 73-88, 1966.

Aki, K., Characteristics of barriers on an earthquake fault, 1977, (to be submitted).

Aki, K., Origin of the seismic gap: what initiates and stops a rupture propagation along a plate boundary? in Proceedings of Conference IV, Methodology for identifying seismic gaps and soon-to-break gaps, 3-46, USGS, Office of Earthquake Studies, 1978.

Alewine, R.W. and T.H. Heaton, Tilts associated with the Pt. Mugu earthquake, in Proceedings of the Conference on Tectonic Problems of the San Andreas Fault System, Kovach, R.L. and A. Nur editor, 86-93, Stanford Univ., Publ., Geol. Sci., Vol. 13, Stanford, CA, 1973.

Atwater, T. and P. Molnar, Relative motion of the Pacific and North American plates deduced from the sea floor spreading in the Atlantic, Indian and South Pacific Oceans, in Proceedings of the Conference on Tectonic Problems on the San Andreas Fault System, Kovach, R.L. and A. Nur, editor, 125-135, Stanford Univ. Publ., Geol. Sci., Vol. 13, Stanford, CA, 1973.

Bakun, W.H., R.M. Stewart, and D. Tocher, Variations in V_p/V_s in Bear Valley in 1972, in Proceedings of the Conference on Tectonic Problems of the San Andreas Fault System, Kovach, R.L. and A. Nur edit., 453-462, Stanford Univ. Publ., Geol. Sci., Vol. 13, Stanford, CA, 1973.

Brace, W.F., Laboratory studies of stick-slip and their application to earthquakes, Tectonophysics, 14, 189-200, 1972.

Brace, W.F. and A.S. Orange, Electrical resistivity changes in saturated rocks during fracture and frictional sliding, J. Geophys. Res., 73, 1433-1445, 1968a.

Brace, W.F., and A.S. Orange, Further studies of the effects of pressure on electrical resistivity of rocks, J. Geophys. Res., 73, 5407-5420, 1968b.

Brune, J.N., T.L. Henyey, and R.F. Roy, Heat flow, stress, and rate of slip along the San Andreas Fault, California, J. Geophys. Res., 74, 3821-3827, 1969.

Castle, R.O., J.N. Alt, J.C. Savage, and E.I. Balazs, Elevation changes preceding the San Fernando earthquake of February 9, 1971, Geology 2, 61-66, 1974.

Castle, R.O., J.P. Church, and M.R. Elliott, Aseismic uplift in southern California, Science, 192, 251-253, 1976.

Danbara, T., Crustal movements before at and after the Niigata earthquake, Report of the coordinate committee for earthquake prediction, 9, 93-96, 1973 (in Japanese).

Fitterman, D.V., Theoretical resistivity variations along stressed strike slip faults, J. Geophys. Res., 81, 4909-4915, 1976.

Forsyth, D. and S. Uyeda, On the relative importance of the driving forces of plate motion, Geophys. J. Roy. Astron. Soc., 43, 163-200, 1975.

Franklin, J., Well-posed stochastic extensions of ill-posed linear problems, J. Math. Anal. Appl., 21, 682-716, 1970.

Friedman, M.E., J.H. Whitcomb, C.R. Allen, J.A. Hileman, Seismicity of the Southern California region, 1 January 1972 to 31 December 1974, Seismological Laboratory, California Institute of Technology, Pasadena, 1976.

Hadley, K., V_P/V_S anomalies in dilatant rock samples, Pure Appl. Geophys., 113, 1-23, 1975.

Hagiwara, Y., Probability of earthquake occurrence estimated from results of rock fracture experiments, Tectonophysics, 23, 99-103, 1974.

Hanks, T.C., Earthquake stress drops, ambient tectonic stress, and stresses that drive plate motions, Pageoph., 115, 441-458, 1977.

Hileman, J.A., C.R. Allen, J.M. Nordquist, Seismicity of the southern California region, 1 January 1932 to 31 December 1972, Seismological Laboratory, California Institute of Technology, Pasadena, 1973.

Ishida, M. and H. Kanamori, The spatio-temporal variation of seismicity before the 1971 San Fernando earthquake, California, Geophys. Res. Lett., 4, 345-346, 1977.

Johnston, M.J.S., Local magnetic field variations and stress changes near a slip discontinuity on the San Andreas fault, J. Geomag. Geoelectr., 30, 511-522, 1978.

Johnston, M.J.S., F.J. Williams, J. McWhister, and B.E. Williams, Tectonomagnetic anomaly during the southern California downwarp, J. Geophys. Rev., 84, 6026-6030, 1979.

Jungles, P.H. and G.A. Frazier, Finite element analysis of the residual displacements for an earthquake rupture: Source parameters for the San Fernando earthquake, J. Geophys. Res., 78, 5062-5083, 1973.

Lachenbruch, A.H. and J.H. Sass, Thermo-mechanical aspects of the San Andreas fault system, in Proceedings of Conference on Tectonic Problems of the San Andreas Fault System, Kovach, R.L. and A. Nur, edit., Stanford Univ. Publ., Geol. Sci., Vol. 13, Stanford, CA, 1973.

Levenberg, K., A method for the solution of certain non-linear problems in least squares, Earthq. Quart. Appl. Math., 2, 164-168, 1944.

Linz, P., Theoretical Numerical Analysis, Wiley-Interscience, NY, 1979.

Mazzella, A., and H.F. Morrison, Electrical resistivity variations associated with earthquakes on the San Andreas fault, Science, 185, 855-857, 1974.

McCowan, D.W., P. Glover, S.S. Alexander, A static and dynamic finite element analysis of the 1971 San Fernando, California earthquake, Geophys. J.R. astr. Soc., 48, 163-185, 1977.

McNally, K.C., H. Kanamori, J. Pechmann, and G. Enis, Seismicity increase along the San Andreas fault, southern California, Science, 201, 814-814, 1978.

Mindlin, R.D., Force at a point in the interior of a semi-infinite solid, Physics, 7, 195-202, 1936.

Mogi, K., Study of elastic shocks caused by the fracture of heterogeneous material and its relation to earthquake phenomena, Bull. Earthq. Res. Inst., Univ. Tokyo, 40, 125-173, 1962.

Morse, P.M. and H. Feshbach, Methods of Theoretical Physics, McGraw-Hill, NY, 1953.

Nur, A., and G. Simmons, The effect of saturation on velocity in low porosity rocks, Earth Planet. Sci. Lett., 7, 183-193, 1969.

Oden, J.T., and J.N. Reddy, Variational Methods in Theoretical Mechanics, Springer-Verlag, NY, 1976.

Prescott, W.H. and J.C. Savage, Strain accumulation on the San Andreas fault near Palmdale, California, J. Geophys. Res., 81, 4901-4908, 1976.

Reid, H.F., Permanent displacement of the ground, in the California earthquake of April 18, 1906, Report of the State of Earthquake Investigation Commission, Vol. 2, 16-28, Carnegie Institution of Washington, Washington, DC, 1910.

Richardson, R.M. and S.C. Solomon, Apparent stress and stress drop for interplate earthquakes and tectonic stress in the plates, Pure Appl. Geophys., 115, 317-331, 1977.

Richardson, R.M., Finite element modeling of stress in the Nazca plate: Driving forces and plate boundary earthquakes, Tectonophysics, 50, 223-248, 1978.

Rikitake, T., Statistics of ultimate strain of the earth's crust and probability of earthquake occurrence, Tectonophysics, 26, 1-21, 1975.

Rikitake, T., Earthquake Prediction, Elsevier, Amsterdam, 1976.

Sassa, K. and E. Nishimura, On phenomena forerunning earthquakes, Trans. Am. Geophys. Un., 32, 1-6, 1951.

Savage, J.C., W.H. Prescott, and W.T. Kinoshita, Geodimeter measurements along the San Andreas fault, in Proceedings of the Conference on Tectonic Problems of the San Andreas Fault System, Kovach, R.L. and A. Nur, ed., 44-53, Stanford Univ. Publ., Geol. Sci., Vol. 13, Stanford, CA, 1973.

Savage, J.C., W.H. Prescott, M. Lisowski, and N. King, Strain in southern California: Measured uniaxial north-south regional contraction, Science, 202, 883-885, 1978.

Savage, J.C. and W.H. Prescott, Geodimeter measurements of strain during the southern California uplift, J. Geophys. Res., 84, 171-177, 1979.

Scholtz, C.H., Static fatigue of quartz, J. Geophys. Res., 77, 2104-2114, 1972.

Semenov, A.M., Variations in the travel-time of transverse and longitudinal waves before violent earthquakes, Izv. Acad. Sci. USSR, Physics of Solid Earth, 4, 245- , 1969.

Smith, A.T., Time-dependent strain accumulation and release at island arcs: Implications for 1946 Nankaido earthquake, Ph.D. Thesis, M.I.T., 1974.

Stesky, R.M., The mechanical behavior of faulted rock at high temperature and pressure, Ph.D. Thesis, M.I.T., 1975.

Stesky, R.M. and W.F. Brace, Estimation of frictional stress on the San Andreas fault from laboratory measurements, in Proceedings of the Conference on Tectonic Problems of the San Andreas Fault System, Kovach, R.L. and A. Nur, ed., 206-214, Stanford Univ. Publ., Geol. Sci., Vol. 13, Stanford, CA, 1973.

Stewart, G.S., Prediction of the Pt. Mugu earthquake by two methods in Proceedings of the Conference on Tectonic Problem of the San Andreas Fault System, Kovach, R.L. and A. Nur, ed., Stanford Univ. Pub., Geol. Sci., Vol. 13, Stanford, CA, 1973.

Thatcher, W., Episodic strain accumulation in southern California, Science, 194, 691-695, 1976.

Tong, P., and J. Rossettos, Finite element method - Basic technique and implementation, M.I.T. Press, 1977.

Whitcomb, J.H., J.D. Garmany, and D.L. Anderson, Earthquake prediction: Variation of seismic velocities before the San Fernando earthquake, Science, 180, 632-635, 1973.

Wiggins, R.A., The general linear inverse problem: implications of surface waves and free oscillations for earth structure, Rev. Geophys. Space Phys., 10, 251-285, 1972.

Wilkinson, J.H., The Algebraic Eigenvalue Problem, Clarendon Press, Oxford, 1965.

Wyss, M., Stress estimates of South American shallow and deep earthquakes, J. Geophys. Res., 75, 1529-1544, 1970.

Wyss, M., Interpretation of the Southern California uplift in terms of the dilatancy hypothesis, Nature, 266, 1977.

Wyss, M., and P. Molnar, Efficiency, stress drop, apparent stress, effective stress and frictional stress of Denver, Colorado earthquakes, J. Geophys. Res., 77, 1433-1438, 1972.

Zienkiewicz, O.C., The Finite Element Method in Engineering Sciences, McGraw-Hill, 1971.

Table 1. Sampling Points and Weight For Gauss-Legendre Quadrature

Order	r_i (sampling point)	a_i (weight)
1	0.000000000000000	2.000000000000000
2	+0.577350269189626	1.000000000000000
	-0.577350269189626	1.000000000000000
3	+0.774596669241483	0.555555555555555
	0.000000000000000	0.888888888888888
	-0.774596669241483	0.555555555555555

Table 2. Values of k, ℓ, m, n

Case	k	ℓ	m	n	Total
1	12	12	12	12	48
2	36	36	36	36	144
3	36	36	120	36	228

Case 1. Five 8 nodes element are used (Fig. 3)

Case 2. Five 20 nodes element are used (Fig. 4)

Case 3. Twelve 20 nodes element are used (Fig. 5)

Table 3. Data Input (Unit MM)

1. Block ABCD Period 1959-1962

Node	u	v	w
1	.0	.0	114.0000
2	.3734927	-.5479640	117.0000
3	.7469853	-1.095928	120.0000
4	-.4361783D-01	-.6053641	117.0000
5	.5166211	-1.427310	123.6000
6	-.8723567D-01	-1.210728	120.0000
7	.9951066D-01	-1.484710	123.6000
8	.2862570	-1.758692	127.2000
9	-.5479640	-1.873492	130.8000
10	-.3612177	-2.147474	130.2000
11	.1227499D-01	-2.695438	136.8000
12	.1990213	-2.969420	139.8000
13	-.6351997	-3.084221	140.4000
14	-.4484533	-3.358203	143.4000
15	-.2617070	-3.632185	146.4000
16	-.8655638	-3.415603	144.0000
17	-.3053248	-4.237549	153.0000
18	-1.095928	-3.746985	147.6000
19	-.7224353	-4.294949	153.6000
20	-.3489427	-4.842913	159.6000

2. Block EFGH Period 1959-1962

Node	u	v	w
1	.0	.0	152.4000
2	.3217809	.2298258	150.6000
3	.6435618	.4596516	148.8000
4	.1379017	-.3229888	156.0000
5	.6205730	.2174995D-01	154.2000
6	.2758034	-.6459776	159.6000
7	.4366938	-.5310647	159.6000
8	.5975843	-.4161517	159.6000
9	.2298258	-1.521781	185.4000
10	.3907163	-1.406868	186.6000
11	.7124972	-1.177042	180.0000
12	.8733876	-1.062129	172.2000
13	.5056292	-2.167759	213.6000
14	.6665196	-2.052846	207.0000
15	.8274101	-1.937933	200.4000
16	.4826404	-2.605660	216.0000
17	.9653118	-2.260921	198.0000
18	.4596516	-3.043562	218.4000
19	.7814325	-2.813736	207.0000
20	1.103213	-2.583910	195.6000

Table 3 (cont'd.)

3. Block EFGH Period 1974-1977

Node	u	v	w
1	.0	.0	-139.7000
2	.3000000	.0	-138.0500
3	.6000000	.0	-136.4000
4	.7500000D-01	-.3250000	-143.0000
5	.5250000	-.3250000	-141.3500
6	.1500000	-.6500000	-146.3000
7	.3000000	-.6500000	-146.3000
8	.4500000	-.6500000	-146.3000
9	.0	-1.300000	-169.9500
10	.1500000	-1.300000	-171.0500
11	.4500000	-1.300000	-165.0000
12	.6000000	-1.300000	-157.8500
13	.1500000	-1.950000	-195.8000
14	.3000000	-1.950000	-189.7500
15	.4500000	-1.950000	-183.7000
16	.7500000D-01	-2.275000	-198.0000
17	.5250000	-2.275000	-181.5000
18	.0	-2.600000	-200.2000
19	.3000000	-2.600000	-189.7500
20	.6000000	-2.600000	-179.3000

Appendix: Code Geodeinverse

Flow Chart.

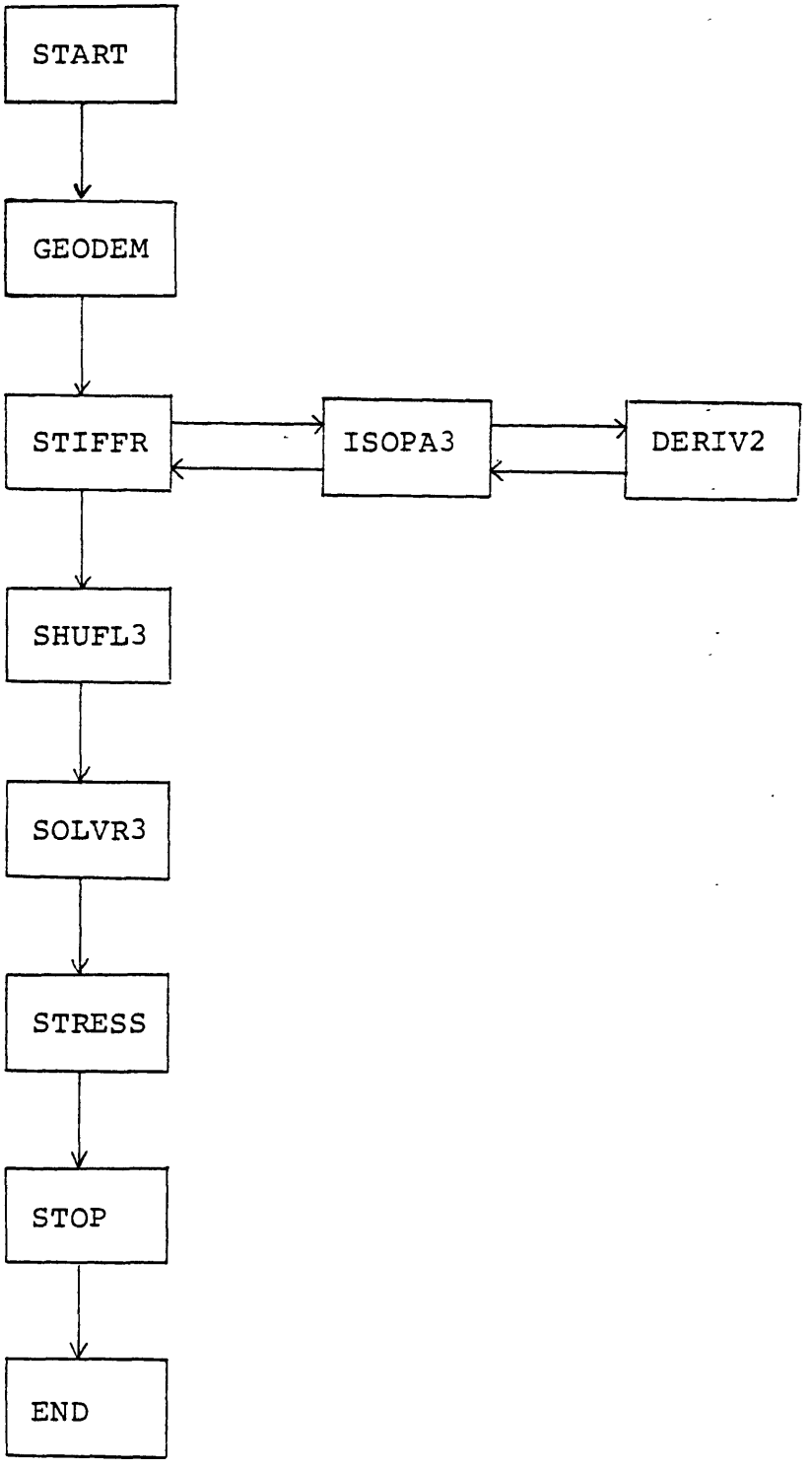

```
CCCCCCCCCCCCCCCCCCCCCCCCCCCCCCCCCCCCCCCCCCCCCCCCCCCCCCCCCCCCCCCCCCCCCCCCC
C                                                                      C
C     PROGRAM GEODINVERSE                                              C
C     THREE DIMENSIONAL GEODETIC INVERSION SCHEME TO OBTAIN STRESS IN   C
C     THE EARTH                                                        C
C     BY                                                               C
C     KEIICHIRO IKEDA                                                  C
C     DEPARTMENT  OF EARTH AND PLANETARY SCIENCES                      C
C     MASACHUSETTS INSTITUTE OF TECHNOLOGY                             C
C     10 DECEMBER 1979                                                 C
C                                                                      C
CCCCCCCCCCCCCCCCCCCCCCCCCCCCCCCCCCCCCCCCCCCCCCCCCCCCCCCCCCCCCCCCCCCCCCCCC
      IMPLICIT REAL*8(A-H,O-Z)
      REAL*8 JUNK,JUNKT,JUNK2
      DIMENSION IDMTX(240),ICOL1(228),IROW1(228),ELAST(6,6),ITEMP(48)
      DIMENSION XCORD(76),YCORD(76),ZCORD(76)
      DIMENSION ICOL2(228),IROW2(228)
      DIMENSION STIFF(228,229),GLOAD(228)
      DIMENSION GLOAD2(228),TEMP(228),ESTOR(12,6,60),STOR2(12,6)
      DIMENSION GSOL1(228),XDATA(20),YDATA(20),ZDATA(20)
CCCCCCCCCCCCCCCCCCCCCCCCCCCCCCCCCCCCCCCCCCCCCCCCCCCCCCCCCCCCCCCCCCCCCCCCC
C                                                                      C
C     USER SHOULD PROVIDE FOLLOWING DATA                               C
C     XCORD,YCORD,ZCORD-----COORDINATES OF OUTER BOUNDARY NODES (KM)   C
C     THETA-----------------DIRECTION OF PRINCIPAL STRAIN AXIS (DEGREE)C
C     SX,SY-----------------PRINCIPAL STRAIN   (MICROSTRAIN)           C
C     ZDATA-----------------VERTICAL DISPLACEMENT  (MM)               C
C     ELAST-----------------ELASTICITY MATRIX   (10**11 DYNE PER CM**2)C
C                                                                      C
CCCCCCCCCCCCCCCCCCCCCCCCCCCCCCCCCCCCCCCCCCCCCCCCCCCCCCCCCCCCCCCCCCCCCCCCC
      DATA CONST1,CONST2,CONST3,CONST4/.5,.5,.5,.5/
      DATA MAXND,MAXEL,MAXSND/76,12,20/
      DATA ITYPE/0/
      DATA MAXCOL,MAXROW/60,168/
      DATA IDMTX/6,8,15,13,49,51,56,54,7,11,14,10,50,53,55,52,69,70,72,7
     X1,49,51,56,54,61,63,68,66,50,53,55,52,62,65,67,64,57,58,60,59,61,6
     X3,68,66,25,27,32,30,62,65,67,64,26,29,31,28,73,74,76,75,6,8,51,49,
     X25,27,63,61,7,70,50,69,26,74,62,73,21,22,58,57,8,15,56,51,27,32,68
     X,63,11,72,53,70,29,76,65,74,22,24,60,58,15,13,54,56,32,30,66,68,14
     X,71,55,72,31,75,67,76,24,23,59,60,13,6,49,54,30,25,61,66,10,69,52,
     X71,28,73,64,75,23,21,57,59,
     X6,1,3,8,25,41,43,27,4,2,5,7,33,42,34,26,21,37,38,22,8,3,20,15,
     X27,43,48,32,5,12,17,11,34,45,36,29,22,38,40,24,15,20,18,13,32,48,
     X46,30,17,19,16,14,36,47,35,31,24,40,39,23,13,18,1,6,30,46,41,25,16
     X,9,4,10,35,44,33,28,23,39,37,21,25,27,32,30,41,43,48,46,26,29,31,
     X28,42,45,47,44,33,34,36,35/
      DATA ICOL1/1,2,3,4,5,6,7,8,9,10,11,12,13,14,15,16,17,18,19,20,21,
     X22,23,24,25,26,27,28,29,30,31,32,33,34,35,36,37,38,39,40,41,42,43,
     X44,45,46,47,48,49,50,51,52,53,54,55,56,57,58,59,60/
      DATA IROW1/10,11,12,13,14,15,16,17,18,19,20,21,22,23,24,28,29,30,3
     X1,32,33,37,38,39,40,41,42,43,44,45,46,47,48,49,50,51,61,62,63,64,6
     X5,66,67,68,69,70,71,72,73,74,75,76,77,78,79,80,81,82,83,84,85,86,8
     X7,88,89,90,91,92,93,94,95,96,97,98,99,100,101,102,103,104,105,106,
     X107,108/
```

```
      DO 1 I=85,168
1     IROW1(I)=60+I
      DATA ITEMP/1,2,3,9,12,18,19,20,37,38,39,40,41,42,43,44,45,46,47,48
     X/
      NUM=MAXCOL/3
      DO 2 I=1,NUM
      IROW2(3*I-2)=3*ITEMP(I)-2
      IROW2(3*I-1)=3*ITEMP(I)-1
2     IROW2(3*I)=3*ITEMP(I)
      MAXDEG=MAXND*3
      MAX1=MAXDEG*2-(MAXCOL+MAXROW)
      MAX2=MAXCOL+MAXROW
      M1=MAXDEG
      M2=MAX1
      M3=M1+1
      MAXID=20*MAXEL
      CALL GEODEM(ITYPE,MAXDEG,MAXND,MAXSND,THETA,SX,SY,SS,
     XXCORD,YCORD,ZCORD,XDATA,YDATA,ZDATA,TEMP)
      CALL STIFFR(MAXND,MAXDEG,MGRID,NGRID,LGRID,ELAST,STIFF,XCORD,
     XYCORD,ZCORD,NFREE,MAXEL,IDMTX,MAXID,ESTOR)
      CALL SHUFL3(MAXDEG,MAXCOL,MAXROW,STIFF,ICOL1,ICOL2,IROW1,IRO
     XW2,GLOAD,TEMP)
      CALL SOLVR3(M1,M2,M3,STIFF,GLOAD,GLOAD2,EPSLON,OMEGA)
      CALL STRESS(MAXDEG,MAXEL,MAXID,MAXCOL,ICOL1,GLOAD2,TEMP,IDMTX,ESTO
     XR,GSOL1,ELAST,STOR2)
      STOP
      END



      SUBROUTINE GEODEM(ITYPE,MAXDEG,MAXND,MAXSND,THETA,SX,SY,SS,
     XXCORD,YCORD,ZCORD,XDATA,YDATA,ZDATA,TEMP)
CCCCCCCCCCCCCCCCCCCCCCCCCCCCCCCCCCCCCCCCCCCCCCCCCCCCCCCCCCCCCCCCCCCCCC
C                                                                      C
C     SUBROUTINE FOR  CALCULATING NECESSARY THREE COMPONTNTS OF        C
C     DISPLACEMENTS ON THE SURFACE                                     C
C                                                                      C
CCCCCCCCCCCCCCCCCCCCCCCCCCCCCCCCCCCCCCCCCCCCCCCCCCCCCCCCCCCCCCCCCCCCCC
      IMPLICIT REAL*8(A-H,O-Z)
      DIMENSION XCORD(MAXND),YCORD(MAXND),ZCORD(MAXND),TEMP(MAXDEG),XDAT
     XA(MAXSND),YDATA(MAXSND),ZDATA(MAXSND),ID(36),ZDATA2(100),ID2(8)
      PI=3.14159265
      DATA ID/1,2,3,3,12,20,20,19,18,18,9,1,1,4,6,3,5,8,20,17,15,18,16,1
     X3,6,7,8,8,11,15,15,14,13,13,10,6/
      DATA ID2/1,3,6,8,13,15,18,20/
C     SS REPRESENTS TENSOR SHEAR
      SS=2.*SS
      THETA2=THETA*PI/180.
      C1=DCOS(THETA2)
      C2=DSIN(THETA2)
      DO 30 I=1,MAXSND
      X=XCORD(I)-XCORD(1)
```

```
      Y=YCORD(I)-YCORD(1)
      DX=C1*X-C2*Y
      DY=C2*X+C1*Y
      IF(ITYPE) 10,10,20
10    DELX=SX*DX
      DELY=SY*DY
      XDATA(I)=DELX*C1+DELY*C2
      YDATA(I)=-DELX*C2+DELY*C1
      GOTO 30
20    DELX=0.
      DELY=-SS*DX
      XDATA(I)=DELY*C2
      YDATA(I)=DELY*C1
30    CONTINUE
      DO 31 I=1,8
31    ZDATA2(ID2(I))=ZDATA(I)
      DO 32 I=1,34,3
      I1=ID(I)
      I2=ID(I+1)
      I3=ID(I+2)
32    ZDATA2(I2)=.5*(ZDATA2(I1)+ZDATA2(I3))
      DO 40 I=1,MAXDEG
40    TEMP(I)=0.
      DO 41 I=1,MAXSND
      TEMP(3*I-2)=XDATA(I)
      TEMP(3*I-1)=YDATA(I)
41    TEMP(3*I)=ZDATA2(I)
      WRITE(6,1000)
      DO 42 I=1,MAXSND
42    WRITE(6,1001) I,TEMP(3*I-2),TEMP(3*I-1),TEMP(3*I)
1000  FORMAT(1H0,'NODE',6X,'X',15X,'Y',15X,'Z',/)
1001  FORMAT(I3,3X,3G15.7)
      RETURN
      END



      SUBROUTINE STIFFR(MAXND,MAXDEG,MGRID,NGRID,LGRID,ELAST,DUMMY,XCORD
     X,YCORD,ZCORD,NFREE,MAXEL,IDMTX,MAXID,ESTOR)
CCCCCCCCCCCCCCCCCCCCCCCCCCCCCCCCCCCCCCCCCCCCCCCCCCCCCCCCCCCCCCCCCCCCCCC
C                                                                      C
C     SUBROUTINE FOR GENERATING STIFFNESS MATRIX BASED ON 20-NODES     C
C     PARABOLIC HEXAHEDRAL ELEMENT                                     C
C                                                                      C
CCCCCCCCCCCCCCCCCCCCCCCCCCCCCCCCCCCCCCCCCCCCCCCCCCCCCCCCCCCCCCCCCCCCCCC
      IMPLICIT REAL*8(A-H,O-Z)
      DIMENSION DUMMY(MAXDEG,MAXDEG),XCORD(MAXND),YCORD(MAXND),ZCORD(MAX
     XND),ELAST(6,6),ID(60),X(20),Y(20),Z(20),S(60,60),IDMTX(MAXID),ESTO
     XR(MAXEL,6,60)
      DO 1 I=1,MAXDEG
      DO 1 J=1,MAXDEG
1     DUMMY(I,J)=0.
```

```
50    DO 60 NEL=1,MAXEL
      NEL2=20*(NEL-1)
      DO 70 I=1,20
      ID1=IDMTX(NEL2+I)
      X(I)=XCORD(ID1)
      Y(I)=YCORD(ID1)
70    Z(I)=ZCORD(ID1)
      DO 80 I=1,20
      ID(3*I)=3*IDMTX(NEL2+I)
      ID(3*I-1)=ID(3*I)-1
80    ID(3*I-2)=ID(3*I)-2
      CALL ISOPA3(NEL,X,Y,Z,ELAST,S,ESTOR,MAXEL)
      DO 90 I=1,60
      DO 90 J=1,60
      ID1=ID(I)
      ID3=ID(J)
90    DUMMY(ID1,ID3)=DUMMY(ID1,ID3)+S(I,J)
60    CONTINUE
100   RETURN
      END
```

```
      SUBROUTINE ISOPA3(NEL,X,Y,Z,ELAST,SMATX2,ESTOR,MAXEL)
CCCCCCCCCCCCCCCCCCCCCCCCCCCCCCCCCCCCCCCCCCCCCCCCCCCCCCCCCCCCCCCCCCCCCC
C                                                                     C
C     SUBROUTINE FOR GENERATING 20-NODES ISOPARAMETRIC ELEMENT        C
C                                                                     C
CCCCCCCCCCCCCCCCCCCCCCCCCCCCCCCCCCCCCCCCCCCCCCCCCCCCCCCCCCCCCCCCCCCCCC
      IMPLICIT REAL*8(A-H,O-Z)
      DIMENSION X(20),Y(20),Z(20),GR(3),GS(3),GT(3),GW(3),
     XELAST(6,6),SMATX(60,60),SMATX2(60,60),A(3,3),B(3,3),C(6,9),D(9,60)
     X,E(6,60),CE(6,60),ET(60,6),DERIV(3,20),ESTOR(MAXEL,6,60)
      DATA GR/.7745966692414 83,0.,-.7745966692414 83/,GS/.7745966692414 83
     X,0.,-.7745966692414 83/,GT/.7745966692414 83,0.,-.7745966692414 83/
     X,GW/.555555555555556,.888888888888889,.555555555555556/
      DO 2 I=1,60
      DO 2 J=1,60
2     SMATX2(I,J)=0.
      DO 3 I=1,6
      DO 3 J=1,9
3     C(I,J)=0.
      DO 4 I=1,9
      DO 4 J=1,60
4     D(I,J)=0.
      DO 10 IR=1,3
      DO 10 IS=1,3
      DO 10 IT=1,3
      DO 11 I=1,3
      DO 11 J=1,3
11    A(I,J)=0.
      R=GR(IR)
```

```
      S=GS(IS)
      T=GT(IT)
      CALL DERIV2(DERIV,R,S,T)
C     WRITE(6,3001)
C     WRITE(6,3000) (DERIV(1,J),DERIV(2,J),DERIV(3,J),J=1,20)
3001  FORMAT(//)
      DO 20 I=1,3
      DO 20 K=1,20
      A(I,1)=A(I,1)+DERIV(I,K)*X(K)
      A(I,2)=A(I,2)+DERIV(I,K)*Y(K)
20    A(I,3)=A(I,3)+DERIV(I,K)*Z(K)
      DET=A(1,1)*A(2,2)*A(3,3)+A(1,2)*A(2,3)*A(3,1)+A(1,3)*A(3,2)*A(2,1)
     X-A(1,3)*A(2,2)*A(3,1)-A(1,2)*A(2,1)*A(3,3)-A(1,1)*A(3,2)*A(2,3)
      IF(DET.LE.1.0E-04) GO TO 80
      B(1,1)=A(2,2)*A(3,3)-A(2,3)*A(3,2)
      B(1,2)=A(3,2)*A(1,3)-A(1,2)*A(3,3)
      B(1,3)=A(1,2)*A(2,3)-A(1,3)*A(2,2)
      B(2,1)=A(2,3)*A(3,1)-A(2,1)*A(3,3)
      B(2,2)=A(1,1)*A(3,3)-A(1,3)*A(3,1)
      B(2,3)=A(1,3)*A(2,1)-A(1,1)*A(2,3)
      B(3,1)=A(2,1)*A(3,2)-A(2,2)*A(3,1)
      B(3,2)=A(1,2)*A(3,1)-A(1,1)*A(3,2)
      B(3,3)=A(1,1)*A(2,2)-A(1,2)*A(2,1)
      DO 30 I=1,3
      DO 30 J=1,3
30    B(I,J)=B(I,J)/DET
      DO 40 I=1,3
      DO 40 J=1,20
      D(I,3*J-2)=DERIV(I,J)
      D(I+3,3*J-1)=DERIV(I,J)
40    D(I+6,3*J)=DERIV(I,J)
      DO 50 J=1,3
      C(1,J)=B(1,J)
      C(2,J+3)=B(2,J)
      C(3,J+6)=B(3,J)
      C(4,J)=B(2,J)
      C(4,J+3)=B(1,J)
      C(5,J)=B(3,J)
      C(5,J+6)=B(1,J)
      C(6,J+3)=B(3,J)
50    C(6,J+6)=B(2,J)
      CALL MULTD(6,9,60,C,D,E)
      CALL MULTD(6,6,60,ELAST,E,CE)
      IF(IR-2) 55,51,55
51    IF(IS-2) 55,52,55
52    IF(IT-2) 55,53,55
53    DO 54 I=1,6
      DO 54 J=1,60
54    ESTOR(NEL,I,J)=E(I,J)
55    CONTINUE
      DO 60 I=1,6
      DO 60 J=1,60
60    ET(J,I)=E(I,J)
      CALL MULTD(60,6,60,ET,CE,SMATX)
```

```
      WT=GW(IR)*GW(IS)*GW(IT)*DET
      DO 70 I=1,60
      DO 70 J=1,60
70    SMATX2(I,J)=SMATX2(I,J)+WT*SMATX(I,J)
10    CONTINUE
C     CALL WRITE(SMATX2)
C     STOP
      GO TO 90
80    WRITE(6,1000) NEL
      WRITE(6,1001)IR,IS,IT
      WRITE(6,2003) R,S,T
1001  FORMAT(1H0,3I5)
1000  FORMAT(1H0,'ERROR/DETERMINANT ZERO AT ELEMENT',I5)
      DO 100 I=1,20
100   WRITE(6,2000)X(I),Y(I),Z(I)
2000  FORMAT(3G15.7)
      DO 101 I=1,3
101   WRITE(6,2001)(DERIV(I,J),J=1,20)
2001  FORMAT(8G15.7)
      DO 102 I=1,3
102   WRITE(6,2002)(A(I,J),J=1,3)
2002  FORMAT(3G15.7)
2003  FORMAT(1H0,3G15.7)
      STOP
90    RETURN
      END



      SUBROUTINE DERIV2(DERIV,R,S,T)
CCCCCCCCCCCCCCCCCCCCCCCCCCCCCCCCCCCCCCCCCCCCCCCCCCCCCCCCCCCCCCCCCCCCCCCCCC
C                                                                       C
C     SUBROUTINE FOR  CALCULATING JACOBIAN MATRIX                       C
C                                                                       C
CCCCCCCCCCCCCCCCCCCCCCCCCCCCCCCCCCCCCCCCCCCCCCCCCCCCCCCCCCCCCCCCCCCCCCCCCC
      IMPLICIT REAL*8(A-H,O-Z)
      DIMENSION DERIV(3,20)
      DATA NODE/20/
      DERIV(1,1)=(1.+S)*(1.+T)*.125
      DERIV(1,2)=(1.+S)*(1.+T)*(-.125)
      DERIV(1,3)=(1.-S)*(1.+T)*(-.125)
      DERIV(1,4)=(1.-S)*(1.+T)*.125
      DERIV(1,5)=(1.+S)*(1.-T)*.125
      DERIV(1,6)=(1.+S)*(1.-T)*(-.125)
      DERIV(1,7)=(1.-S)*(1.-T)*(-.125)
      DERIV(1,8)=(1.-S)*(1.-T)*.125
      DERIV(2,1)=(1.+R)*(1.+T)*.125
      DERIV(2,2)=(1.-R)*(1.+T)*.125
      DERIV(2,3)=(1.-R)*(1.+T)*(-.125)
      DERIV(2,4)=(1.+R)*(1.+T)*(-.125)
      DERIV(2,5)=(1.+R)*(1.-T)*.125
      DERIV(2,6)=(1.-R)*(1.-T)*.125
```

```
DERIV(2,6)=(1.-R)*(1.-T)*.125
DERIV(2,7)=(1.-R)*(1.-T)*(-.125)
DERIV(2,8)=(1.+R)*(1.-T)*(-.125)
DERIV(3,1)=(1.+R)*(1.+S)*.125
DERIV(3,2)=(1.-R)*(1.+S)*.125
DERIV(3,3)=(1.-R)*(1.-S)*.125
DERIV(3,4)=(1.+R)*(1.-S)*.125
DERIV(3,5)=(1.+R)*(1.+S)*(-.125)
DERIV(3,6)=(1.-R)*(1.+S)*(-.125)
DERIV(3,7)=(1.-R)*(1.-S)*(-.125)
DERIV(3,8)=(1.+R)*(1.-S)*(-.125)
IF(NODE.EQ.8) GOTO 10
DERIV(1,9)=-.5*R*(1.+S)*(1.+T)
DERIV(1,10)=-.25*(1.-S*S)*(1.+T)
DERIV(1,11)=-.5*R*(1.-S)*(1.+T)
DERIV(1,12)=.25*(1.-S*S)*(1.+T)
DERIV(1,13)=-.5*R*(1.+S)*(1.-T)
DERIV(1,14)=-.25*(1.-S*S)*(1.-T)
DERIV(1,15)=-.5*R*(1.-S)*(1.-T)
DERIV(1,16)=.25*(1.-S*S)*(1.-T)
DERIV(1,17)=.25*(1.+S)*(1.-T*T)
DERIV(1,18)=-.25*(1.+S)*(1.-T*T)
DERIV(1,19)=-.25*(1.-S)*(1.-T*T)
DERIV(1,20)=.25*(1.-S)*(1.-T*T)
DERIV(1,1)=DERIV(1,1)-.5*(DERIV(1,9)+DERIV(1,12)+DERIV(1,17))
DERIV(1,2)=DERIV(1,2)-.5*(DERIV(1,9)+DERIV(1,10)+DERIV(1,18))
DERIV(1,3)=DERIV(1,3)-.5*(DERIV(1,10)+DERIV(1,11)+DERIV(1,19))
DERIV(1,4)=DERIV(1,4)-.5*(DERIV(1,11)+DERIV(1,12)+DERIV(1,20))
DERIV(1,5)=DERIV(1,5)-.5*(DERIV(1,16)+DERIV(1,17)+DERIV(1,13))
DERIV(1,6)=DERIV(1,6)-.5*(DERIV(1,13)+DERIV(1,14)+DERIV(1,18))
DERIV(1,7)=DERIV(1,7)-.5*(DERIV(1,14)+DERIV(1,15)+DERIV(1,19))
DERIV(1,8)=DERIV(1,8)-.5*(DERIV(1,15)+DERIV(1,16)+DERIV(1,20))
DERIV(2,9)=.25*(1.-R*R)*(1.+T)
DERIV(2,10)=-.5*(1.-R)*S*(1.+T)
DERIV(2,11)=-.25*(1.-R*R)*(1.+T)
DERIV(2,12)=-.5*(1.+R)*S*(1.+T)
DERIV(2,13)=.25*(1.-R*R)*(1.-T)
DERIV(2,14)=-.5*(1.-R)*S*(1.-T)
DERIV(2,15)=-.25*(1.-R*R)*(1.-T)
DERIV(2,16)=-.5*(1.+R)*S*(1.-T)
DERIV(2,17)=.25*(1.+R)*(1.-T*T)
DERIV(2,18)=.25*(1.-R)*(1.-T*T)
DERIV(2,19)=-.25*(1.-R)*(1.-T*T)
DERIV(2,20)=-.25*(1.+R)*(1.-T*T)
DERIV(2,1)=DERIV(2,1)-.5*(DERIV(2,9)+DERIV(2,12)+DERIV(2,17))
DERIV(2,2)=DERIV(2,2)-.5*(DERIV(2,9)+DERIV(2,10)+DERIV(2,18))
DERIV(2,3)=DERIV(2,3)-.5*(DERIV(2,10)+DERIV(2,11)+DERIV(2,19))
DERIV(2,4)=DERIV(2,4)-.5*(DERIV(2,11)+DERIV(2,12)+DERIV(2,20))
DERIV(2,5)=DERIV(2,5)-.5*(DERIV(2,16)+DERIV(2,17)+DERIV(2,13))
DERIV(2,6)=DERIV(2,6)-.5*(DERIV(2,13)+DERIV(2,14)+DERIV(2,18))
DERIV(2,7)=DERIV(2,7)-.5*(DERIV(2,14)+DERIV(2,15)+DERIV(2,19))
DERIV(2,8)=DERIV(2,8)-.5*(DERIV(2,15)+DERIV(2,16)+DERIV(2,20))
DERIV(3,9)=.25*(1.-R*R)*(1.+S)
DERIV(3,10)=.25*(1.-R)*(1.-S*S)
```

```
      DERIV(3,11)=.25*(1.-R*R)*(1.-S)
      DERIV(3,12)=.25*(1.+R)*(1.-S*S)
      DERIV(3,13)=-.25*(1.-R*R)*(1.+S)
      DERIV(3,14)=-.25*(1.-R)*(1.-S*S)
      DERIV(3,15)=-.25*(1.-R*R)*(1.-S)
      DERIV(3,16)=-.25*(1.+R)*(1.-S*S)
      DERIV(3,17)=-.5*(1.+R)*(1.+S)*T
      DERIV(3,18)=-.5*(1.-R)*(1.+S)*T
      DERIV(3,19)=-.5*(1.-R)*(1.-S)*T
      DERIV(3,20)=-.5*(1.+R)*(1.-S)*T
      DERIV(3,1)=DERIV(3,1)-.5*(DERIV(3,9)+DERIV(3,12)+DERIV(3,17))
      DERIV(3,2)=DERIV(3,2)-.5*(DERIV(3,9)+DERIV(3,10)+DERIV(3,18))
      DERIV(3,3)=DERIV(3,3)-.5*(DERIV(3,10)+DERIV(3,11)+DEPIV(3,19))
      DERIV(3,4)=DERIV(3,4)-.5*(DERIV(3,11)+DERIV(3,12)+DERIV(3,20))
      DERIV(3,5)=DERIV(3,5)-.5*(DERIV(3,16)+DERIV(3,17)+DERIV(3,13))
      DERIV(3,6)=DERIV(3,6)-.5*(DERIV(3,13)+DERIV(3,14)+DERIV(3,18))
      DERIV(3,7)=DERIV(3,7)-.5*(DERIV(3,14)+DERIV(3,15)+DERIV(3,19))
      DERIV(3,8)=DERIV(3,8)-.5*(DERIV(3,15)+DERIV(3,16)+DERIV(3,20))
10    RETURN
      END



      SUBROUTINE SHUFL3(MAXDEG,MAXCOL,MAXROW,STIFF,ICOL1,ICOL2,IROW
     X1,IROW2,GLOAD,TEMP)
CCCCCCCCCCCCCCCCCCCCCCCCCCCCCCCCCCCCCCCCCCCCCCCCCCCCCCCCCCCCCCCCCCCCCC
C                                                                     C
C     SUBROUTINE FOR ARRANGING KNOWNS AND UNKNOWNS                    C
C                                                                     C
CCCCCCCCCCCCCCCCCCCCCCCCCCCCCCCCCCCCCCCCCCCCCCCCCCCCCCCCCCCCCCCCCCCCCC
      IMPLICIT REAL*8(A-H,O-Z)
      REAL*8 JUNK,JUNK2
      DIMENSION STIFF(MAXDEG,MAXDEG),GLOAD(MAXDEG),TEMP(MAXDEG),
     XICOL1(MAXDEG),ICOL2(MAXDEG),IROW1(MAXDEG),IROW2(MAXDEG)
      DO 11 I=1,MAXDEG
11    GLOAD(I)=0.
      DO 12 I=1,MAXDEG
      DO 12 J=1,MAXCOL
12    GLOAD(I)=GLOAD(I)-STIFF(I,ICOL1(J))*TEMP(J)
      DO 20 I=1,MAXDEG
      DO 20 J=1,MAXROW
20    STIFF(I,J)=STIFF(I,J+MAXCOL)
      DO 21 I=1,MAXDEG
      DO 21 J=1,MAXCOL
      STIFF(I,J+MAXROW)=0.
21    IF(IROW2(J).EQ.I) STIFF(I,J+MAXROW)=-1.
      RETURN
      END
```

```
      SUBROUTINE SOLVR3(M1,M2,M3,DUMMY4,GLOAD,GLOAD2,EPSLON,OMEGA)
CCCCCCCCCCCCCCCCCCCCCCCCCCCCCCCCCCCCCCCCCCCCCCCCCCCCCCCCCCCCCCCCCCCCCC
C                                                                      C
C     SUBROUTINE FOR SOLVING LINEAR EQUATION                           C
C     BASED ON GAUSS JORDAN ELIMINATION USING PARTIAL PIVOTING         C
C                                                                      C
CCCCCCCCCCCCCCCCCCCCCCCCCCCCCCCCCCCCCCCCCCCCCCCCCCCCCCCCCCCCCCCCCCCCCC
      IMPLICIT REAL*8(A-H,O-Z)
      ABS(X)=DABS(X)
      DIMENSION DUMMY4(M1,M3),GLOAD(M1),GLOAD2(M1)
      IMAX=M1
      DO 10 I=1,IMAX
10    DUMMY4(I,IMAX+1)=GLOAD(I)
C      GAUSS JORDAN ELIMINATION
       NUM=IMAX+1
       DO 130 K=1,IMAX
C     CALL WRITE2(DUMMY4)
       LMAX=K
       D2=DUMMY4(K,K)
       AMAX=ABS(D2)
       DO 80 I=K,IMAX
       D1=DUMMY4(I,K)
       IF(AMAX.GE.ABS(D1)) GO TO 80
       LMAX=I
       AMAX=ABS(D1)
80     CONTINUE
       IF(LMAX.EQ.K) GO TO 100
       DO 90 J=1,NUM
       DUMMY6=DUMMY4(LMAX,J)
       DUMMY4(LMAX,J)=DUMMY4(K,J)
       DUMMY4(K,J)=DUMMY6
90     CONTINUE
100    CONTINUE
C      CHECK SINGULAR MATRIX
       D2=DUMMY4(K,K)
       IF(ABS(D2).GT.EPSLON) GO TO 91
       DUMMY4(K,K)=DUMMY4(K,K)+OMEGA
       WRITE(6,2300)K
       STOP
91     CONTINUE
       DDIV=DUMMY4(K,K)
       DO 110 J=1,NUM
       DUMMY4(K,J)=DUMMY4(K,J)/DDIV
110    CONTINUE
       DO 121 I=1,IMAX
       IF(I.EQ.K) GO TO 121
       DMULT=DUMMY4(I,K)
       DO 120 J=K,NUM
      DUMMY4(I,J)=DUMMY4(I,J)-DMULT*DUMMY4(K,J)
120    CONTINUE
121    CONTINUE
130   CONTINUE
      DO 140 I=1,M1
140   GLOAD2(I)=DUMMY4(I,IMAX+1)
```

```
2300  FORMAT(1H0,'KMATRIX BECAME SINGULAR AT ROW',I5)
      RETURN
      END



      SUBROUTINE STRESS(MAXDEG,MAXEL,MAXID,MAXCOL,ICOL1,GLOAD2,TEMP,IDMT
     XX,ESTOR,GSOL1,ELAST,STOR2)
CCCCCCCCCCCCCCCCCCCCCCCCCCCCCCCCCCCCCCCCCCCCCCCCCCCCCCCCCCCCCCCCCCCCCCC
C                                                                      C
C     SUBROUTINE FOR   CALCULATING STRESS AND STRAIN IN EACH ELEMENT   C
C                                                                      C
CCCCCCCCCCCCCCCCCCCCCCCCCCCCCCCCCCCCCCCCCCCCCCCCCCCCCCCCCCCCCCCCCCCCCCC
      IMPLICIT REAL*8(A-H,O-Z)
      DIMENSION ICOL1(MAXDEG),GLOAD2(MAXDEG,1),TEMP(MAXDEG,1),
     XIDMTX(MAXID),ESTOR(MAXEL,6,60),GSOL1(MAXDEG,1),ID(60),DISPL(60,1)
     X,E(6,60),S1(6,1),S2(6,1),ELAST(6,6),A(3,3),V(3,3),D(3),B(3),Z(3)
      DIMENSION STOR2(MAXEL,6)
      EPSL2=0.1D-08
      M1=MAXDEG-MAXCOL
      DO 10 I=1,MAXCOL
10    GSOL1(ICOL1(I),1)=TEMP(I,1)
      DO 11 I=1,M1
11    GSOL1(MAXCOL+I,1)=GLOAD2(I,1)
      DO 20 NEL=1,MAXEL
      NEL2=20*(NEL-1)
      DO 30 I=1,20
      ID(3*I)=3*IDMTX(NEL2+I)
      ID(3*I-1)=ID(3*I)-1
30    ID(3*I-2)=ID(3*I)-2
      DO 40 I=1,60
40    DISPL(I,1)=GSOL1(ID(I),1)
      DO 50 I=1,6
      DO 50 J=1,60
50    E(I,J)=ESTOR(NEL,I,J)
      CALL MULT(6,60,1,E,DISPL,S1)
      CALL MULT(6,6,1,ELAST,S1,S2)
C     GOTO 70
71    CONTINUE
      WRITE(6,1000) NEL
      WRITE(6,1001) S1(1,1),S2(1,1)
      WRITE(6,1002) S1(2,1),S2(2,1)
      WRITE(6,1003) S1(3,1),S2(3,1)
      WRITE(6,1004) S1(4,1),S2(4,1)
      WRITE(6,1005) S1(5,1),S2(5,1)
      WRITE(6,1006) S1(6,1),S2(6,1)
70    CONTINUE
      DO 52 I=1,6
52    STOR2(NEL,I)=S2(I,1)
C     GOTO 20
51    CONTINUE
      A(1,1)=S1(1,1)
```

```
      DIMENSION A(N,N),V(N,N),D(N)
      ITM=200
      IT=0
      DO 10 I=1,N
      DO 10 J=1,N
      V(I,J)=0.
   10 IF(I.EQ.J) V(I,J)=1.
   15 T=0.
      M=N-1
      DO 20 I=1,M
      J1=I+1
      DO 20 J=J1,N
      IF(DABS(A(I,J)).LE.T) GO TO 20
      T=DABS(A(I,J))
      IR=I
      IC=J
   20 CONTINUE
C     IF(IT.EQ.0) T1=T*ERR
C     IF(T.LE.T1) GOTO 999
      IF(T.LE.ERR) GO TO 999
      PS=A(IR,IR)-A(IC,IC)
      TA=(-PS+DSQRT(PS*PS+4.*T*T))/(2*A(IR,IC))
      C=1./DSQRT(1.+TA*TA)
      S=C*TA
      DO 50 I=1,N
      P=V(I,IR)
      V(I,IR)=C*P+S*V(I,IC)
   50 V(I,IC)=C*V(I,IC)-S*P
      I=1
  100 IF(I.EQ.IR) GOTO 200
      P=A(I,IR)
      A(I,IR)=C*P+S*A(I,IC)
      A(I,IC)=C*A(I,IC)-S*P
      I=I+1
      GO TO 100
  200 I=IR+1
  300 IF(I.EQ.IC) GOTO 400
      P=A(IR,I)
      A(IR,I)=C*P+S*A(I,IC)
      A(I,IC)=C*A(I,IC)-S*P
      I=I+1
      GO TO 300
  400 I=IC+1
  500 IF(I.GT.N) GOTO 600
      P=A(IR,I)
      A(IR,I)=C*P+S*A(IC,I)
      A(IC,I)=C*A(IC,I)-S*P
      I=I+1
      GO TO 500
  600 P=A(IR,IR)
      A(IR,IR)=C*C*P+2.*C*S*A(IR,IC)+S*S*A(IC,IC)
      A(IC,IC)=C*C*A(IC,IC)+S*S*P-2.*C*S*A(IR,IC)
      A(IR,IC)=0.
      IT=IT+1
```

```
      IF(IT.LT.ITM) GOTO 13
  999 DO 998 I=1,N
  998 D(I)=A(I,I)
      RETURN
      END
```